This document was prepared for the ETI by third parties under contract to the ETI. The ETI is making these documents and data available to the public to inform the debate on low carbon energy innovation and deployment.

Programme Area: Marine

Project: PerAWAT

Title: Tidalfarmer Model Validation And Uncertainties

Abstract:

Validation of the numerical models developed in TidalFarmer is essential in order to predict the expected energy yield with a quantifiable level of uncertainty. This will provide stakeholder confidence in the planning, investment and maintenance of a tidal array and will help accelerate growth of the tidal energy industry. The various numerical and experimental studies performed throughout the PerAWaT project can be used to form comparisons with the array-scale model to test whether it is an accurate representation of a tidal stream farm. In this work, it is assumed that each of these studies is comparable to the full-scale Tidal Generation Ltd device. As such, discussions relating to the accuracy of the studies to the full-scale device are provided throughout. In order to check the adequacy of the modelling assumptions and limitations of each model component, a comparison to experimental and numerical studies has been undertaken. In addition, an uncertainty analysis is provided whereby the impact of standard measurement uncertainty on the model outputs is discussed. Suggestions for further work, in order to decrease uncertainty in energy yield predictions, are provided.

Context:

The Performance Assessment of Wave and Tidal Array Systems (PerAWaT) project, launched in October 2009 with £8m of ETI investment. The project delivered validated, commercial software tools capable of significantly reducing the levels of uncertainty associated with predicting the energy yield of major wave and tidal stream energy arrays. It also produced information that will help reduce commercial risk of future large scale wave and tidal array developments.

Disclaimer:

The Energy Technologies Institute is making this document available to use under the Energy Technologies Institute Open Licence for Materials. Please refer to the Energy Technologies Institute website for the terms and conditions of this licence. The Information is licensed 'as is' and the Energy Technologies Institute excludes all representations, warranties, obligations and liabilities in relation to the Information to the maximum extent permitted by law. The Energy Technologies Institute is not liable for any errors or omissions in the Information and shall not be liable for any loss, injury or damage of any kind caused by its use. This exclusion of liability includes, but is not limited to, any direct, indirect, special, incidental, consequential, punitive, or exemplary damages in each case such as loss of revenue, data, anticipated profits, and lost business. The Energy Technologies Institute does not guarantee the continued supply of the Information. Notwithstanding any statement to the contrary contained on the face of this document, the Energy Technologies Institute confirms that the authors of the document have consented to its publication by the Energy Technologies Institute.

GL Garrad Hassan

ETI Marine Programme Project
PerAWaT MA1003
WG3WP4 D19: TIDALFARMER MODEL VALIDATION AND UNCERTAINTIES

Client	**Energy Technologies Institute**
Contact	Simon Cheeseman
Document No	104329/BR/17
Issue	1.0
Classification	Not to be disclosed other than in line with the terms of the Technology Contract
Date	30 August 2013

Author: S. Parkinson

Checked by: M. Thomson

Approved by:

Garrad Hassan & Partners Ltd

St Vincent's Works, Silverthorne Lane, Bristol BS2 0QD, UK Tel: +44 (0)117 972 9900, Registered in England 1878456

IMPORTANT NOTICE AND DISCLAIMER

This report ("Report") is prepared and issued by Garrad Hassan & Partners Ltd ("GH" or "Garrad Hassan") for the sole use of the client named on its title page (the "Client") on whose instructions it has been prepared, and who has entered into a written agreement directly with Garrad Hassan. Garrad Hassan's liability to the Client is set out in that agreement. Garrad Hassan shall have no liability to third parties (being persons other than the Client) in connection with this Report or for any use whatsoever by third parties of this Report unless the subject of a written agreement between Garrad Hassan and such third party. The Report may only be reproduced and circulated in accordance with the Document Classification and associated conditions stipulated or referred to in this Report and/or in Garrad Hassan's written agreement with the Client. No part of this Report may be disclosed in any public offering memorandum, prospectus or stock exchange listing, circular or announcement without the express written consent of Garrad Hassan. A Document Classification permitting the Client to redistribute this Report shall not thereby imply that Garrad Hassan has any liability to any recipient other than the Client.
This report has been produced from information relating to dates and periods referred to in this report. The report does not imply that any information is not subject to change.

KEY TO DOCUMENT CLASSIFICATION

Strictly Confidential	:	For disclosure only to named individuals within the Client's organisation.
Private and Confidential	:	For disclosure only to individuals directly concerned with the subject matter of the Report within the Client's organisation.
Commercial in Confidence	:	Not to be disclosed outside the Client's organisation
GH only	:	Not to be disclosed to non GH staff
Client's Discretion	:	Distribution for information only at the discretion of the Client (subject to the above Important Notice and Disclaimer).
Published	:	Available for information only to the general public (subject to the above Important Notice and Disclaimer and Disclaimer).

© 2013 Garrad Hassan & Partners Ltd

REVISION HISTORY

Issue	Issue date	Summary
Draft	26/09/2013	

Not to be disclosed other than in line with the terms of the Technology Contract

CONTENTS

Not to be disclosed other than in line with the terms of the Technology Contract

Not to be disclosed other than in line with the terms of the Technology Contract

Not to be disclosed other than in line with the terms of the Technology Contract

EXECUTIVE SUMMARY

Validation of the numerical models developed in TidalFarmer is essential in order to predict the expected energy yield with a quantifiable level of uncertainty. This will provide stakeholder confidence in the planning, investment and maintenance of a tidal array and will help accelerate growth of the tidal energy industry.

The various numerical and experimental studies performed throughout the PerAWaT project can be used to form comparisons with the array-scale model to test whether it is an accurate representation of a tidal stream farm. In this work, it is assumed that each of these studies is comparable to the full-scale Tidal Generation Ltd device. As such, discussions relating to the accuracy of the studies to the full-scale device are provided throughout.

The array-scale model is a combination of interlinked components. These components are; the flow field, blockage, near wake and far wake models. In order to check the adequacy of the modelling assumptions and limitations of each component, a comparison to experimental and numerical studies has been undertaken. In addition, an uncertainty analysis is provided whereby the impact of standard measurement uncertainty on the model outputs is discussed.

Together the different components can estimate the energy yield and the effect of negative device interactions, such as wake losses, of a tidal stream farm. To test this assertion a comparison to measured data, from the array scale experiments, is made against the prediction of the downstream loadings on devices. The aggregated uncertainty of the combined model is then assessed using a Monte Carlo method. Taking experimentally observed system properties, such as the thrust coefficient and turbulence intensity, these values can be perturbed by a small amount. By repeatedly evaluating the model and comparing to measurements, sensitive parameters can be identified. Suggestions for further work, in order to decrease uncertainty in energy yield predictions, are provided.

Not to be disclosed other than in line with the terms of the Technology Contract

1 INTRODUCTION

1.1 Scope of this document

This document forms the 19th deliverable (D19) of the PerAWAT project and constitutes a discussion of the overall model validation of TidalFarmer. This model has been developed as part of working group 3, work package 4 (WG3WP4) of the PerAWAT (Performance Assessment of Wave and Tidal Arrays) project commissioned and funded by the Energy Technologies Institute (ETI). Garrad Hassan (GH) is the sole contributor to this work package.

1.2 Purpose of this document

The purpose of WG3WP4 is to develop, validate and document an engineering tool that allows a rapid assessment of the energy yield potential of a tidal turbine array on non-specialist hardware. The specific objective of WG3 WP4 D19 is to both document and provide technical justification for the use of the existing GH blockage, near wake, far wake and flow field models within the suite of models that make up the engineering tool: TidalFarmer.

This includes discussions of the various model components such as the blockage, near wake, far wake and flow field models with comparison to numerical and experimental studies. In addition, an assessment of the overall model adequacy is presented, that takes into consideration measurement and model uncertainty whereby the most sensitive parameters are identified and additional work is suggested in order to help further reduce uncertainties.

1.3 Specific tasks associated with WG3 WP4 D19

WG3WP4 D19 comprises of the following:

- A description of the GH blockage, near wake, far wake and flow field models and their assumptions.
- An evaluation of each GH model against experimental and numerical data sets.
- Discussions of the assumptions, model limitations and sensitivities.
- A discussion of the uncertainty in model predictions with respect to measurement uncertainty.
- Discussions of the aggregated accuracy of the array-scale model, with comparison to scaled experimental testing and suggestions of future work that can help reduce uncertainties.

1.4 Acceptance criteria for WG3WP4 D19

The acceptance criteria as stated in schedule five of the PerAWAT technology contract is as follows:

D19: TidalFarmer interim model validation report:

- Description of validation methodology for the blockage model.
- Assessment of blockage model performance via the analysis of the boundless rotor characteristics, the device scale experiment data (RPM, power and thrust) and the model results.
- Quantification of the uncertainties of the GH blockage model
- Discussion of the overall validity, sensitivities and limitations of the GH blockage model

Not to be disclosed other than in line with the terms of the Technology Contract

- Description of validation methodology for the near wake model.
- Assessment of near wake model performance via the comparison of the device scale experiment data with the GH near wake models – particularly, the near wake form (in terms of deficit and turbulence intensity).
- Analysis of the effect of varying the shear profiles on the near wake form in a variety of ambient flow conditions (waves and seabed generated turbulence intensities).
- Assessment of the effect of including the flow field data from the ReDAPT project on near wake model performance.
- Quantification of the uncertainties of the GH near wake model.
- Discussion of the overall validity, sensitivities and limitations of the GH near wake model.

- Description of the validation methodology for the flow field model.
- Assessment of model performance via the comparison of the detailed 2-d Telemac model against the rationalised flow model with the basin scale data form ReDAPT.
- Assessment of model performance via the comparison of the flow field model with the basin scale data from ReDAPT.
- Validation of depth profile models (data from ReDAPT).
- Quantification of the uncertainties of the GH flow field model.
- Discussion of the overall validity, sensitivities and limitations of the GH flow field model.

- Description of validation methodology for the far wake model.
- Assessment of model performance via comparison of the device scale experiment data and the GH far wake models, particularly wake deficit and added turbulence; ambient turbulence intensity conditions and wave generated turbulence.
- Assessment of the impact of large scale eddies on wake recovery.
- Assessment of wake interaction modelling – via comparison with experimental data.
- Quantification of the uncertainties of the GH far wake model.
- Discussion of the overall validity, sensitivities and limitations of the GH far wake model.

- A clear definition of resulting overall inter-array scale modelling methodologies, model integration and the associated uncertainties of the final combined model.
- A clear comparison of measured and predicted loading and performance along with critique of discrepancies.
- Identification of components of models that contribute significantly to levels of uncertainty and suggestions for further work to further reduce uncertainty.
- Discussion of the overall validity, sensitivities, and limitations of the overall inter-array scale model.

1.5 Definitions of terminology

In order to discuss uncertainty in energy yield predictions and how the PerAWaT project has decreased this uncertainty in these predictions, a common language has been developed. In particular, some key terms used in this report are defined below to fully identify what we can and cannot quantify through the report, as well as in the numerical and experimental studies undertaken as part of this project.

In performing experimental studies, there is always a degree of uncertainty surrounding the results. The **accuracy** is referred to as the degree of closeness of a measured quantity to the true value of the quantity itself. Given that the true value of an observation can never be known or measured perfectly,

Not to be disclosed other than in line with the terms of the Technology Contract

there can be many factors that contribute to poor accuracy in experiments, including **bias** where testing errors favour some outcomes over others. Accuracy is in fact a qualitative object whereby the accuracy of an experiment can be defined as low, fair, high. A related concept is the **error**; this is defined to be the difference between a computed or measured value and a true or theoretically correct value. In the following work, the error statistic that is used is the root mean square error which can be written as

$$RMSE = \Sigma_i^N (u_i - z_i)^2 /N, \quad [1\text{-}1]$$

where u_i is a model output and z_i is an experimental output and N is the number of data items.

A related concept to accuracy is **precision** which in this context is defined as the degree to which the repeated measurements, under unchanged conditions, show the same results. This is also referred to as repeatability. One important feature of a carefully performed experiment is that they exhibit repeatability, such that the results can be recreated at a later time. By re-running experiments for an extended period repeatability can be observed when the degree of scatter in the observations is small.

Given that the true value to an experiment can never be known, defined or realised perfectly, the term **uncertainty** acknowledges that no observation can be perfect. It is defined as the parameter associated with the results of a measurement that characterises the dispersion of values that could reasonably be attributed to the measurand. Or, for a statistical definition is – the estimated percentage by which an observed or calculated value may differ from the true value. Typically this is expressed as a range of values within which the true value is estimated to lie for a given statistical confidence, but it does not attempt to define or rely on a unique true value.

For the purposes of the PerAWaT project, we wish to understand the degree to which the models can be used to predict the expected energy yield for a tidal farm. In order to be able to begin to quantify the amount of uncertainty inherent in the model we define three further types of uncertainty:

1. **Input uncertainty –** imprecise knowledge of the input parameter or focing functions.
2. **Model uncertainty –** errors that occur when transforming model inputs into outputs to predict the natural system.

The uncertainty is generally a measure of dispersion around a value. Another factor that should therefore be considered is the **model discrepancy**. This is the difference between the ability of the model to predict properties of a system (such as fluid velocity) to measured values. The larger the model discrepancy, the more likely it is the model will not provide accurate forecasts of the energy yield.

Two further sub categories of uncertainty exist relating to both imperfect knowledge of a situation and the random nature of physical events that cannot be replicated in a deterministic model.

Epistemic uncertainty is engendered by a lack of knowledge. While the purpose of the PerAWaT project is to gain an understanding surrounding array interactions, there will inherently be epistemic uncertainty due to a lack of knowledge of how experiments reflect full-scale demonstration farms.

Aleatory uncertainty is linked to random or chance events that may serve to change the expected energy yield of a project. Examples of factors that can be attributed to aleatory uncertainty are adverse meteorological conditions or maintenance issues. These cannot be foreseen ahead of time, aleatory uncertainty must be quantified using appropriate statistical tools, for instance Monte Carlo simulations.

Not to be disclosed other than in line with the terms of the Technology Contract

1.6 Description of energy extraction model

The energy extraction model, otherwise referred to as TidalFarmer, is a combination of interlinked models which output an estimate for the potential energy yield of a Tidal stream device farm. In this document the accuracy of each model and of the overall combined model is discussed. The individual models are: the flow field, blockage, near wake and far wake models. The manner in which these models are related is described in the WG3 WP4 D6 document, however, a quick summary is provided below.

The flow field model (see section 4 and also WG3 WP4 D4) allows the rotor averaged flux, at the device locations to be evaluated. From the predictions of rotor averaged flux, second and third order moments of the rotor averaged velocity can be calculated giving the thrust and power coefficients. These thrust and power coefficients require modification however, as the presence of bounding surfaces and other rotors changes the bounding streamtube surrounding the device, thus changing the operating point. The blockage model (see section 2 and also WG3 WP4 D1) corrects for the change in operating point of the device so that accurate predictions for both the power production and the downstream wake deficit can be obtained. The near wake model (see section 3 and also WG3 WP4 D2) takes the blockage corrected thrust coefficient and ambient turbulence intensity and outputs an inflow profile to the far wake model. The far wake model (see section 5 and also WG3 WP4 D5) then models the recovery of the inflow profile back to a quasi free-stream state. The reduction in flow speed that is obtained from the far wake model is then imposed on the flow field. The process is then repeated until all wake effects have been resolved and the power at each rotor has been calculated. This algorithm is described in more detail in section 6 and the reader is also referred to the previous work on the combined inter-array algorithm (WG3 WP4 W6).

Not to be disclosed other than in line with the terms of the Technology Contract

SUMMARY OF NOTATION

Channel characteristics

A	Cross-sectional area (m^2)
b	Width of channel (Diameters)
D_H	Hydraulic radius of the channel (m)
Fr	Froude number (channel)
h	Channel height (Diameters)
d	Flume water depth (m)
r	Radial distance (m)
z	Vertical height measured from the sea bed or channel floor (m)

Turbine characteristics

C_p	Power coefficient
Cp_b	Power coefficient of the rotor in a boundless flow
C_t	Thrust coefficient
Ct_b	Thrust coefficient of the rotor in a boundless flow
D	Rotor diameter (m)
hh	Turbine hub height (Diameters)
$Re_{turbine}$	Reynolds number across the rotor

Flow Field

a	Axial induction factor
B	Blockage ratio
B_l	Lateral blockage ratio
B_v	Vertical blockage ratio
E	Specific energy (m^2/s^2)
f	Body forces (per unit volume) acting on the fluid (N/m^3)
g	Gravitational acceleration (m/s^2)
J_0	Bessel function
k	Wave number (1/m)
M	Momentum (Ns)
m	Strength of the source
p	Pressure (N/m^2)
q	Flow rate (m^3/s)
R	Radius of streamtube (m)
S	Area of the streamtube (m^2)
s_t	Equivalent 2-D turbine diameter (m)
s_0	Width of streamtube upstream (m)
s_2	Width of streamtube downstream (m)
u	Axial velocity component (m/s)
v	Lateral velocity component (m/s)
w	Vertical velocity component (m/s)
u’	Axial turbulent velocity fluctuation (m/s)
u_{wake}	Axial flow speed of the wake flow (m/s)
U_0	Mean free stream flow speed (m/s)
U_i	Incident flow speed on rotor (m/s)
TI_{amb}	Ambient turbulence intensity (%)

Not to be disclosed other than in line with the terms of the Technology Contract

TI_{added}	Added turbulence intensity (%)
α	Fractional reduction in velocity downstream in the wake (m/s)
β	Fractional reduction in velocity at the rotor (m/s)
Φ	Velocity potential (m^2/s)
κ	Drag coefficient
ρ	Density (kg/m^3)
τ	Fractional increase in flow speed (m/s)
x	Streamwise coordinate
y	Cross stream coordinate
z	Vertical coordinate
z_0	Roughness length
1-d	one dimension (typically in the x-direction)
2-d	Numerical solution of the two-dimensional, axisymmetric, free-shear layer equations
3-d	Numerical solution of the three-dimensional, Cartesian, free-shear layer equations

Modelling

$\hat{U}$	Normalised velocity deficit
μ_x	Mean x-position for Gaussian fit to measured data
μ_y	Mean y-position for Gaussian fit to measured data
σ_x	Standard deviation in x-direction for Gaussian fit to measured data
σ_y	Standard deviation in y-direction for Gaussian fit to measured data
RMSE	Root mean square error between measured and GH model predictions
ν	Eddy-viscosity mixing parameters
s_0	Start of the near wake

Statistical notes

Φ	Standard Normal cumulative distribution function
ϵ_I	Internal model discrepancy
ϵ_E	External model discrepancy
e	Measurement error
σ_I	The internal model discrepancy standard deviation
σ_E	External model discrepancy standard deviation
σ_e	Measurement error standard deviation
u_C	Combined uncertainty

Not to be disclosed other than in line with the terms of the Technology Contract

2 BLOCKAGE MODEL

This section contains a discussion of the validation of the GH blockage model. A full description of the model is given in WG3 WP4 D1 and both model verification and validation of the model are discussed in WG3 WP4 D18. The critical aspects to recall are that the blockage model aims to estimate the change in operating rotor performance (i.e. C_t and C_p) due to the presence of bounding surfaces. The blockage model can also be used to predict the flow acceleration around the outside of the rotor streamtube.

The findings from the interim D18 report indicated that the GH (potential flow) model under-predicted the impact of blockage when compared to an analytical model and that this different increased with the level of blockage (as shown in Figure 2-1 below). However, the level of local blockage that might be expected at a tidal array is generally considered to be lower that 20% due to pratical spacing constraints. At this upper bound of 20% blockage the error in the model is 20%.

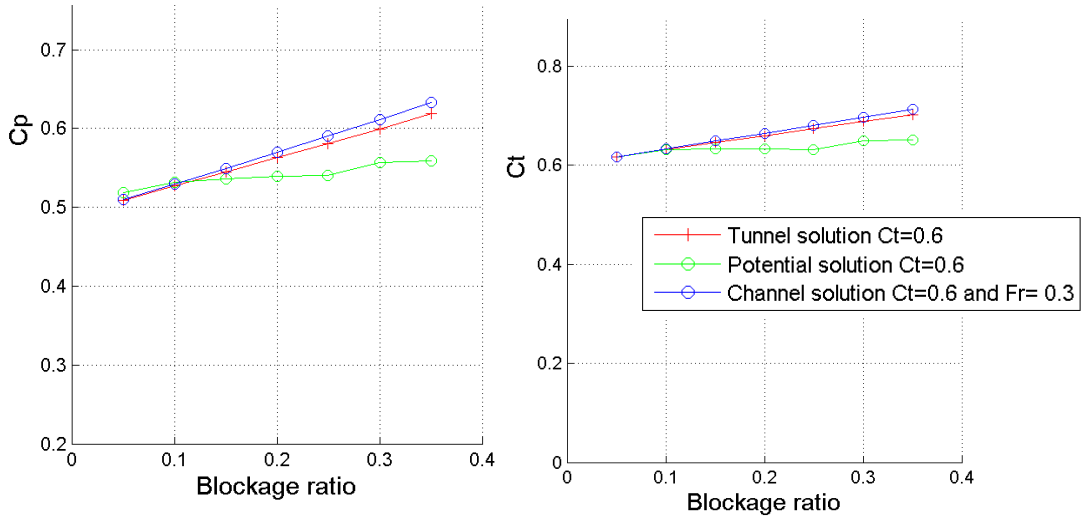

Figure 2-1: Analytical model comparison (Cp vs Blockage ratio)

The analytical models (channel and tunnel) reduce the complexity of the real life situation and although various other studies have looked to validate these models, there remains some uncertainty around the limits to the analytical model (for example when there is high blockage >10% the flow acceleration around the outside of the rotor may interact with the wake development downstream casuing additional changes in to the rotor performance).

Within PerAWaT there have been various studies to explore the sensitivity of rotor performance to bounding effects, however, a common challenge is the accurate and repeatable measurement of Cp&Ct. As outlined in D18, understanding the effect of high blockage, upon a rotor of sufficient scale for power measurement, was complicated due to the uncertainty around the EDF rotor geometry.

Not to be disclosed other than in line with the terms of the Technology Contract

2.1 Further work beyond D18

To address the uncertainty around the EDF rotor design and testing, a sensitivity analysis was undertaken. The figure below illustrates the prediction of rotor Ct (using standard methods which have been shown to be valid at full scale) varys with differing set-up changes. As discussed in D18, the built rotor had a differing geometry to the designed rotor which has resulted in a very different Ct characteristic. The "as built" geometry was used to give a new prediction of rotor performance (yellow line in the figure below), but this prediction disagrees with the measured data. After correcting the measured data for tunnel blockage and inflow shear the comparison of measured data and prediction is poor (comparing mauve and yellow lines). When assuming only a 2deg blade pitch angle error, the magnitudes are better aligned. Assuming a 10% error in RPM measurement (brown line) pushes the measurements to align with the prediction for the low and near peak parts of the curve. The higher TSR predictions still show large discrepancies and it is thought that this is due to interactions between the expanding streamtube wake and the by-pass flow. The point to note is that without testing the same rotor into a much large flume it is difficult to conclude whether simply applying an analytical correction to the boundless prediction is sufficient (as suggested by the other literature).

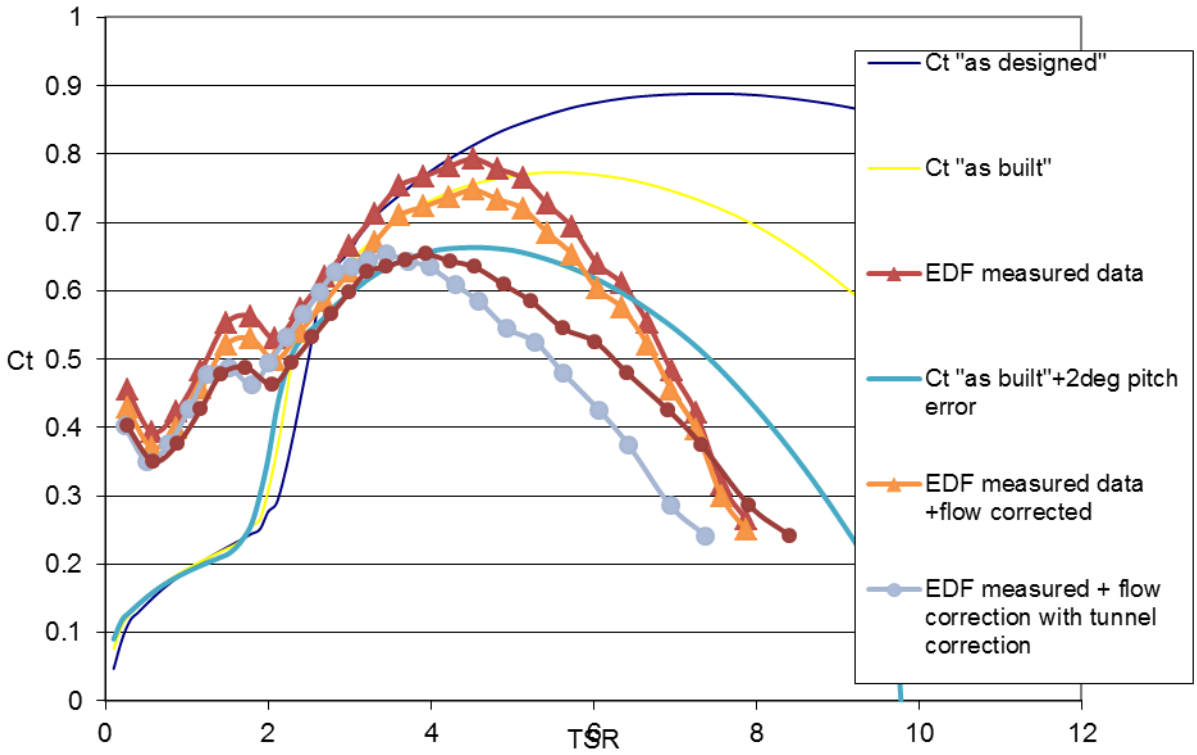

Figure 2-2: Comparison of measured and prediction rotor Ct for the EDF rotor

The table below was constructed after D18 and presents a comparison of results from a number of 1/70th scale rotor experiments where the lateral and vertical placement or bounding surface is altered. As would be expected, the thrust on the rotor increases with reduced depth and this is shown via comparion of the first three rows of data. However, note that the changes in Ct are very small and well within the bounds of experimental error. To provide some indication of the repeatability of the tests, and hence the uncertainty around this comparison, experiments 9, 9.1 and 13 are compared (see

Not to be disclosed other than in line with the terms of the Technology Contract

rows 5-13). Experiment 9, 9.1 and 13 are repeats of the same test and it can be seen that the measurements fluctuate and a standard error of 5% is evaluated.

The remaining data sets (row 14 onwards) show how the Ct measurements increase with reduced lateral spacing. However, the changes are small when compared to the error. For this reason it is hard to justify the use of this data set for the validation of the blockage model.

Table 2-1: Blockage dataset

Test	No. of rotors	Rotor lateral position [Dia.	Lateral gap [Dia]	Lateral Blockage [%]	Vertical Blockage [%]	Area Blockage [%]	Ct for normalisation	local Ct (corrected)	Ct/Ctb
EDF_UoM_2-1	1	0	0	18	34	5	0.83	0.83	1.00
UoM_05	1	0	0	5	54	2	0.86	0.88	1.02
UoM_05	1	0	0	5	59	2	0.83	0.86	1.04
UoM_09	3	-1.50	3	16	59	7	0.93	0.89	0.95
UoM_09	3	0.00	3	16	59	7	0.93	0.93	1.00
UoM_09	3	1.50	3	16	59	7	0.93	0.88	0.95
UoM_09,1	3	-1.50	3	16	59	7	0.87	0.85	0.97
UoM_09,1	3	0.00	3	16	59	7	0.87	0.87	1.00
UoM_09,1	3	1.50	3	16	59	7	0.87	0.82	0.94
UoM_13	3	-1.50	3	16	59	7	0.87	0.85	0.98
UoM_13	3	0.00	3	16	59	7	0.87	0.87	1.00
UoM_13	3	1.50	3	16	59	7	0.87	0.83	0.95
UoM_08	2	mean of 2	3	11	59	5	0.86	0.86	1.00
UoM_07	2	mean of 2	2	11	59	5	0.86	0.89	1.03
UoM_06	2	mean of 2	1.5	11	59	5	0.86	0.87	1.01
UoM_11	3	central rotor	3	16	59	7	0.76	0.76	1.00
UoM_10	3	central rotor	2	16	59	7	0.76	0.87	1.14
UoM_09,1	3	central rotor	1.5	16	59	7	0.76	0.87	1.15
UoM_11	3	mean of outer 2	3	16	59	7	0.86	0.86	1.00
UoM_10	3	mean of outer 2	2	16	59	7	0.86	0.85	0.98
UoM_09,1	3	mean of outer 2	1.5	16	59	7	0.86	0.88	1.02
UoM_18	5	-3.00	1.5	27	59	12	0.84	0.86	1.03
UoM_18	5	-1.50	1.5	27	59	12	0.84	0.85	1.01
UoM_18	5	0.00	1.5	27	59	12	0.84	0.80	0.95
UoM_18	5	1.50	1.5	27	59	12	0.84	0.88	1.05
UoM_18	5	3.00	1.5	27	59	12	0.84	0.81	0.96
UoM_05	1		0	5	59	2	0.86	0.86	1.00

Not to be disclosed other than in line with the terms of the Technology Contract

UoM_06	2	mean	1.5	11	59	5	0.86	0.87	1.01
UoM_09,1	3	central rotor	1.5	16	59	7	0.86	0.87	1.01
UoM_18	5	0.00	1.5	27	59	12	0.86	0.84	0.98

The GH potential model **(as used in TidalFarmer) has been used to predict the change in power and thrust for a full scale turbine and the comparison with the measured data was favourable. However, this data cannot be disclosed and hence it is recommended that various aspects of the ReDAPT project be used to further publically demonstrate the performance of the blockage model.**

Not to be disclosed other than in line with the terms of the Technology Contract

3 NEAR WAKE MODEL

This section involves the description of the validation methodology for the GH near wake model and the comparison with experimental and numerical data that has been generated through the PerAWaT project. The models that have been developed were discussed in WG3 WP4 D2 (Thomson *et al*, 2010a) and the reader is referred to this report for the modelling details.

The near wake is a region of complex flow characteristics and has been discussed in some detail by Vermeer *et al* (2003). The fluid velocity immediately downstream of the rotor retards causing the bounding streamtube to expand while vortices are shed from the blade tips. Given the relative complexity of the near wake, modelling the flow is not considered an option. Instead, the preferred strategy is to formulate some relationship between the known environmental, geometric and operating conditions of the rotor with the velocity deficit and wake width generated through energy production. This information can then be fed into the far wake model (Ainslie, 1988).

As a consequence, the primary questions concerning the near wake are: how does one link the performance of the device with the velocity deficit and where does the near wake end? In answer to the latter, the near wake ends when the flow becomes self-preserving. A flow is said to be self-preserving (Tennekes & Lumley, 1972) if the flow is in a state of equilibrium where the inertia (convection of fluid) is dissipated through the shear stress (turbulent diffusion). In this situation, the free-shear flow equations describe the motion and the wake profile is similar to a Gaussian curve.

The end of the near wake position will be informed through analysis of the centreline velocity deficit. From this starting point, a Gaussian profile will be fitted to the data at the near wake location. In combination with environmental conditions, the geometry of the experiment and the rotor performance, the semi-empirical model can then be validated for tidal stream energy extraction.

3.1 The end of the near wake

Through the PerAWaT project several data sets have been made available of the wake recovery downstream of a horizontal axis turbine. The reciprocal of the centreline recoveries ($1/u_{wake}$) from the different experiments and numerical studies are provided in figure 3-1. There are some discrepancies across the data sets which is of some concern. An external data set has been documented in Myers et al, (2007) and has also been included and shows good agreement with some of the tests performed within PerAWaT.

To gain some insight into how the data sets differ we refer to textbook analytical tools. For instance, in Pope (2000), a description of how the centreline fluid velocity of a turbulent jet scales by $u \sim 1/x^p$, where x is the downstream distance and p is some fraction. In the case of an axisymmetric jet $p = 1$, or in a plane wake then $p = ½$. In figure 3-1, the reciprocal of the downstream distance against the centreline wake flow has been plotted ($x,u_0/u_{wake}$). As discussed in Pope (2000), WG3 WP4 D2 and WG3 WP4 D5 there are two regions of primary interest, the near wake and the far wake. In the far wake the flow will scale as $u \sim 1/x^p$. Therefore, in figure 3-1 three lines have been added to each data set. From the lines of best fit, three distinct regions are observed. From left to right these are; the near wake, axisymmetric wake, and shallow water or plane wake. The axisymmetric wake and shallow water wake both form part of the far wake region and can be differentiated by the flow dynamics. While the asixymmetric wake is bounded on all sides by fast moving fluid, the plane wake is bounded from above and below and can only expand into faster moving fluid laterally.

Not to be disclosed other than in line with the terms of the Technology Contract

The points at which the relationships change (different lines of best fit) mark the transition regions between the flow dynamics. The point at which the near wake ends and the far wake begins is the first transition region. In the literature (Vermeer *et al*, 2003) the near wake is said to end around 1-5D downstream of the rotor plane. Here we observe that the end of the near region occurs at around 2-2.5D for all data sets except WG4 WP1 and WG3 WP1. This helps justify the choice of 2.5D as both the start of the far wake (start of the axisymmetric wake) and also the point at which a Gaussian curve best approximates the data. Here the flow is self-preserving and therefore satisfies the criterion of the near wake.

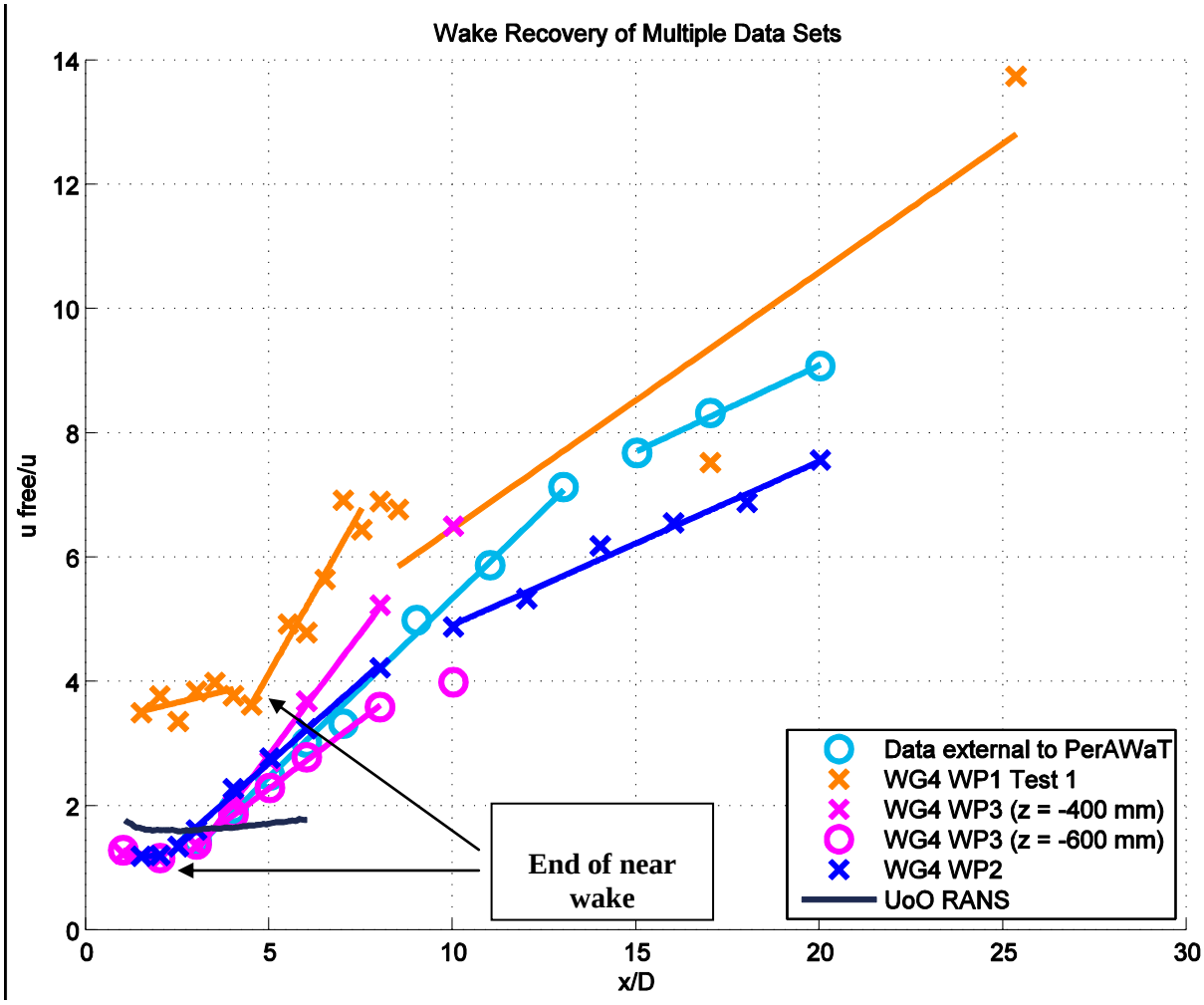

Figure 3-1: Plot of the inverse centreline wake recovery of multiple datasets including trend lines for different phases of the recovery.

Care must be taken when comparing the different data sets. The tests have been performed at different Reynolds number and blockage ratios. Pope, (2000) suggests the spreading and recovery rate of jets is Reynolds number independent. In addition, the geometry of the scaled rotors had to be modified such that they produced similar performance to the full-scale Tidal Generation Limited (TGL) device geometry. Some of the results reflect the geometry of the flume, for instance, the WG4 WP3 quasi-unbounded tests where the rotor was placed at z = -400 shows a very fast recovery. Unlike in other

Not to be disclosed other than in line with the terms of the Technology Contract

experiments where the flume floor and free-surface suppress large scale eddies, in this test the flow is re-energised more rapidly. In the external data set example the axisymmetric wake continues for a greater distance and this could be due to a lower cross sectional blockage.

In some scenarios the near wake region ends later, for instance WG4 WP1. In addition, some studies show that the near wake, and far wake, develop at a much slower rate. These will be discussed in more detail later in this section (see Section 3-3).

3.2 Brief description of model

In Tennekes & Lumley (1972), if the wake flow in the lee of an obstacle, is self-preserving, then the form of the velocity deficit can be taken to be Gaussian (Tennekes, 1972) as given below,

$$f(u_{def,}\ \mu_y\ ,\ \sigma_y\ ,\ \mu_z\ ,\ \sigma_y\ ) = u_{def}\ \exp(\ -\ y^2/2\sigma_y^{\ 2}\ -\ z^2/2\sigma_z^{\ 2}) \qquad [3\text{-}1]$$

It is expected that the near wake profile is dependent on physical quantities such as the turbulence intensity, type of rotor (i.e. ducted and unducted), blockage effects and the operating point, Cp, Ct. In WG3 WP4 D2, it was described how the quantities for the wake width σ_y, σ_y and u_{def} were obtained using semi-empirical formulae

$$u_{def} = C_t - 0.05 - (16C_t - 0.5)TI/1000, \quad \text{and} \qquad [3\text{-}2]$$

$$\sigma_y = \sigma_y = \sqrt{(\ C_t/8/(\ 2\ u_{def}\ (\ 1\ -\ 0.5\ u_{def}\ )\ )\ ).} \qquad [3\text{-}3]$$

In order to validate the GH near wake model, a comparison betwee the Gaussian profile approximation and experimental or numerical data needs to be carried out. To do this, the end of the near wake position is defined by studying the experimental results. This fixes the distance downstream at which to fit the Gaussian profile. Then, a Gaussian curve is fitted to the data and this allows the wake width and velocity deficit to be determined from the data. Once the width and centreline velocity deficit have been calculated, the near wake model can be evaluated in order to compare against an observed deficit and then a discussion of model validity can follow.

The centreline readings from experiments could also be used to predict the velocity deficit for the near wake model. However, the lateral and vertical traverses are required in order to estimate the wake width. In addition, the axial flow velocity will be normalised against axial inflow such that the normalised profile represents purely the velocity deficit due to the operation of the rotor.

The main assumptions of the near wake model are as follows:

- Gaussian – The end of near wake flow is taken to be Gaussian (Tennekes & Lumley, 1972) and this is based upon the assumptions that the flow is unbounded, self-preserving, incompressible and turbulent.
- No boundary layer – Linked to the assumption that the flow is unbounded, and therefore axisymmetric, the data is normalised against inflow velocity. This allows us to directly compare a shear-free wake profile with the Gaussian curve.

Not to be disclosed other than in line with the terms of the Technology Contract

Table 3-1: Dataset parameter and blockage summary

Dataset	Lateral Blockage	Vertical Blockage	Ct range	TI_{amb} range
WG3 WP1 (full scale CFD)	25 / 67%	50%	0.8 – 1.0	0.5 – 6%
WG4 WP1 (1/30th device scale)	40%	60 / 75%	0.65 – 0.95	5 – 15%
WG4 WP2 (1/70th array scale)	5 – 30%	60%	0.45 – 0.9	8-10 %
WG4 WP3 (1/70th device scale: unbounded)	18%	34%	0.8 – 0.9	5-8%

3.3 Comparison to data sets

In the following sections, the Gaussian near wake profile is fitted against the various data sets in order to assess the model limitations. In addition, an in-depth discussion of the different data sets is made.

3.3.1 WG3 WP1 UoO CFD Simulations

The WG3 WP1 CFD simulations were designed to investigate the near wake region and therefore simulations end at a distance of 6D downstream. In comparison to the experimental results we observe a turning point close to 2 D and then a steady recovery. However, trends are not obvious from this data set.

Reynolds-Averaged Navier-Stokes (RANS) equations assume that a flow can be decomposed into a fluctuating component and mean flow term. The equations can then be time averaged and suitable assumptions made to model turbulence phenomena. The main drawback of the RANS approach is an inability to capture the interaction of multiple length and velocity scales that are usually present in more complex problems such as fluid flow through a tidal stream turbine. This means that the wake flow is not well described due to a failure to predict the correct shear gradients. While the wake flow isn't captured well, the model can be used to accurately describe the steady loadings and mean power output of a device. More complicated techniques such as Large Eddy Simulations (LES) may well be able to better resolve the multiple length scale issue.

A literature review of other RANS studies (McNaughton, *et al*, 2012) reveals that the choice of turbulence model has a strong effect on the rate of recovery in the wake. In particular an isotropic k-ω model results in a persistent wake, as can be seen in the results shown below in figure 3-1. For a similar tip speed ratio (3.5) as the EDF and UoM experimental results, as discussed in Sections 3.3.2 and 3.3.3, the shear layer for the WG3 WP1 base case does not reach the centreline until around $x \geq 5D$. It is also clear from examination of the centreline axial flow speed, in figure 3-1, that the recovery in the region $x < 5D$ does not follow the same trends as observed in the experimental data.

The shape of the near wake profile could also be linked to the slow recovery rate. As depicted in figure 3-2 at 1D downstream the shape of the wake should be similar to a top hat profile (WG3 WP4 D2, Thomson, *et al*, 2010b), in this case it is more Guassian in shape with a central dip. This means that the shear gradients along the mixing layer are not as sharp and therefore will not transfer momentum as quickly and the transformation to a Gaussian profile will take longer.

In particular, the turbulent mixing in the near wake takes longer to develop. The expected top hat profile is not observed and the formation of two clear mixing layers is not present. It is observed in McNaughton, *et al,* (2012) that the wake formation and recovery is sensitive to the selection of turbulence model and in particular the isotropic assumption. The flow is strongly anisotropic, whereas

Not to be disclosed other than in line with the terms of the Technology Contract

the model adopted in WG3 WP1 is isotropic, hence it is expected that the simulations would under predict the mixing as compared to both experimental and field measurements.

The profile that was found to best approximate the Gaussian curve is shown in figure 3-2 to be at 5D downstream. Therefore, the wake width and centreline velocity deficit was taken at this point and included in the near wake analysis. This was done for several of the tests that were undertaken as part of the (WG3 WP1 D4) studies. These studies included varying the shear layer, the nacelle height in the flume, the width of the flume, the yaw strategy. Simulations were undertaken with a rigid lid assumption.

From this comparison we can see that a Gaussian profile is a reasonable approximation to the data, if the end of the near wake position is correctly defined. In addition, we can also predict the wake width and the normalised velocity deficit from the data. In this case the normalised velocity deficit is a combination of the bypass velocity and calculated wake flow term.

For both the blade resolved and embedded BEM CFD model, simulations have been performed with the rotor speed and pitch angle held constant.

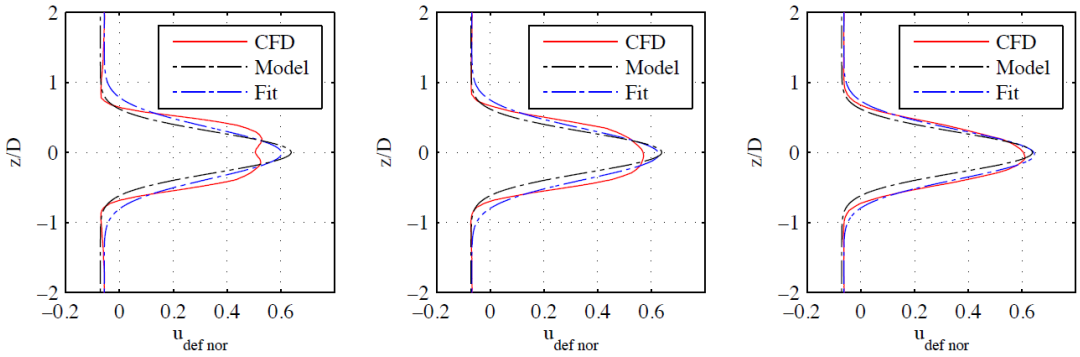

Figure 3-2: Gaussian fitting to WG3 WP1 (CFD), Test A, blade resolved simulations at tip-speed-ratio of 4.5. Left-right: at 1D, 2D, and 5D. The Model results use a blockage correction method to fit to the CFD results, while the Fit refers to a curve fitting using a Gaussian function (see WG3 WP1 D4 for more details).

3.3.2 WG4 WP1 EDF flume experiments

From figure 3-1, it is shown that the centreline recovery of the WG4 WP1 experiments observed is different from all other studies. Two reasons are attributed to these discrepancies; first, although the rotor was designed to have a similar Cp/Ct ratio as the generic full scale PerAWaT rotor, the built rotor differed and performed more like an over-speed type turbine (see section 2). Secondly the blockage ratio of the flume is high at 75%. The impact of high blockage acts to increase the thrust on the rotor, but also accelerate the bypass flow. Hence it could be expected that the near wake would differ to that of an unbounded rotor, resulting in a persistant wake deficit until around 4-5D downstream.

Results from tests performed with a flume depth of 0.8 m, are provided in figures 3-3, 3-4. From these figures, negative normalised velocities are observed and this is caused by high lateral blockage

Not to be disclosed other than in line with the terms of the Technology Contract

causing flow acceleration around the rotor plane. This makes the flow dynamics very complicated as was discovered in Buvat (2010b).

The GH models that have been developed to describe wake flow assume that there are no bounding side walls and that drag is created only from devices in an unbounded domain. From the Gaussian comparisons to the WG4 WP1 data in figure 3-3 and 3-4, the limitations in the application of the near wake model to highly blocked cases are clear. Across the rotor swept area (-0.5D < y < +0.5D) the Gaussian curve provides an acceptable approximation to the data, however, none of the flow acceleration in the bypass region is captured [Whelan 2009, Gretton 2012].

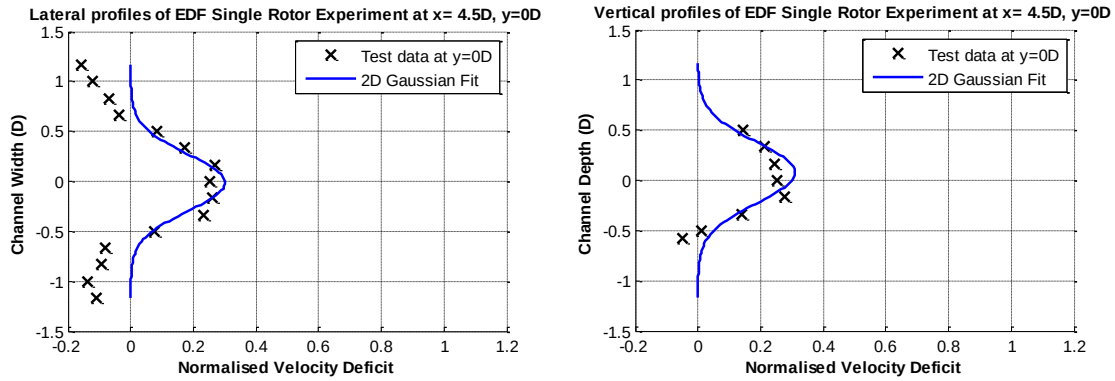

Figure 3-3: Gaussian fitting to measured data in WG4 WP1 (1/30th scale, U_o = 0.27 m/s, TI_{amb} = 5%) at x=4.5D.

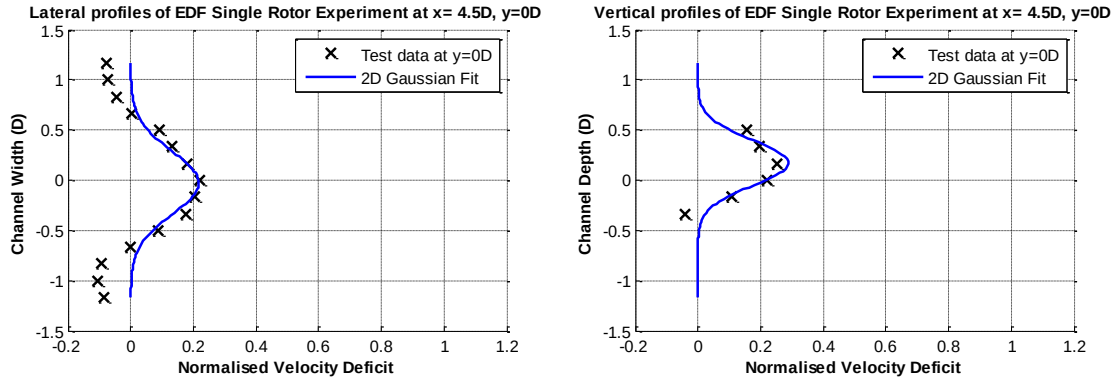

Figure 3-4: Gaussian fitting to measured data in WG4 WP1 (1/30th scale, U_o = 0.27 m/s ,TI_{amb} = 15%) at x=4.5D.

3.3.3 WG4 WP2 UoM flume experiments

Detailed readings of the near wake were taken in the WG4 WP2 array scale experiments (see WG4 WP2 D5) at a downstream distance of 2D and 4D of the rotor plane. Gaussian profiles were fitted across all the data sets, results of some of these are presented in figures 3-5, 3-6 and 3-7. Note that, given the close lateral spacing of some of the devices (such as 1.5 D centre to centre) the data had to be curtailed so that the Gaussian profile was not fitted to data generated from another wake. Figures 3-5, 3-6, 3-7 clearly show that even when closely spaced the rotors generate a distinct axisymmetric Gaussian near wake.

Not to be disclosed other than in line with the terms of the Technology Contract

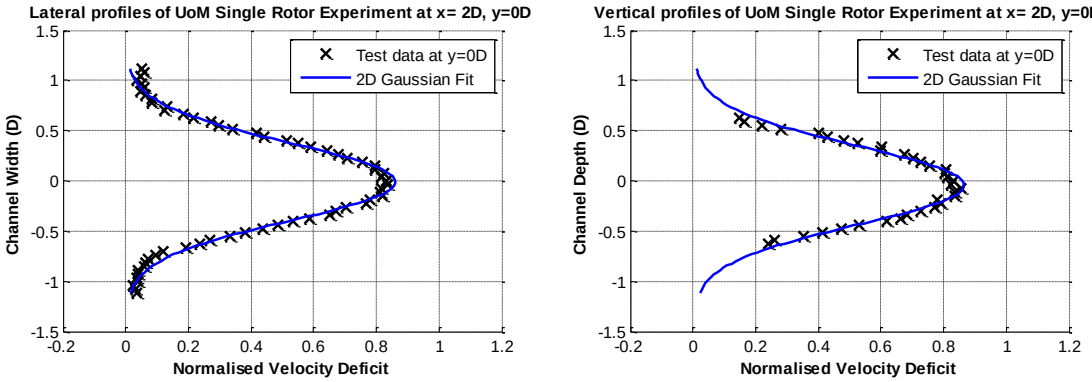

Figure 3-5: Gaussian fitting to WG4 WP2 single rotor (1/70th scale, U_o = 0.47 m/s, TI_{amb} = 5%) at x=2D

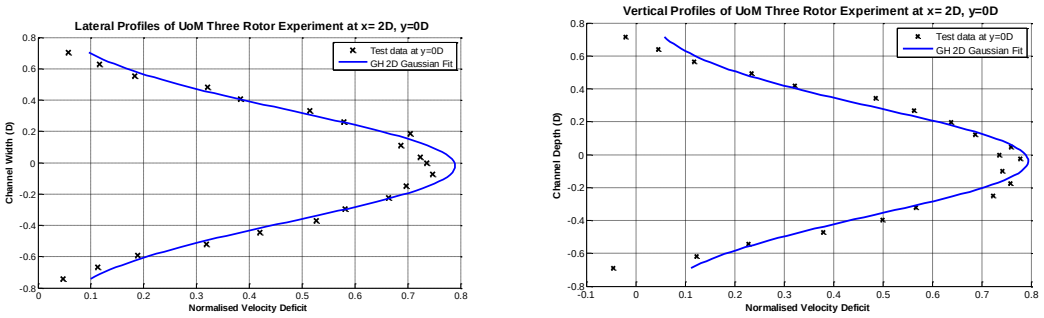

Figure 3-6: Gaussian fitting to the rotor at y=0D in wave experiment WG4 WP2 ,(1/70th scale, U_o = 0.27 m/s, TI_{amb} = 5%) three rotors side by side at x=2D.

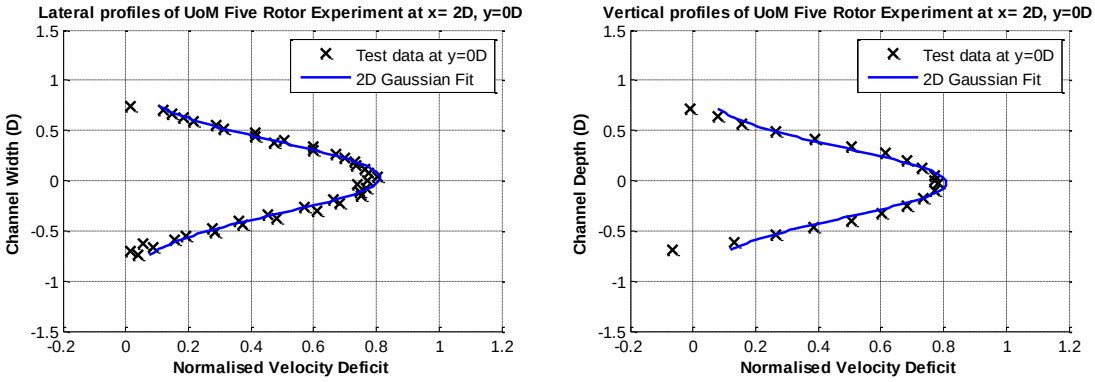

Figure 3-7: Gaussian fitting to the rotor at y=0D in five rotor experiment, WG4 WP2 (1/70th scale, U_o = 0.27 m/s, TI_{amb} = 5%) at x=2D.

In the vertical, there is some asymmetry in the profile which is caused by the boundary layer, however, although, the vertical blockage for this set of experiments is high (>50 %) the normalised results still show an axisymmetric wake. Figure 3-8 shows that surface waves have little effect on the near wake shape (same magnitude of deficit and wake width to other experiments). The general effects of waves, as discussed in further work performed at the Manchester university testing facilities by Olczak et al,

Not to be disclosed other than in line with the terms of the Technology Contract

(2013) is that more energetic waves increase the rate of wake recovery downstream. In particular, Deep water waves, where kd > π, (where k = 2π/λ = the wave number) causes the most rapid flow recovery.

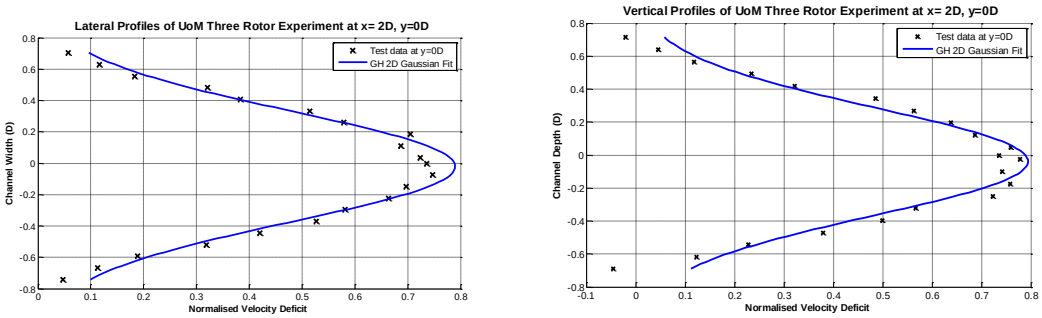

Figure 3-8: Gaussian fitting to the rotor at y=0D in wave experiment WG4 WP2 ,(1/70th scale, U_o = 0.27 m/s, TI_{amb} = 5%) three rotors side by side at x=2D.

Once parameters are determined for the wake width σ_y, σ_z and maximum velocity deficit u_{def}, as well as the centreline μ_y, μ_z a comparison between the Gaussian model fit, using eq. 1, and the measured observations from the experiments can be made. The root mean square error (RMSE) has been calculated using eq. 1-1. This analysis shows that the end of near wake profile shows good agreement with the theoretical Gaussian curve. The results of the error between model and measured are given in Table 3-2, where it is clear that the theory fits well with observations.

Table 3-2: Average RMSE for Gaussian fitting to WG4 WP2 data.

Average Error (RMSE), %			
Row 1	Row 1	Row 2	Row 2
2.7	3.6	2.9	3.7

3.3.4 WG4 WP3 UoM rotor in the EDF flume (unbounded experiments)

This series of tests were undertaken by placing the 1/70th scale rotor in a large flume with cross-sectional area of 1.5 m x 0.8 m (width x height), such that the blockage ratio is small and the flow is quasi-unbounded. The investigations were meant to quantify the effect of unbounded operation on the device. There were two primary investigations, one where the rotor was at mid depth (z = -0.4m) such that the flow can be assumed to be unbounded and second, where the rotor was placed near the seabed (z = -0.6m) such that the effect of high shear on the near wake assumptions could be better understood.

Following the discussion concerning figure 3-1, the end of the near wake for the WG4 WP3 tests was determined to be approximately x=2-3D. Gaussian comparisons are made at x=2D in figure 3-9, 3-10. In some cases only partial traverses of the lateral profiles were measured as detailed in the experimental specification (WG3 WP4 D1).

Not to be disclosed other than in line with the terms of the Technology Contract

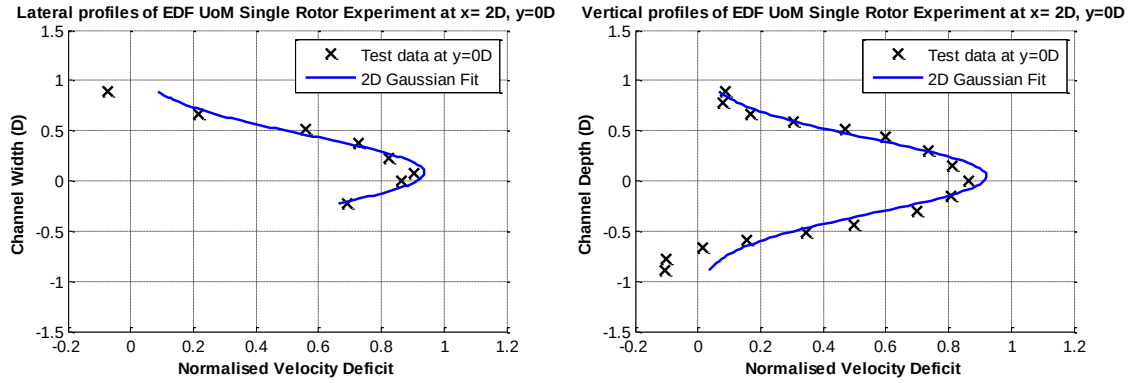

Figure 3-9: Gaussian fitting to measured data in WG4 WP3 (-0.4m depth, 1/70th scale U_o = 0.45 m/s, TI_{amb} = 5%) at x=2D.

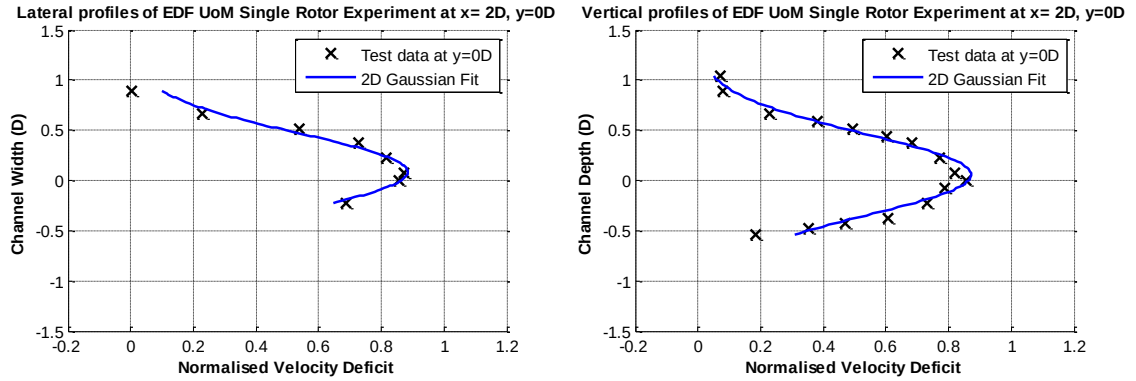

Figure 3-10: Gaussian fitting to measured data in WG4 WP3 (-0.6m depth, 1/70th scale U_o = 0.45 m/s, TI_{amb} = 5%) at x=2D.

The lower hub-height test exposes the rotor to higher turbulence intensity and places the device in a region of strong bed shear. From the above comparisons we can see the Gaussian profile approximates the data well, even in the seabed proximity test where the device was situated in close proximity to the flume bed in a region of high shear. In both tests the error between model prediction and measurements was found to be comparable to the WG4 WP2 data with a RMSE of less than 3%.

3.4 Assessment of model performance

The outputs of the GH Near Wake model are normalised velocity deficit and wake width (WG3 WP4 D2). The near wake model inputs are the recorded thrust coefficient Ct and the turbulence intensity TI for the baseflow. For each experiment, the near wake model was evaluated using the respective (Ct ,TI) values. A scatter plot of the near wake model prediction of u_{def} against estimated values for u_{def} using experimental readings, across the different studies presented in Sections 3.2.1 – 3.2.4, is presented in figure 3-11. Likewise a graph of predicted σ_y, σ_z against wake width estimated from experimental data is presented in figure 3-12.

For the WG4 WP1 experiments all 4 tests are presented where the device was operating at peak performance at around TSR = 4.5. For the WG4 WP2 data, only the first row Gaussian fits are provided. In addition, these plots show the centreline velocity deficit at 2.5 D as this is where it was

Not to be disclosed other than in line with the terms of the Technology Contract

chosen to start the far wake model and therefore gives the best comparison. Finally, for the WG4 WP3 data it was chosen to make a comparison at 3D for the centreline velocity deficit, as at 2D the near wake is still developing. Likewise, the external data set was compared at 3D for the same reason.

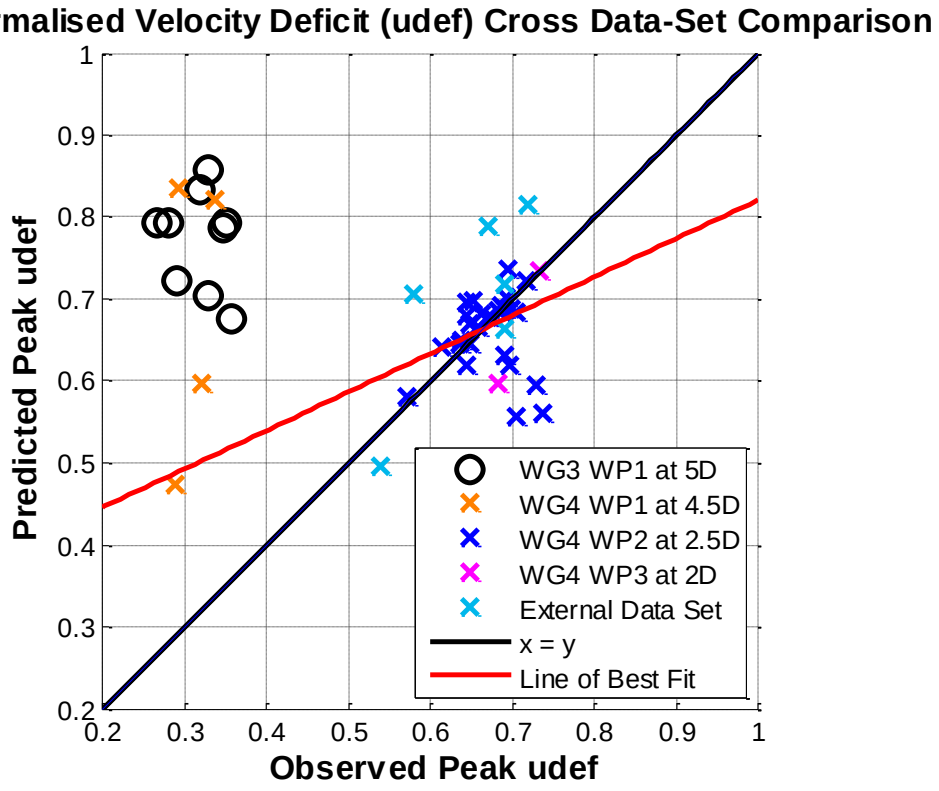

Figure 3-11: Validation of the GH Near Wake Model's prediction of normalised velocity deficit across applicable PerAWaT datasets.

From this comparison across the various datasets, it is observed that there are two clusters of data. The 1/70th array scale tests (WG4 WP2) show that the model can give a good approximation of the velocity deficit at the end of the near wake. This trend is also reflected in other data sets such as the external data sets and also the WG4 WP3 experiments. In contrast, the RANS results and WG4 WP1 experimental data suggests a different pattern in the near wake region.

If agreement of the model with measured data was good then the best fit curve would ideally coincide with x=y as denoted by the black line in figure 3-11. However, a different underlying trend is suggested by the model. The Pearson correlation coefficient yields a value of around 0.327 for the WG4 WP2 data. Ignoring the highly blocked cases, as discussed earlier, the majority of data from the external data set 1/20th device scale and 1/70th lie close together. In addition, the mean absolute error between model prediction u_{def} and model observed x_i (for N measurements) was analysed using eq. 1-1 and found to be 4.3 %, the sample standard deviation was observed to be 5.8 %. Therefore, the suggestion is that, while the correct trend observed in the experiments is not captured by the model (resulting in a best fit line which does not lie on top of the x=y line), overall the model does manage to predict a deficit 'close' to the observed value.

Not to be disclosed other than in line with the terms of the Technology Contract

Likewise the predicted wake width has been plotted against the observed value in figure 3-12, for all tests, except the external data set. One remark is that, while the RANS numerical modelling (WG3 WP1) may not produce the correct velocity deficit, the wake width is reasonably well predicted. In addition, all other tests, apart from the WG4 WP1 experiments result in reasonable agreement with the model. It is also clear, that one would not expect values of the wake width much less than 0.8 as the wake width is approximately of order one, i.e. one rotor diameter. A Pearsons' correlation coefficient of model vs. observed yields a value of -0.509 suggesting that, once again, there is a different trend to the data that the model has not captured. However, examining the mean absolute error we obtain a value of 6.24 % showing that while the incorrect trend is captured a reasonable prediction can still be obtained. There are some cases where the wake width is observed to be much greater than is observed in the experiments. This may be linked to the effect of tip speed ratio on the bounding stream tube. If the tip speed ratio is high this may cause an increased rate of recovery and therefore a faster wake expansion may be observed.

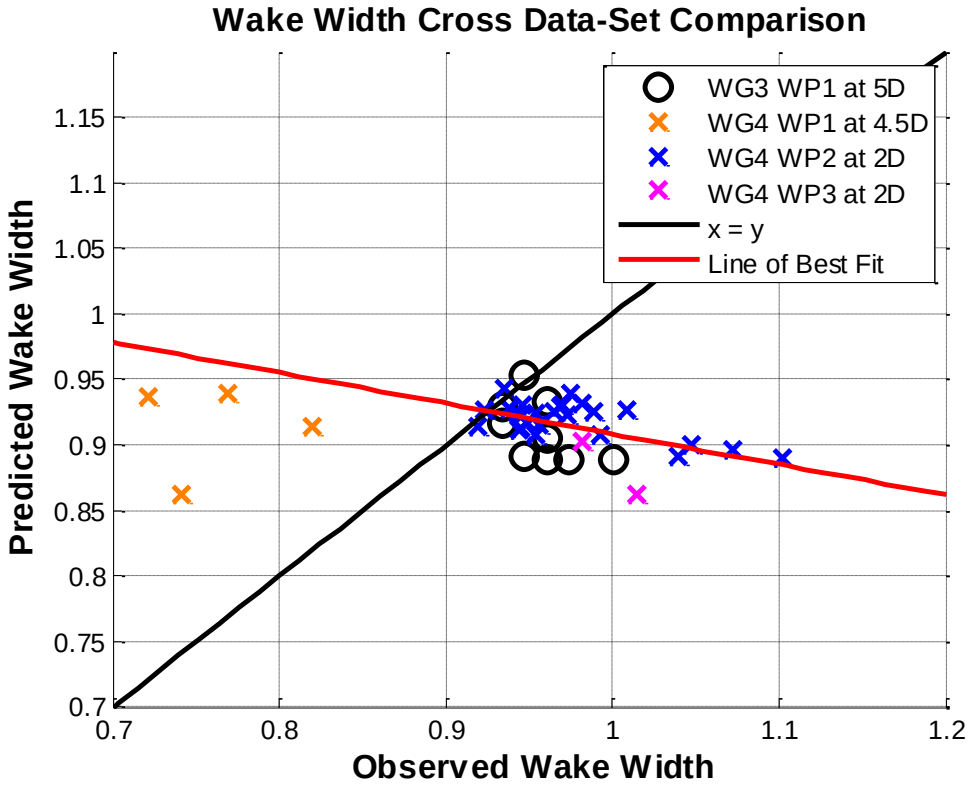

Figure 3-22: Validation of the GH Near Wake Model's prediction of wake width across applicable PerAWaT datasets.

A mean absolute error of 6.24 % is greater than measurement error and given that the near wake model is used to inform the far wake model, the impact of this modelling imprecision/discrepancy needs to be quantified when the aggregated model uncertainty is considered. However, from Ainslie (1988), the initial velocity deficit and wake width provide the initial conditions for the far wake models described in section 5. It was commented that the model is insensitive to the exact form of the initial flow profile and in addition, as the equations are solved the uncertainty around the initial condition will diminish as the flow recovers to the free-stream. Therefore, although the prediction may

Not to be disclosed other than in line with the terms of the Technology Contract

not be very accurate, it may still be sufficient to resolve the wake effects. This is discussed in section 6 in more detail later.

The results from both WG4 WP2 and WG4 WP3 show reasonable agreement with the near wake model. This is encouraging as rotors are operating in different flumes and for different turbulent ambient conditions. The WG3 WP1 and WG4 WP1 data have been discussed and these results are deemed inaccurate for a number of reasons (see Sections 3.2.1 and 3.2.2.). In the case of the numerical RANS simulations it has been shown that the wake does not develop at the same rate as observed experimentally. Further work through the ReDAPT (Reliable Data Acquisition Platform) project could be used to help quantify the level of inaccuracy. Finally, the WG4 WP1 data is not an accurate representation of the TGL device in unbounded flow conditions as the rotor was not built as designed and is operating in a highly blocked flume. The rotor exhibits strange performance that could be explained by the high blockage and therefore it is inappropriate to use this data to validate the near wake model.

3.5 Model limitations and uncertainties

A discussion of the validity of the model assumptions is provided below:

- Gaussian profile – the assumption that the Gaussian profile (Tennekes & Lumley, 1972) is a suitable approximation to the data, where the GH near wake model can determine the wake width and normalised velocity deficit is derived under the assumption that the flow is unbounded, turbulent, incompressible and self-preserving. In situations where the flow was not significantly blocked (note that, as observed in the WG4 WP1 expeirments, while vertical blockage can be high, lateral blockage cannot) the model gave good agreement. The experiments were performed at a sufficiently high channel Reynolds number such that the flow was sufficiently turbulent. In addition, the point at which the flow became self-preserving was understood by plotting the inverse axial flow velocity, whereby regions of the near wake and far wake could be identified and then used to inform Gaussian fitting.

- Boundary layer – The WG4 WP3 testing, where the location of the device was varied in order to understand the impact on the wake, has shown that the near wake can still be well approximated by the Gaussian profile. Therefore, the seabed boundary proximity does not seem to be an issue. Observations from the WG4 WP1 experiments show that the dominant effect would be the presence of bounding sidewalls as noted in the Gaussian profile assumption.

When assessing the near wake model uncertainty due to measurement error we can perturb the model inputs by a percentage amount and evaluate the error that would occur due to this uncertainty. The measurement uncertainty from WG4 WP2 data has been analysed and shown to be ±5% for thrust coefficient and ±2-5% for the flow speeds. Upon examination of the near wake model (eq. 3-2) and using standard methods for assessing combined uncertainties (JCGM, 2008) if the thrust coefficient and turbulence intensity standard uncertainties are p and q respectively then linearisation of (eq. 3-1) yields

$$u_C^2 = (\partial u_{def}/\partial C_t)^2 p^2 + (\partial u_{def}/\partial TI)(\partial u_{def}/\partial C_t) pq + (\partial u_{def}/\partial TI)^2 q^2$$

$$= (1- 16TI/1000)^2 p^2 + (1- 16TI/1000)(16 C_t/1000 – 0.5)pq + (16 C_t/1000 – 0.5)^2 q^2$$

Not to be disclosed other than in line with the terms of the Technology Contract

The leading order error term is related to perturbation of the thrust coefficient p, and q carries a small variation. In fact, it is not the uncertainty surrounding the value of the turbulence intensity itself that gives a greater contribution to the uncertainty of the model predictions. Supposing that the error in estimating thrust coefficient is 5% and for the turbulence intensity it is 3 % then in the near wake model we see that the model uncertainty due is 4.2 %. Any further lack of fit to model data is then due to a combination of measurement error or the simple fact that the model is not sufficient for the task at hand.

A similar analysis for the wake width (eq. 3-3) can be performed where it is found that the model uncertainty is 3.9 %. Here it is seen that, when compared measured data the RMS error is found to be 6.24% and so the model may be missing some physics. Several explanations can be offered for the model discrepancy. The exact point of the near wake end has been shown to lie at the 2.5D position. However, there only exists readings at 2D and 3D and therefore a complete comparison is difficult to make. In addition, when the flow is relatively unbounded the wake width is observed to expand quicker and this is reflected in the results for the unbounded test cases in WG4 WP3 and the single rotor test of WG4 WP2.

3.6 Summary

The validation methodology was discussed in Section 3.2 where a Gaussian curve was fitted to measured and simulated data sets made available through the PerAWaT project in order to calculate the normalised centreline velocity deficit and wake width.

The model performance was assessed whereby the near wake model predictions were compared to the observed velocity deficit and wake width. This analysis of the various data sets took into account the ambient conditions such as the turbulence intensity, the thrust coefficient, and tip speed ratio. The comparison shows that the models can generally predict the correct values but the results do suggest that the trends were not always captured correctly.

The effect of shear, waves and seabed generated turbulence intensities has been investigated in both the WG4 WP2 and WG4 WP3 data sets. It was found that shear had little impact on the near wake form. In the case of the array-scale tests further studies have shown that energetic deep water waves cause the wake to recover more quickly. The differences observed in the wave experiments carried out within PerAWaT suggested that waves had little effect on the flow recovery or the validity of the near wake model. However, other studies could be used in future work in order to gain a more detailed insight (Olczak *et al*, 2013).

Where uncertainty can be quantified investigations have been undertaken. The mean absolute error in predicting the normalised velocity deficit and wake width was observed to be 4.3% and 6.24 % respectively. In addition, the effect of input uncertainty has been analysed using analytic methods. In the case of the normalised velocity deficit the model uncertainty was found to match with the error observed between the model predictions and observations. Therefore, this discrepancy could be accounted for by improving uncertainty around the inputs rather than focusing on the models themselves. In particular, it was found that C_t contributed most significantly to errors concerning input uncertainty and therefore, thrust curve and far wake model accuracies, are important when determining the correct thrust coefficient on downstream devices.

Generally the near wake model has performed well in comparison to relatively unbounded flow conditions. The testing in both WG4 WP2 and WG4 WP3 appears to give an accurate representation

Not to be disclosed other than in line with the terms of the Technology Contract

of the wake of a horizontal axis turbine and the observations show that the experiments are repeatable and that these results can be used to validate numerical wake models. The biggest epistemic uncertainty that is currently faced is whether the results are representative of full scale. It is believed that with data from the ReDAPT project, better understanding will be gained on this last point.

Not to be disclosed other than in line with the terms of the Technology Contract

4 FLOW FIELD MODEL

In order to accurately predict the performance and loadings on devices in a tidal farm, the flow velocity at the device locations must be estimated. This flow velocity field is typically referred to as the resource and the primary focus of this section is understanding whether the spatial variability of the resource can be correctly represented across the tidal farm. A more detailed discussion concerning the flow field model is given in WG3 WP4 D4.

Recent research (Kutney, *et al*, 2013, Stock-Williams, *et al* ,2013) suggests that while tidal heights are deterministic and can be predicted using harmonic analysis the flow velocity can be significantly affected by aharmonic components, such as eddy shedding from local bathymetry. While a deterministic method would appear at first sight to be a better approach given the apparent predictability of the resource it has been shown that using histograms and treating the resource as stochastic can yield more accurate estimates for the long term energy yield. However, the one advantage of tidal energy that must not be lost is the ability to predict the inter-annual variation that will occurs due to the 18.6 year cycle.

The process of using histograms to represent a time varying resource is referred to as binning or the 'frequency domain'. One advantage of summarising 18.6 years of time series data into a finite number of 'bins' is computational efficiency and this is discussed in more detail in Section 6, whereby fast models can be used to quantify uncertainty in model predictions.

Assuming the resource is stochastic allows us to equate a probability of occurrence to each flow state. However, for each flow state, the fluid flow needs to be well modeled. In particular, the vertical velocity profiles that occur during these flow states needs to be applied such that accurate prediction of the fluid flux through the turbine can be calculated. Flow shear is particularly important as the device sits in a sizeable portion of the boundary layer and therefore accurate flux predictions rely on a good approximation of the flow shear. In this section an examination of the power law profile is given and when the traditional model fails to predict the vertical flow profile in tidally energetic sites, suggestions for further improvement shall be provided.

4.1 Brief description of models

The hydrograph, at a reference location denoted by **x,** can be obtained from outputs of a hydrodynamic model, given by **u**(**x**,t). The hydrograph can be constructed from the model, where the velocity components, denoted (u,v) or in polar coordinates ($|\mathbf{u}| = \sqrt{(u^2 + v^2)}$) and $\alpha = \text{atan}(u/v)$, are recorded at each time step and then presented as a scatter plot. One method of `binning' the data would be to divide the flow into two directions denoted α_i for i=1,2. Then, if a series of flow speed bins with bin centres denoted by $[u_1,u_2,\ldots,u_N]$ are constructed, the flow solution at the reference location can be partitioned into the following sets $\mathcal{B}_{i,j} = \{\mathbf{u}(\mathbf{x},t) : u_i<|\mathbf{u}|<u_{i+1}$ and $\alpha_i - \pi/2< \alpha < \alpha_i + \pi/2\}$. If the bins defined above denote the event space $\mathcal{B}_{i,j}$ of all possible flow speeds and directions that occur at the reference point over the lifetime of the project, then they fill the event space Ω of all possible outcomes such that an estimate for the energy yield can be made.

Provided the tidal cycle can be represented as a number of discrete flow states (direction sectors and flow speed bins) this enables the mean power of each device per flow state to be converted into an energy yield. Using a device scale parametric model which adequately describes the device performance for a given flow state (i.e. a dynamic power curve) the power output of the device can be calculated. An energy calculation then combines mean power at each flow state with the occurrence

Not to be disclosed other than in line with the terms of the Technology Contract

distribution of that flow state, resulting in the expected energy yield. This is covered in more detail in the WG3 WP4 D6 report.

The model takes input parameters for the seabed surface roughness that can then predict the shape of the velocity profile in the vertical. Therefore, given a surface roughness value k_s the Darcy friction function f, can be calculated using

$$\sqrt{(1/f)} = 2 \log(D_h/k_s) + 1.14,$$

where D_h is the hydraulic diameter (Chanson, 2004). The Power law is determined via the equation

$$N = K\sqrt{(8/f)},$$

In order to obtain the horizontal velocity through the water column in a free-surface flow of depth H with friction velocity u_h we use the equation (Pope, 2010),

$$u/u_h = (z/h)^N. \quad [4\text{-}1]$$

The primary assumptions of the flow field modelling approach are:

- Stochastic – The flow velocities contain noise such that the flow speeds are not deterministic and a traditional harmonic fit is not the most suitable approach.
- Quasi-steady – In order to predict the spatial variability across a site, the frequency domain approach assumes that the fluid flow is sufficiently steady such that the average flow speed is representative of the binned time series data.
- Power Law – Vertical profile is well approximated by a power law profile which implies that the flow must be steady, turbulent, incompressible and fully developed – not accelerating or decelerating.
- Small farm – It is assumed that the kinetic energy flux is a suitable measure of the amount of energy that can be extracted from a tidal farm and in order for this assumption to be valid the farm must be sufficiently small such that there is no large scale blockage of the flow due to the array.

4.2 Validation methodology

In order to test whether the frequency domain is a suitable approach for predicting the expected energy yield, an investigation using the Telemac 2d simulations developed as part of WG3 WP3 D1 was undertaken. In this study a frequency domain and a time domain simulation are compared to assess the adequacy of the frequency domain approach.

In order to compare the time series and frequency domain a resource analysis of the flow fields was performed. This is achieved by calculating the kinetic energy flux. While it has been argued that the kinetic energy flux is not a suitable measure of the total potential energy that can be extracted at a tidal site, (Garrett & Cummins, 2005) it is noted here that the energy extraction model developed as part of this study uses the rotor averaged flow speed in order to calculate the power and thrust values at each device. As discussed in WG3 WP6 D6, the kinetic energy flux is a suitable metric provided that small, demonstration type farms are considered. This approach is suitable for arrays which do not extract a

Not to be disclosed other than in line with the terms of the Technology Contract

significant proportion of the driving head of the flow. In this way, global blockage effects and the impacts on the large scale hydrodynamics will be minimal.

The time series kinetic energy flux at a point $\mathbf{x}$ is given by $K_t(\mathbf{x}_i) = \Sigma_{t=1}^{nt}\ 1/2\ \rho\ |\mathbf{u_j}(\mathbf{x}_i)|^3$, where n_t is the number of simulation time steps. Meanwhile the frequency domain analogy assumes that there exists a probability distribution (PDF) of the flow over the same period as the time series simulation. If such a PDF exists then the kinetic energy flux is written $K_f(\mathbf{x}_i) = \Sigma_{j=1}^{n\alpha}\ \Sigma_{i=1}^{nu}\ 1/2\ \rho\ P(\Re_{i,j})\mathbf{u_j}(\mathbf{x}_i)^3$ where n_α is the number of direction bins and n_u is the number of speed bins.

In addition, we shall also assess the adequacy of the flow profile predictions using the data from Telemac 3d simulations to compare against the power law profile.

4.3 Assessment of model performance

A number of studies are presented in order to help determine whether the approaches adopted in section 4.2 are appropriate in the context of this study.

4.3.1 Frequency versus time domain

In this investigation, representing the overall epistemic uncertainty surrounding the expected energy yield of a tidal farm, it is assumed that the time domain simulation gives the 'correct' solution. Here it is desirable to understand how much disagreement exists between the frequency and time domain simulations when examining the resource and energy yield predictions for an array of tidal stream devices.

To inform this investigation the authors have undertaken a study of simulations of tidal currents across northern European waters that have been earmarked for the development of tidal farm arrays. These simulations have been undertaken as part of the PerAWaT project WG3 WP3 D1 and are presented to help quantify the differences between a time domain and frequency domain analysis, to understand what the primary factors are involving any discrepancies and to inform decision making in this subject. These models have been calibrated against ADCP and tidal elevation data at sites across regions of interest for tidal stream deployment.

The three Telemac2d simulations were run using Thompson type boundary conditions (Telemac, 2013) and the Coriolis force was included in the computation. A summary of the format of the results is provided in table 4-1.

A reference point for each of the studies was identified as the point with maximum resource. The data was then binned according to the methodology described in Section 4.1 and then a comparison between the time-averaged and frequency kinetic energy flux was made. In order to understand the spatial variability of the resource, these comparisons were performed over a circular area of increasing radius. The size of the radii considered were 1/2, 1 and 2 kms.

Given that the hydrograph determines how the flow will be binned, it is interesting to examine these to understand the variability in the results. Presented in figure 4-1 are the tidal ellipses for Alderney, Paimpol-Brehat and the Pentland Firth. From figure 4-1, it is clear to see that the Alderney hydrograph shows the largest directional variability. This appears to be reflected in the errors between the time series kinetic energy estimates using the frequency and time domain approaches in figure 4-2. Otherwise, the velocity roses show strong bi-directionality in tidal currents.

Not to be disclosed other than in line with the terms of the Technology Contract

Table 5-1: Box and Whisker plots of the root mean square error between model and measured data for single row and multiple row tests: Centreline, lateral, and vertical profile comparisons were made. Shown are the minimum, maximum, median and quartile errors.

Region	Mesh Resolution	Time step	Simulation Time
Alderney	< ½ km	10 minutes	6 days
Paimpol-Brehat	< ½ km	10 minutes	4 days
Pentland Firth	½ km	15 minutes	17 days

The errors between kinetic energy flux predictions are provided in figure 4-2. As expected, it can be seen that as the number of flow speed bins is increased, the error decreases as the frequency domain tends to a time series analysis. Further remarks to be made are that the maximum error for a site radius of up to 1 km is generally below 5 % while the maximum site error ranged up to 30 % for the Alderney data at radii of 2 km. The mean absolute error by contrast was less than 2.5 % across all the different sites and different radii.

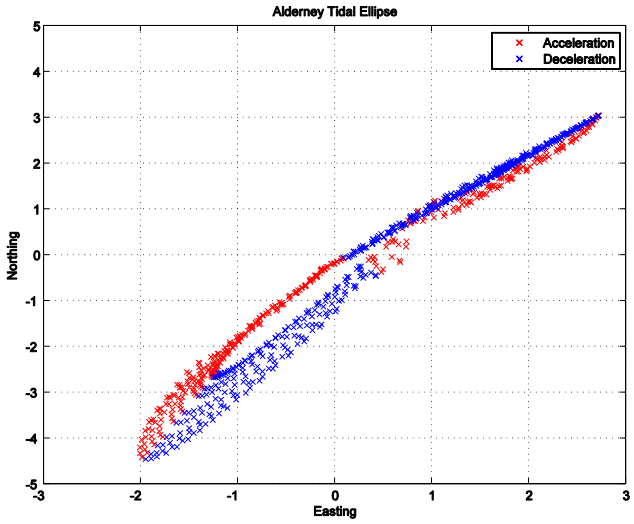

Not to be disclosed other than in line with the terms of the Technology Contract

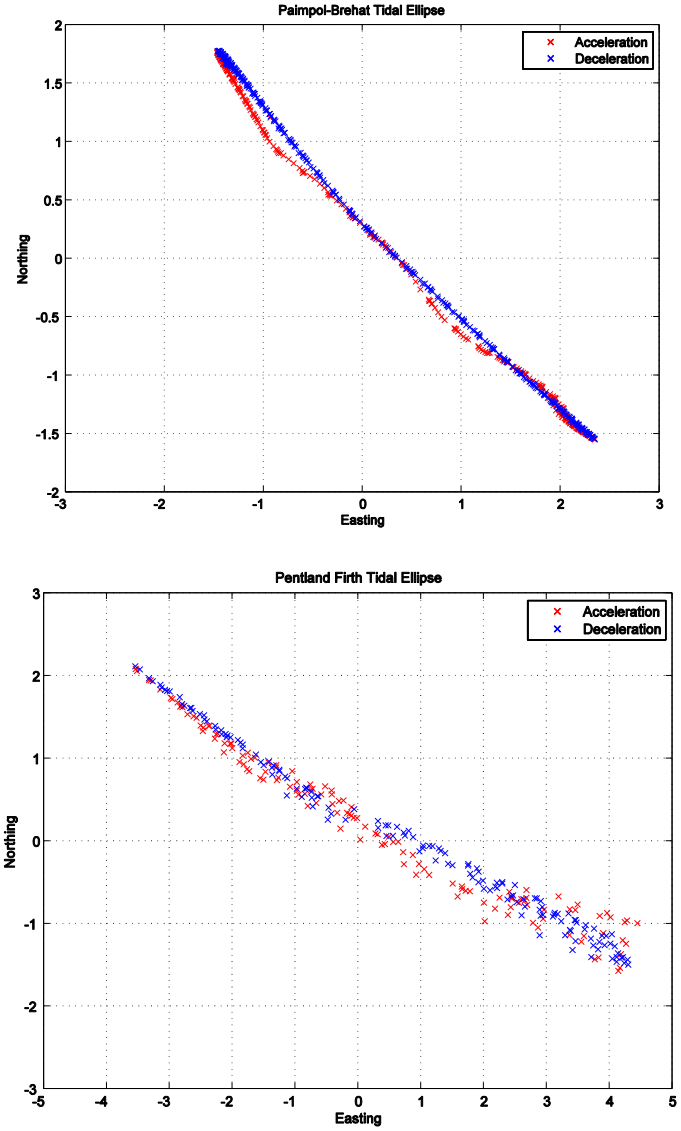

Figure 4-1: Tidal Hydrographs at reference locations for the three data sets Alderney (top), Paimpol (middle) and Pentland Firth (bottom). Red/blue shows accelerating/decelerating time series points.

Not to be disclosed other than in line with the terms of the Technology Contract

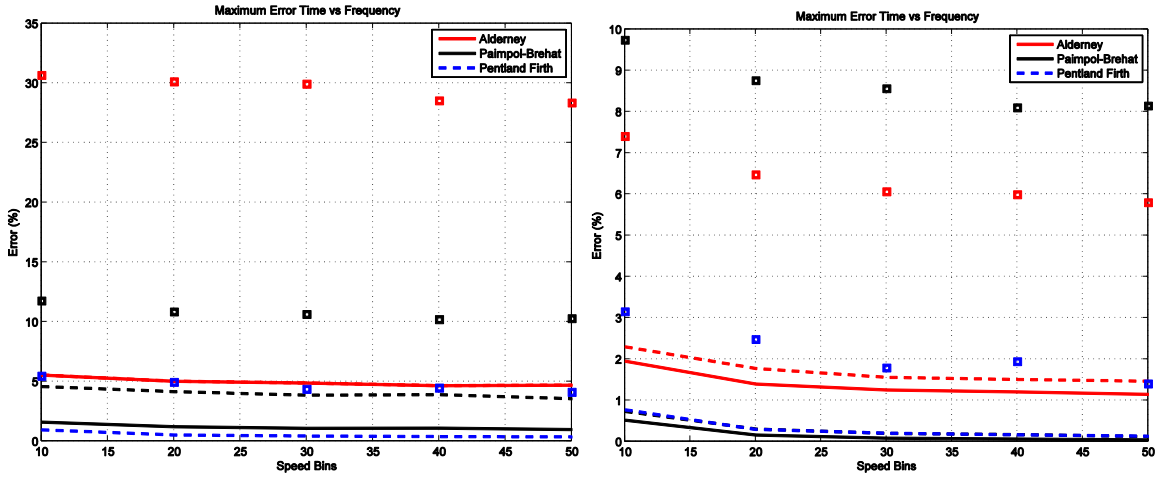

Figure 4-2: Absolute error between time series and frequency domain kinetic energy flux predictions. The left figure shows results adopting the standard 'binning' method, while the figure on the right presents results using the accelerating-decelerating decomposition. The ½, 1 and 2 km radii zones are denoted by (-----), (- - -) and (□) respectively.

The dynamics of accelerating and decelerating flow are different, certainly through the water column the turbulence can deviate from a parabolic profile (Ni *et al*, 2012). Therefore, in order to improve the results the flow at the reference point was decomposed into accelerating and decelerating flow (AD decomposition) see red and blue markers in figure 4-2.

The results of such a decomposition are presented in figure 4-2 and show a clear improvement, suggesting that there is very little difference between a time and frequency domain simulation. In fact, the maximum error for radii of up to 1 km is never above 2.5 % and the mean error is approximately less than 1 %. These results may not come as a surprise given that the number of flow speed bins in the frequency domain has been doubled. However, the improvement is better than linear with respect to the increase in the number of bins. For instance, in the case of 20 bins with AD decomposition the results show an improvement over 40 bins without AD decomposition.

Given that the difference between resource estimates has been analysed for three different sites, the next step is to calculate the energy yield due to an array. A power curve is therefore inputted into the energy model and device positions specified. From the depth-averaged flow solution the flow field is extrapolated into three-dimensions and consequently a prediction at hub height can then be made. This is subsequently used to calculate the operating power coefficient and then the power output. An energy yield analysis modelled array interactions due to speed ups and wakes. These simulations were not performed using the AD decomposition as presented earlier. A simulation of the Pentland Firth over a two-day period (tidal cycle) of half hourly outputs was used for the calculation. The results for a time and frequency domain simulation were compared between the baseline, gross (speed-ups) and net (speed ups and wakes) energy yield predictions resulting in means errors of 0.675, 1.13 and 1.3256 % respectively. Baseline prediction simply uses flow speed at a reference location and produces an inferred power reading. Given that the operating conditions at devices for a time simulation will be slightly different when compared to the averaged flow state, the wake effects will also vary causing differences in energy yield production. One of the flow wake maps is presented in figure 4-3.

Not to be disclosed other than in line with the terms of the Technology Contract

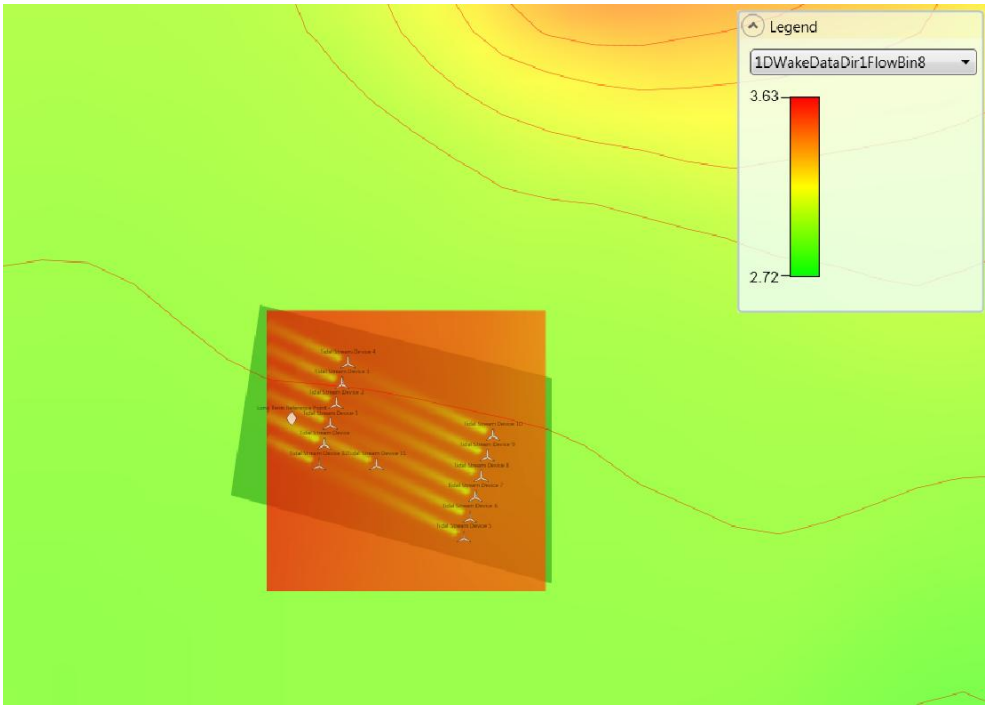

Figure 4-3: Wake map of a flow speed bin using the frequency domain method for predicting energy yield. This is a demonstration of a farm and is not representative of any particular device or real life project.

4.3.2 Depth profile comparison with Telemac3d

In addition to depth-averaged simulations being undertaken as part of WG3 WP3 D1, Telemac3d simulations were also provided. In this section the velocity profiles through the water column, provided by the three-dimensional model, are compared with the GH model for predicting the velocity shear.

Figure 4-4 shows a sample of different shape velocity profiles obtained by the model outputs. In addition, an approximation to the time series outputs using a power law approximation has been superimposed to compare with the data. In the majority of cases the power law profile provided a suitable approximation as the flow followed a roughly logarithmic/power law shape. However, it is clear to see that in some cases these profiles are not sufficiently accurate, such that accurate inflow predictions would not be possible. An error analysis to help quantify the difference between model prediction and observed yields a mean absolute error of 11.7 %. It is worthy of note that the biggest dependence on the flow profile for the combined inter-array model is the flow speed and not the shape parameters, see Section 6.

Not to be disclosed other than in line with the terms of the Technology Contract

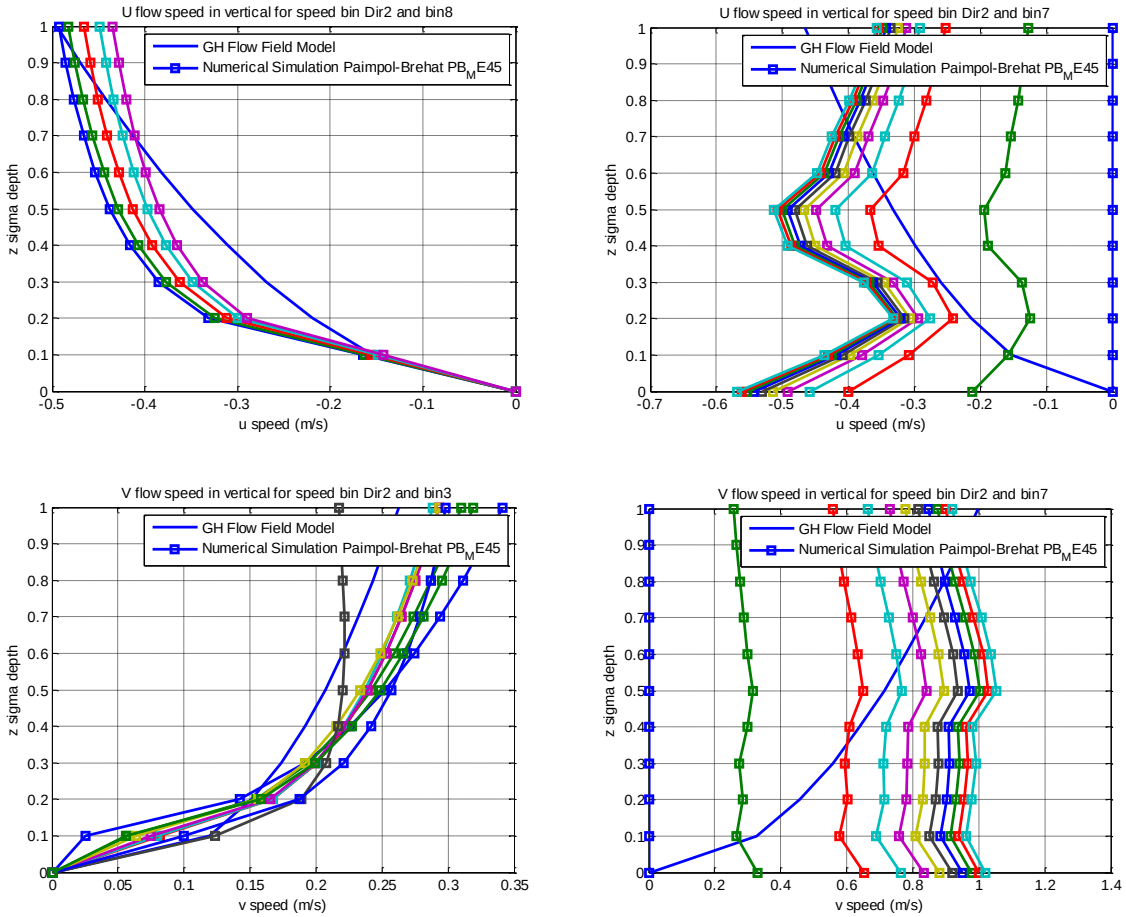

Figure 4-4: Results comparing the velocity profiles from a Telemac 3d simulation to the GH flow field model. Telemac 3d results are denoted by the (□) and GH flow field results given by (-).

In tidally energetic sites, the flow profile can deviate from the traditional power law formula [Gunn & Stock-Williams, 2013]. More recent research has led us to conclude that different curves could produce better results and this is presented in the following section.

4.3.3 Depth profile comparison within ReDAPT

As reported by Gunn & Stock-Williams (2013) measurements taken at the TGL device location reveal velocity profiles that are in fact quite different from what conventional analytical expressions can predict. In highly energetic tidal sites, vortex shedding from islands, secondary flows, wind driven currents and waves produce quite different velocity profiles from the power law that has been proposed. Therefore, it is suggested that a different model is adopted such that velocity profiles that are observed, such as shown in figure 4-5. The following equation is suggested,

$u(z) = a[\log(z/z_0) + bz^{n+1} + cz^n]$, $a > 0$, $z_0 > 0$. [4-2]

For the standard log law $a = u_s/\kappa$ and $b = c = 0$. The parameter u_h is the max flow speed, h is the free-surface height, and $1/\alpha$ is typically referred to as the power law. In addition, u_s is the surface friction

Not to be disclosed other than in line with the terms of the Technology Contract

speed, κ is the von-Kármán constant and finally z_0 the surface roughness. In addition, in eq. 4-2, a, b and c are constants while n is set equal to 2.

It is the intention of GH to improve on the existing work within the PerAWaT and ReDAPT project in order to develop the most appropriate models.

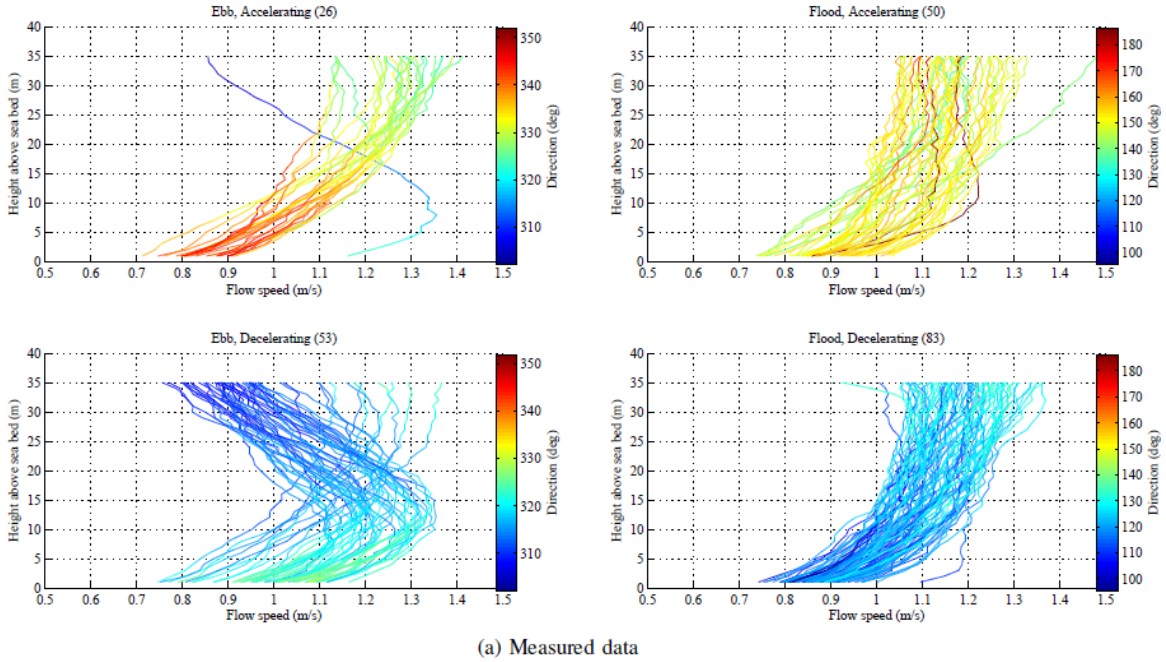

(a) Measured data

Figure 4-5: Measured flow velocity profiles from the ReDAPT project that do not generally show the traditional logarithmic or power law results.

4.4 Quantification of uncertainties

A comparison between frequency and time domain predictions, using a variety of flow models made available through the PerAWaT project representing sites earmarked for tidal deployment has been made. In addition an energy yield analysis has been performed for a 48 hour tidal period. The key findings are:

1. As the number of bins is increased, the magnitude of the error decreases.

2. As the radii of the domain becomes larger, the error grows as the frequency domain flow states do not adequately represent the time series flow.

3. If the flow is binned according to acceleration and deceleration as well as speed and direction then the results show significant improvement.

4. The mean error between the frequency and time domain simulations is generally small, less than 2 %.

Not to be disclosed other than in line with the terms of the Technology Contract

5. The error between time series and frequency domain energy yield predictions is small, justifying the use of frequency domain in the analysis.

In order to quantify uncertainties with respect to fitting velocity profiles to measured data, each of the models was fitted to the base flow readings from the WG4 WP2 data set. By examining the data it was found that the best fit was obtained using $u_h = 0.5067$ and $\alpha = 10.6$ in eq. 4-1; this profile will be denoted by $u_{fit.}$ For the log law and modified log law profiles (eq. 4-2) a suitable approximation to the power law was found and then the inputs perturbed by 5% using a Monte-Carlo type analysis. In this manner, numbers were drawn randomly from a normal distribution such that $\eta \sim N(1,p)$ and $p = 0.05$. As an example, the random variable $\eta\ u_s$ would have an expectation of $E[\eta\ u_s] = u_s$ and a standard deviation $SD[\eta\ u_s] = p\ u_s$. The standard deviation between the fitted profile and perturbed profile was then calculated for all the simulations $\sigma = SD[u_{fit} - u(z)]$. For each model 1000 evaluations were computed in an attempt to account for a high proportion of the input parameter space.

For the power law profile it was found that:

1. When varying the u_h parameter the standard deviation was found to be 0.0300 m/s.

2. When the exponent α was perturbed the standard deviation was found to be 0.00234 m/s.

3. If all parameters were perturbed then $\sigma = 0.0302$ m/s. This last point is useful as it shows that variation of the two parameters u_h and α are effectively uncorrelated as σ, is roughly equal to the standard deviation when only u_h is perturbed.

For the log law it was found that

1. The roughness parameter yielded $\sigma = 0.001281$ m/s.

2. The speed parameters yielded $\sigma = 0.01427$ m/s.

3. When all parameters were perturbed then the result was found to be $\sigma = 0.01439$ m/s. Again, the log law shows a similar story such that the difference between the standard deviation when all parameters are perturbed is roughly equal to the difference when speed parameters only are perturbed.

4. For the modified log law the additional parameters were found to be small ~ 0.00001 m/s.

It is clear that the most sensitive fitting parameter, unsurprisingly, is u_h or u_s depending on whether a power law or log law is adopted. Given that the base flow profile is well approximated by the power law, it is not a fair test of the sensitivity of the additional parameters in eq. 4-2. Only further work will reveal the sensitivity of these parameters on prediction of flow speed.

4.5 Discussion of model validity, sensitivities and limitations

A range of studies have been undertaken to quantify the level of uncertainty in model predictions when attempting to understand the resource from which energy will be extracted. This has included a study examining the frequency domain assumption and the adequacy of the vertical flow profile representation.

A review of the assumptions is undertaken:

Not to be disclosed other than in line with the terms of the Technology Contract

- Stochastic - An attempt has been made to understand the level of error in assuming the resource is stochastic. It appears that, provided the method of binning and a time series analysis of the resource are similar, then the energy results will most likely be similar as well. This could form the first step of any energy resource analysis such that confidence in the energy yield predictions can be increased. In addition, it has been found that by distinguishing between accelerating and decelerating flow, the accuracy of the results can be significantly improved. Other methods are likely to be computationally expensive and the primary drawback of using a shallow water model to produce an energy yield prediction is that the wakes between devices and the loadings on downstream rotors will not be correctly captured. In addition, studies have shown that aharmonic components exist in the current data and that the resource is not purely deterministic (Kutney *et al,* 2013)

- Quasi-steady – assuming the flow can be treated as quasi-steady appears valid. In particular, an energy yield calculation performed both in the time and frequency domains reveals that there is little difference between the two approaches.

- Power Law - The model limitations of the power law fit are that the power law and log law assume that the flow is quasi-steady, fully developed and in a channel of infinite width. In reality, at highly energetic sites we find the standard log and power law profiles do not give an accurate description of the flow. It is the intention of GL GH to improve the modelling process so that an accurate three-dimensional model of the flow around a complex tidal site can be developed. A perturbation of the various parameters used to define vertical velocity profile was made and compared to the base flow profile for an experiment. It was found that the most sensitive parameter was the maximum flow speed and that the uncertainty when all parameters were perturbed was generally found to be in line with the flow speed parameter uncertainty. Therefore, there appears to be little correlation between the two.

- Small farm – It was assumed that the farm was small in order for this analysis to be performed. This cannot easily be tested as no data exists of operational farms. As farms are deployed data will be used to quantify the level of impact.

Not to be disclosed other than in line with the terms of the Technology Contract

5 FAR WAKE

In order to predict inter-array effects of a series of tidal stream turbines, the velocity deficit imposed on the flow due to upstream turbines must be predicted with sufficient accuracy to ensure that the overall uncertainty is within acceptable limits (see Section 6 for the aggregated uncertainty analysis). Here, the far wake models that calculate the recovery of the flow velocity after energy has been extracted are discussed. These models have been reported in more detail in WG3 WP4 D5.

The far wake model is based on the drag that is generated when flow moves past a bluff body in an unbounded domain. In this case, the wake blockage generated by an operational turbine mimics the drag generated from a blunt body. This phenomenon can be modelled using the free-shear layer equations (Ainslie 1988, Tennekes & Lumley, 1972). These equations assume that the flow is self-preserving such that the turbulence is in local equilibrium. In other words, the turbulence can be related to the mean flow variables such as the velocity deficit and width of the wake. The effects of turbulent dissipation and production are considered to be unimportant such that vorticity is merely transported downstream.

The far wake model outputs have been compared to various experiments undertaken as part of the PerAWaT project, and good agreement is found. The range of experiments includes those with multiple wake merging, and different environmental conditions, such as free surface waves. There is however, a lack of validation data around the operating point and uncertainty in the rotor thrust measurements. A detailed analysis of the various possible source of uncertainty, from measurement error to modelling assumption, is discussed and an indication of the overall model uncertainty is presented.

5.1 Lesson for Tidal Energy using full-scale results from the wind industry

When an effort to model physical processes is undertaken, assumptions must be made to simplify the physics. It is acknowledged that these models will not provide a complete description of the real world. Measurements from complex real-life systems include noise and rarely fall on a smooth curve. Therefore, an assessment of the limitations in the modelling approaches must be made by measuring the appropriate quantities and making fair comparisons.

The results from LIDAR measurements of a horizontal axis turbine are provided to form a comparison with the current level of knowledge between the Wind and Tidal energy industries with respect to wake modelling. The measurements are provided courtesy of Aitken *et al*, (2012) as part of the NREL laboratory study to improve levels of uncertainty in the prediction and modelling of wind turbine wakes, similar to the objectives outlined in the mission statement for the PerAWaT project. These results are provided in figure 5-1.

These studies were undertaken as wind turbine wake modelling still suffers from uncertainty, even at this stage in the industry. Not being able to accurately predict the wake impacts negatively on the optimisation and control of wind turbines operating as an array. The high resolution Lidar (HRDL) at NRELs national wind technology centre is the current ‘state of the art’ for wind measurements and shows a clear wake deficit is generated behind the rotor. The regeneration of the flow deficit at a real site is rapid. From figure 5-1 it is observed that the flow has recovered from 2-5 m/s back to the value of the free-stream 10-12 m/s by 8D. In addition, measurements of the vertical velocity profile clearly show a Gaussian wake.

Not to be disclosed other than in line with the terms of the Technology Contract

From examination of figure 5-1, one can note that in reality, the recovery is described by anything but a smooth curve. The presence of large scale eddies and random fluctuations caused by turbulence create scatter in the data. However, trends can be observed and this is what the work below attempts to predict for wakes generated using tidal stream devices.

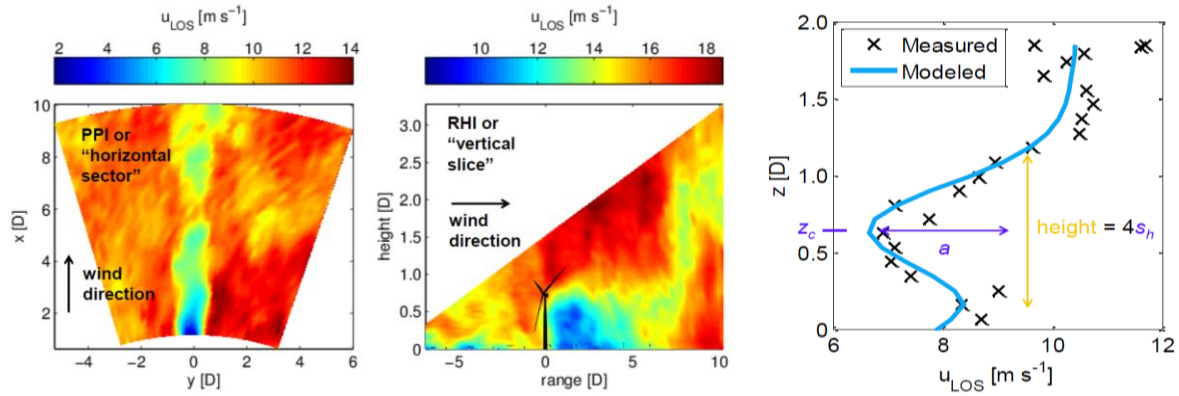

Figure 5-1: Lidar measurements of a 2.3 MW wind turbine operating in stable atmospheric conditions. Results show the reduction in velocity due to device operation and fluctuations due to turbulence.

5.2 Brief description of the models

TidalFarmer utilises three different far wake models that can be used separately to model array interactions. The first is an empirical formula that relates the downstream distance, thrust coefficient and mixing parameters to predict the flow deficit and will be referred to as the Park model. The second is a standard model that has been successfully applied in the wind industry. It is an axisymmetric description of the wake deficit and uses the eddy-viscosity turbulence closure model described in Ainslie (1988) and is hereby referred to as the 2-d model. A third model has been developed to address the issue of modelling wake mixing due to multiple operational turbines in a bounded flow. It was developed by extending the 2-d model and will be referred to as the 3d model. For more detail the reader is directed to an earlier PerAWaT deliverable WG3 WP4 D5. The 2-d and 3-d eddy-viscosity models are based on the free-shear layer equations (Tennekes & Lumley, 1972). This system of equations is derived on the following assumptions:

- Free-shear layer equations – The free-shear layer equations are derived upon the assumption that the flow is incompressible, turbulent and that the ratio of lateral (cross stream) to longitudinal length scales (downstream) is small such that the only lateral shear gradients are important. In fact, lateral (or cross stream) flow is neglected. This reduces the full set of RANS equations to a simple system of equations that can be solved much more quickly than those used in general purpose RANS solvers.

- Unbounded – the boundary conditions assume that the flow is unbounded such that the far field condition is for a slip wall. The greatest area of uncertainty is whether the boundary layer has an impact on wake development as this would normally be modelled as a no-slip boundary condition.

- Eddy-viscosity model – The primary assumption of the far wake models lies in the turbulence model that has been adopted. The eddy-viscosity assumes that turbulent dissipation mimics molecular diffusion. This is a valid assumption, provided that turbulent eddies are not stretched or

Not to be disclosed other than in line with the terms of the Technology Contract

compressed and are merely transported downstream. In the case of free-shear flow, such as the wake of a turbine, this is a valid assumption as the flow is self-preserving. In this situation, the turbulent properties are dependent on the flow.

Table 1 gives a number of input parameters that form part of the far wake models and the effect that these inputs will have on the form and shape of the far wake. These parameters were described in Thomson, et al (2010). The primary inputs to the model are:

1. Thrust coefficient, Ct.

2. Turbulence intensity, TI.

3. The wake start position, s_0.

4. The mixing parameters due to wake generated turbulence and ambient turbulence.

The Park model and 2-d model assume that the flow is unbounded and give a prediction of the centreline recovery. From these predictions a Gaussian profile is then used to describe the off-centre deficit. When two or more wakes lie closely together they are merged together using simplistic approaches.

The 2-d model is a numerical solution to the axisymmetric free-shear equations using a finite difference technique. These equations are solved for each device independently and then the solution is merged together using some simplistic formulae. The 'linear superposition', 'largest deficit' and the 'root mean square' algorithms have been adopted for the GH far wake models (Thomson *et al*, 2011b). These simplified wake merging models were developed in the wind industry for speed of calculation at the expense of accuracy and hence it is of importance to assess the effectiveness of such approaches.

The 3-d model is a numerical solution to the free-shear layer equations on a Cartesian grid using a finite difference technique. The grid is aligned to the flow direction (streamwise direction) as the lateral flow velocity is considered negligible. As the 3-d model solves the entire flow field, the merging of multiple wakes is obtained as part of the solution. The mixing length model or eddy-viscosity model is parameterised differently in both models. This is detailed in (Thomson, *et* al, 2011c). However, both models have the same inputs parameters to model the turbulence.

5.3 Validation methodology

A far wake model should be able to predict the reduction in flow speed due to the operation of upstream rotors. This should take into consideration different environmental conditions, such as seabed proximity, geometry, turbulence intensity and flow shear. The validation methodology that has been adopted is to first calibrate the model to the single wake experiment performed in the array-scale experiments. Then to compare against the different experiments performed as part of the PerAWaT project.

In particular, heavy focus will be on the array scale experiments that were undertaken (WG4 WP2 D5) as these have evidence of repeatability and are representative of real site conditions, in terms of blockage ratio, turbulence intensity and the merging of wakes between several rotors. In addition, the wave tests that were performed in these experiments will help in the understanding of wave-wake interaction.

Not to be disclosed other than in line with the terms of the Technology Contract

The single device testing in WG4 WP1 and WG4 WP3 allows a comparison of the model to measured data for different turbulence intensity and thrust operating points. In addition, the WG4 WP3 tests series allows an analysis of the effect of unbounded flow and seabed proximity on wake recovery. This will test the assumptions that have been made with respect to the boundary conditions that have been used to solve the system of equations in order to model the wake.

In all the studies performed in this section, the inputs to the far wake model were the normalised centreline velocity deficit and the wake width at the near wake position. These were chosen to match measurements taken in the flume, thus minimising any uncertainty around what the actual inputs to the model should be.

5.4 Calibration

The model was calibrated to match the centreline flow readings of the WG4 WP2 single rotor studies – this data set has been widely documented in both the PerAWaT documents WG4 WP2 D5 and in the academic literature (Whelan & Stallard, 2011, Stallard et al, 2011 and Olczak et al, 2013). It has good evidence of repeatability and is most representative of real-site conditions in terms of blockage ratio and turbulence intensity.

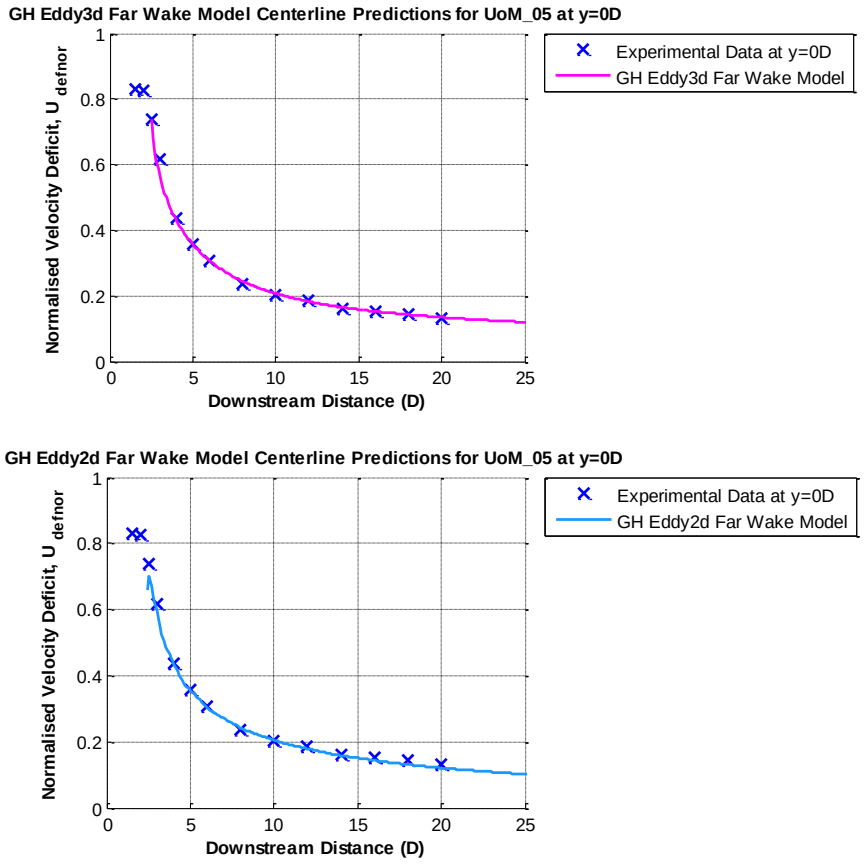

Figure 5-2: Comparison between the GH 3d model (top figure) and 2d model (bottom figure) and experimental data from WG4 WP1 single wake experiment (1/70th scale).

Not to be disclosed other than in line with the terms of the Technology Contract

Figure 5-2 shows the results of the calibration curve fits. As expected, good agreement is found; however, the 3-d model clearly captures the transition to a shallow water wake around 10D downstream (see discussion in section 3.1). Once the model parameters are calibrated they are not changed at any further point during the analysis. It is noted, that the end of near wake point is chosen to be 2.5D as suggested by the discussion in Section 3.1. However, in some comparisons this is changed if the data suggests that the far wake begins later.

5.5 Assessment of model performance

In this section, we will compare the far wake models discussed above in section 5.2 with the various data sets that have been made available through the PerAWaT project.

5.5.1 WG4 WP1

For the WG4 WP1 single device testing the near-far wake transition did not produce similar results to the other experimental data sets. As discussed in Section 3.3, the rotor was not built as designed and is operating in a highly blocked flume and these two aspects do not provide results that accurately represent the wake or performance of an quasi-unbounded horizontal axis turbine.

The comparison between the 3-d far wake model and an experiment from WG4 WP1 is given in figure 5-3. In this test the water depth = 0.8 m, the axial flow velocity was U = 0.27m/s and the TI = 15%. For an operating tip speed ratio of 4.5 the blockage corrected C_t was found to be 0.8. The velocity deficit only reaches 30% in the near wake region (WG4 WP1 D4) and does not start recovering until round 4.5D downstream, after which there is good agreement between the model and measurements.

5.5.2 WG4 WP2

The array scale tests provided a large set of multiple rotor and wake merging data. These tests investigate devices at different lateral and longitudinal spacings and measurements have been taken at lateral and vertical traverses behind each rotor. In some multiple row tests, and for efficiency reasons, data has been ‘sewn’ together to provide a complete experimental data set.

In the interim validation report, WG3 WP4 D18, it was shown that the wake models provide good agreement with experimental measurements in terms of wake decay and shape of the velocity profiles, both along the centreline, laterally and vertically for one row of devices. As in the interim validation report the model input parameters will be chosen to match with experimental measurements. Therefore, the TI is chosen to corresponts with readings observed in the experiments, and C_t was chosen such that the initial flow deficit matches the experimental observations. This is deemed acceptable as the accurate prediction of the initial velocity deficit for the far wake model is dealt with by the blockage and near wake models.

Not to be disclosed other than in line with the terms of the Technology Contract

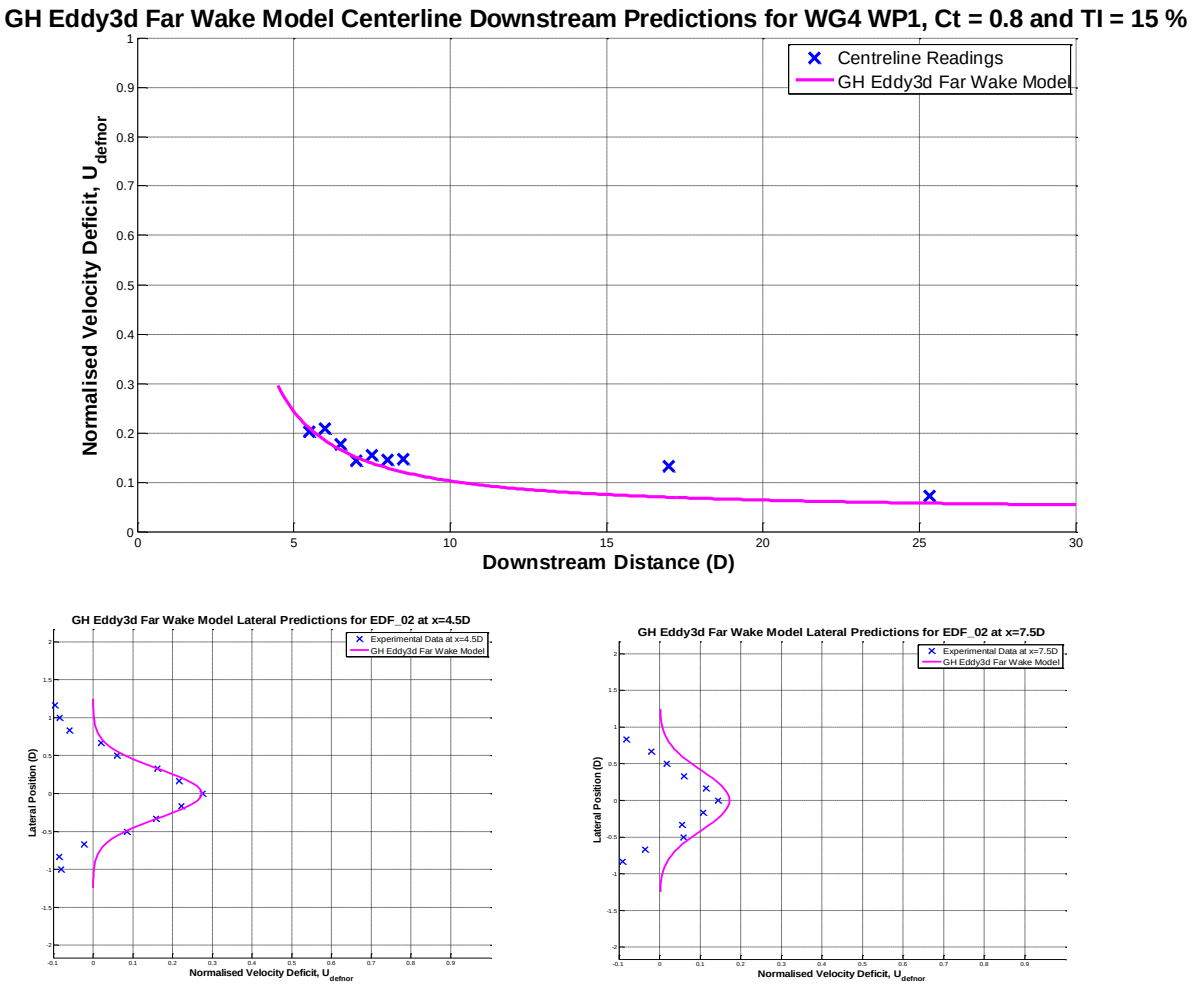

Figure 5-3: Centreline (top figure) and Lateral (bottom figure) wake recovery profiles for the WG4 WP1 experiments of 1/30th scale rotor at inflow U0 = 0.27 m/s, TI_{amb} = 10 %.

The focus of this report is upon the accuracy of the prediction of both loading and power production on downstream rows. Note that power production could not be robustly estimated from the small scale rotor experiments and therefore the primary method of assessing the potential for power production is in the inflow flow speed and profile. Estimates of the accuracy of the far wake models are made by comparing both the model prediction of increased TI and inflow speed upon the downstream rotors to the experimental data.

The tests that were compared to the far wake model featured a row of three rotors operating with a lateral spacing of 1.5D. These, along with other array formations are provided in figure 5-4. Various combinations were then considered downstream, including a second row of 3 aligned rotors (from herein referred to as test A), 4 staggered rotors (test B) and a larger test case with a second staggered row of 4 rotors and then a third row of 5 rotors (test C). The single row study of three rotors provides readings at 2D, 4D,...,12D. These lateral and vertical readings can be used to predict the inflow to a second row of rotors at either 4D or 8D downstream. This can then be used to assess how accurately the models will predict the downstream thrust coefficient for loadings onto the second row.

Not to be disclosed other than in line with the terms of the Technology Contract

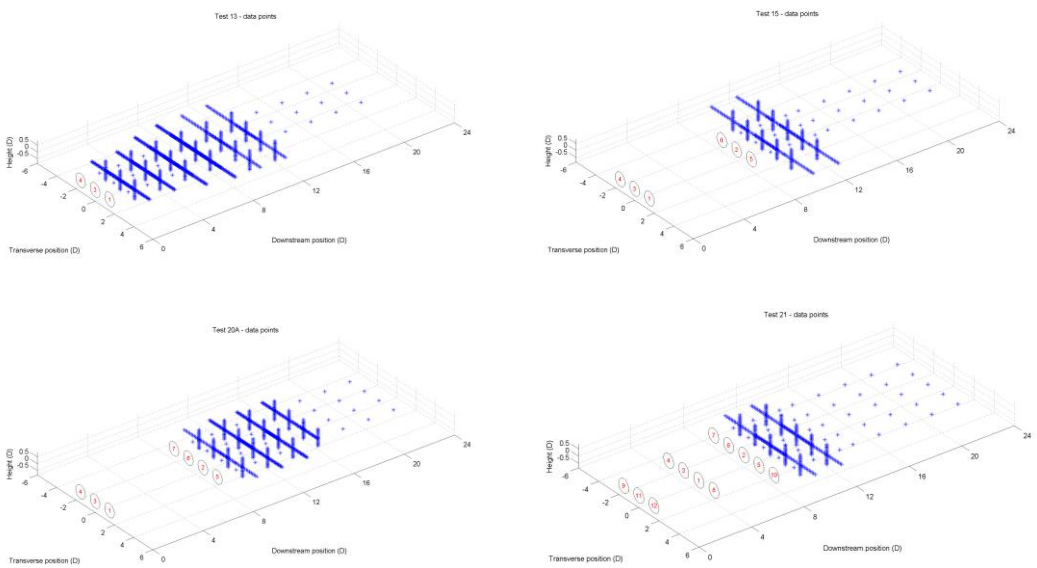

Figure 5-4: Summary of detailed array scale (WG4 WP2, 1/70th) investigations for single row with multiple readings downstream (top left), test A - two rows of three rotors aligned (top right), test B - row of three then staggered row of four (bottom left) and finally, test C - three rotors with staggered second row of four and further staggered row of 5 rotors, U0 = 0.47 m/s, TI_{amb} = 10 %.

Assessment of wake interactions

Comparison using the far wake models discussed in Section 5-2 was made to the experiments shown in figure 5-4. The lateral profiles can be seen in figures 5-5, 5-6, and 5-7. For these investigations the inputs to the model were experimentally observed centreline velocity deficit, wake width, and turbulence intensity.

In figure 5-5 it is observed that the three models capture the general trend of the wake merging across the rotor groups. The centreline velocity deficit is well predicted by all three models, and in addition, the 3-d model gives a good match with the data at 8D downstream yielding good predictions for the inflow to the second row of devices. In order to resolve the wake flow downstream of the second row, readings from the experiments were inputted in order to match with the value of turbulence intensity at the rotor plane. We again see that good results are found showing that the wake merging is well captured for the models.

While the Park model is very efficient computationally speaking, it generally over-predicts the wake deficit downstream. It was believed that while the Park model was useful in gaining a quick assessment of wake effects, in order to quantify uncertainty, the model will not be adequate as it generally gives a biased prediction. Therefore, no further analysis was undertaken with the Park model.

Likewise, in figure 5-6, good results are observed for a staggered formation. This study was undertaken in the same manner using inputs taken from experimental readings, such as matching centreline velocity deficit, wake width and the turbulence intensity. The increase in turbulence

Not to be disclosed other than in line with the terms of the Technology Contract

intensity was set to match with the experimental results as well. Here we again see good agreement with both the 2-d and 3-d models.

A stress test of the models is given in Figure 5-7 where the velocity deficit is applied at 4D downstream of the first row. Given the level of agreement the models are clearly capable of capturing the correct deficit provided appropriate inputs are provided.

Not to be disclosed other than in line with the terms of the Technology Contract

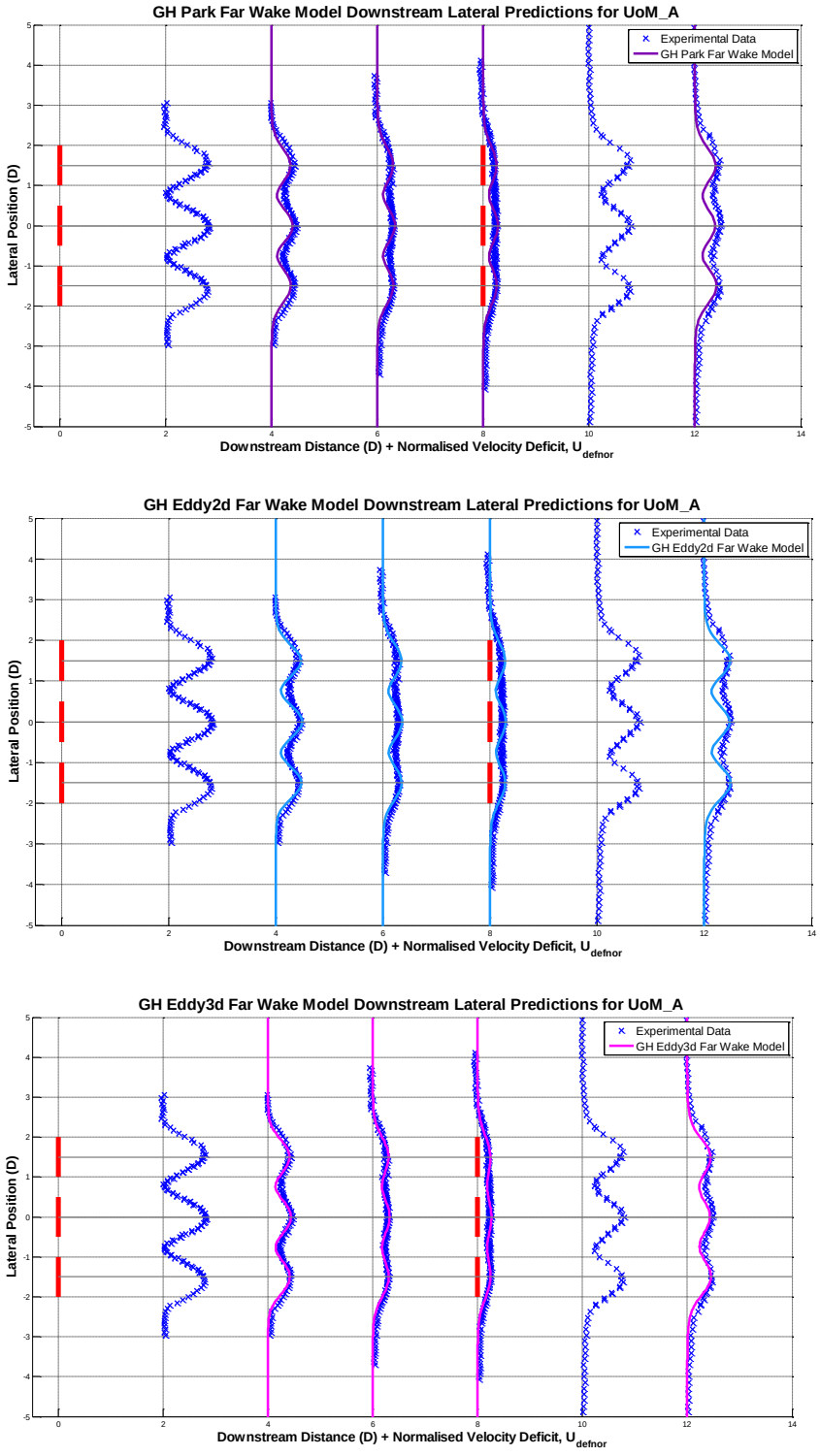

Figure 5-5: Combined data set for two rows of rotors with 1.5 lateral spacing and 8D longitudinal. Free stream flow speed was around, U0 = 0.47 m/s, TI_{amb} = 10 %. The red lines represent the rotor positions. The first graph (top) shows results of the Park model, second graph is the 2d model (middle) and the final set of results (bottom) compare the 3d model to the experimental measurements.

Not to be disclosed other than in line with the terms of the Technology Contract

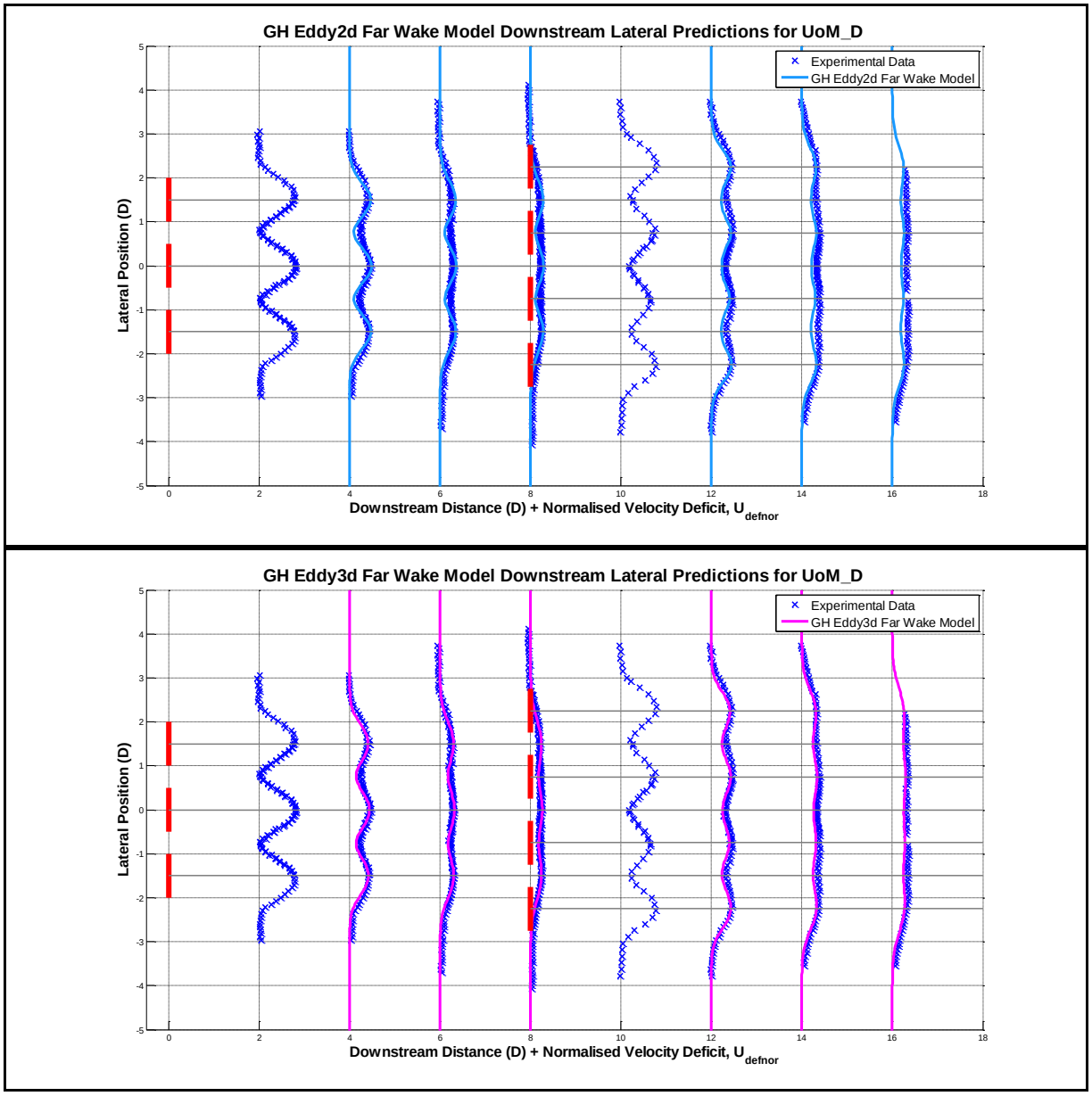

Figure 5-6: Combined data set for one row of 3 rotors and a second row of 4 rotors with 1.5 lateral spacing and 8D longitudinal. Free stream flow speed was around, U0 = 0.47 m/s, TI_{amb} = 10 %. The red lines represent the rotor positions. The first graph (top) shows results of the 2-d model and the second set of results (bottom) compare the 3-d model to the experimental measurements.

Not to be disclosed other than in line with the terms of the Technology Contract

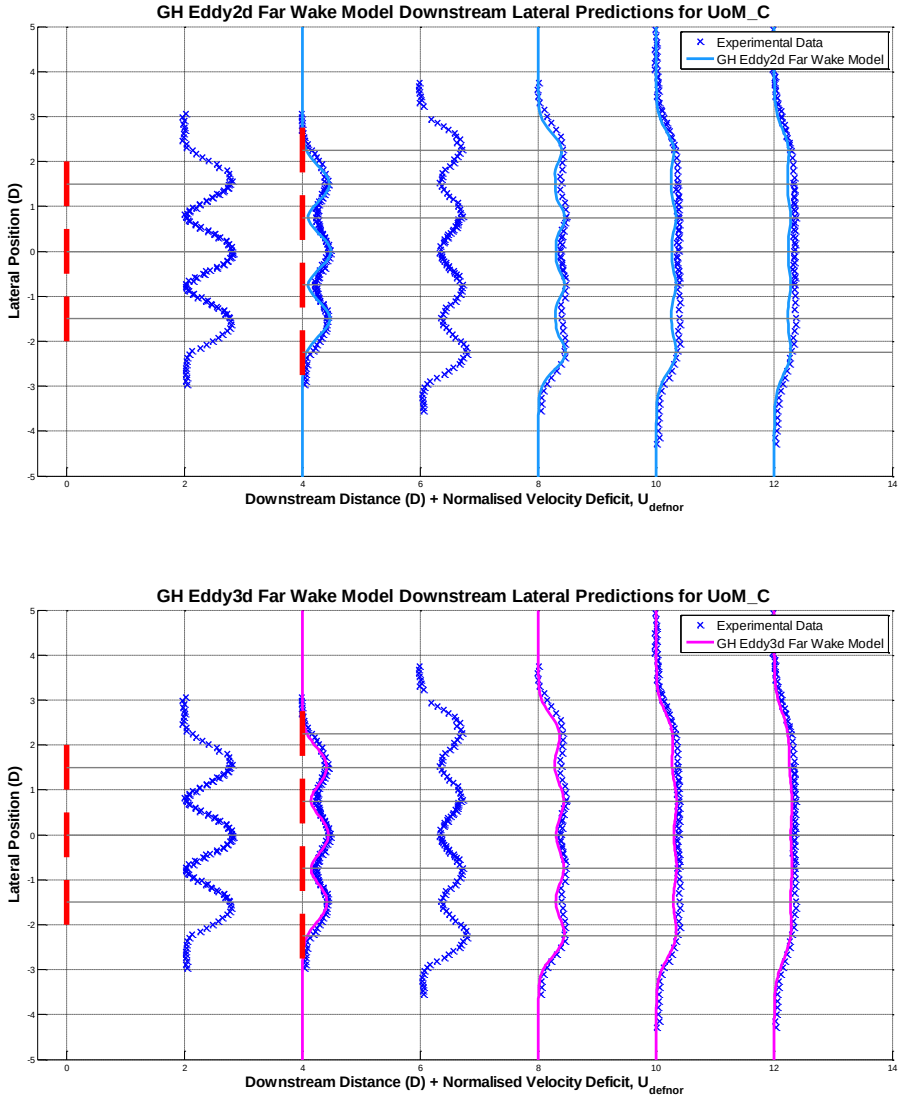

Figure 5-7: Combined data set for one row of 3 rotors and a second row of 4 rotors with 1.5 lateral spacing and 4D longitudinal. Free stream flow speed was around, U0 = 0.47 m/s, TI_{amb} = 10 %. The red lines represent the rotor positions. The first graph (top) shows results of the 2-d model and the second set of results (bottom) compare the 3-d model to the experimental measurements.

Discussion of wave-flow interaction on wake recovery

Figure 5-8 shows lateral profiles of the downstream flow for a test that includes the effect of opposing waves on currents. The waves correspond to a 'full-scale' period of 10.5 s and a significant wave height of 3.5 m giving a wave number of approximately k = 0.3 representing a shallow water wave ($k<\pi/10$). The layout of the test in figure 5-8 is that of test A in figure 5-4, two aligned rows of three turbines. Here it is seen that while the centreline velocity deficit is reasonably similar to that observed in other tests, in between the centrelines the wake deficit is much greater.

Not to be disclosed other than in line with the terms of the Technology Contract

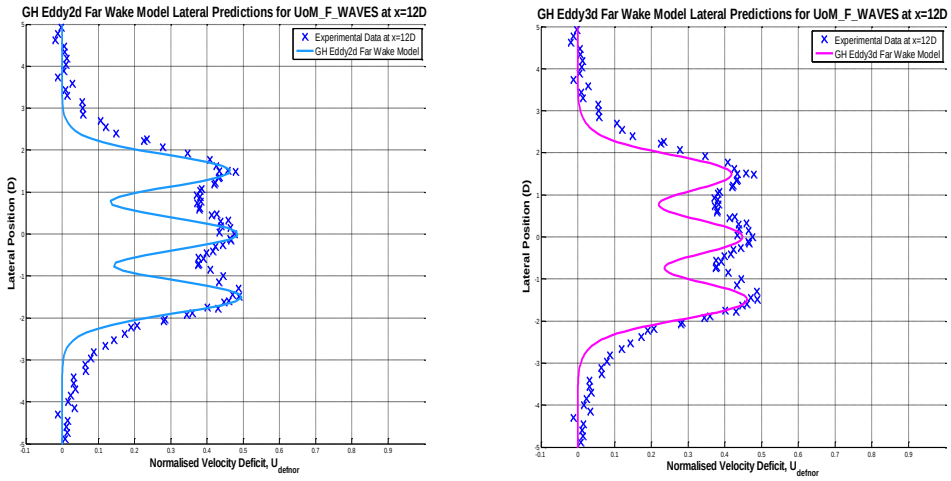

Figure 5-8: Comparison of lateral profiles between measurements and model predictions for the wave test case at 4D downstream of second row of devices. Waves have a 'full-scale' period of 10.5s and a significant wave 3.5 m.

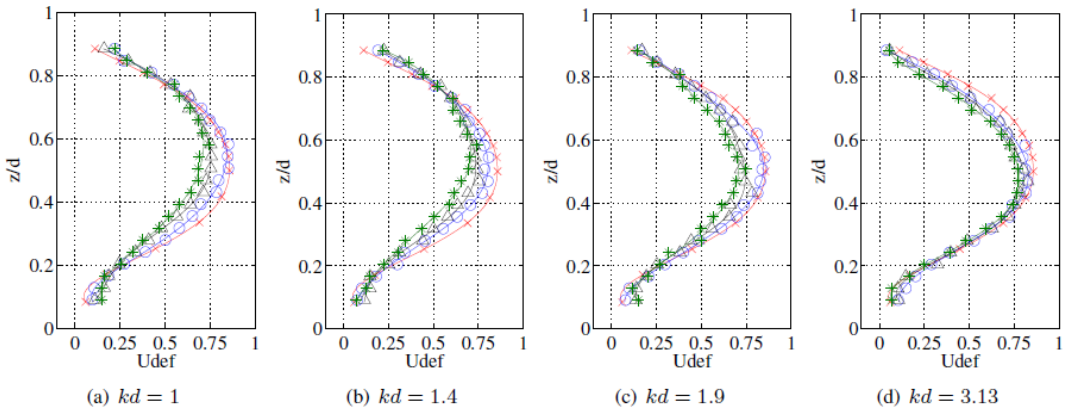

Velocity deficit 2D downstream for increasing wave heights. No Wave (x), Wave I (O), Wave II (△), Wave III (*)

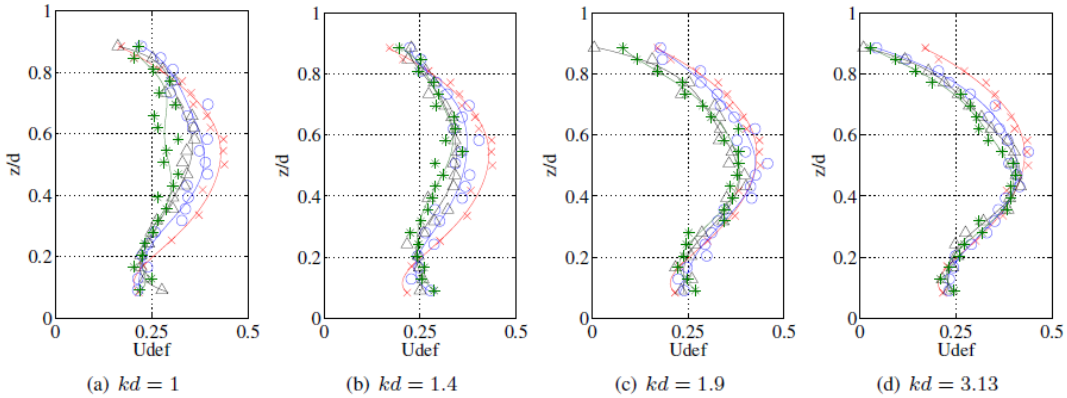

Velocity Deficit 4D downstream for increasing wave heights. No Wave (x), Wave I (O), Wave II (△), Wave III (*)

Figure 5-9: Vertical profiles showing the effect of varying the wave number and flume depth parameters on wake recovery at 2D and 4D downstream of a series of rotors.

Not to be disclosed other than in line with the terms of the Technology Contract

Further tests have been undertaken to observe the effect of wave current interactions. In figure 5-9, the impact of varying the wave number on the vertical profile is observed. The different wave conditions, Wave I, II and III are summarised in Olczak et al (2013) representing intermediate ($\pi/10<k<\pi$), and deep water waves ($k>\pi$). It is clear to see from the results that the deep water waves increase the rate of recovery (by 25 % in some cases).

5.5.3 WG4 WP3 – Single device quasi-unbounded and seabed proximity tests

In order to measure the unbounded rotor performance of the WG3WP2 1/70th scale rotor, the rotor was tested in the EDF (WG4 WP1) flume. Using the same ambient conditions as one of the studies in WG4 WP1 (TI_{amb} = 5 % and U0 = 0.55 m/s) the wake was mapped and the results are presented in figures 5-11 and 5-12. These studies were designed to investigate the impact of bounding surfaces upon rotor performance, wake structure and recovery.

In order to compare against the far wake model the rotor average turbulence for each device needed to be calculated. This was done by assuming that the only variation of TI across the rotor plane was in the vertical direction, therefore, a cubic polynomial was fitted to the data and the turbulence intensity was predicted as shown in figure 5-10. Here, the mid-level rotor is operating with an ambient TI ~ 5 % while the low-level rotor TI ~ 8 %.

Figure 5-11 shows that the recovery of the rotor in mid flume is substantially quicker than the recovery of that predicted by the 3-d model, the single wake WG4 WP2 tests (see figure 5-2) or the rotor that is close to the flume floor (see figure 5-12). As the rotor is in the mid-flume position there will be a large amount of free stream flow surrounding the stream tube that will help re-energize the flow quicker than if the device was bounded.

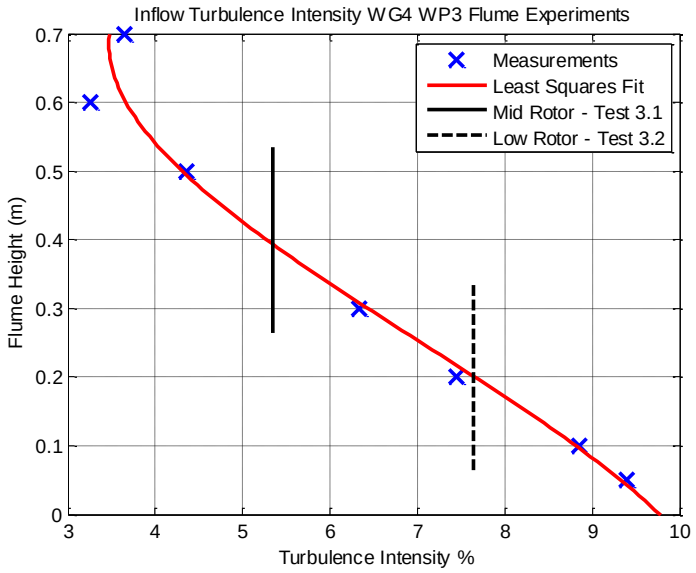

Figure 5-10: Vertical profile of the inflow turbulence intensity for the WG4 WP3 flume. The rotor positions and magnitude of the rotor averaged turbulence intensity is shown.

In general the 2-d model assumes the same boundary conditions, therefore the main factors influencing wake recovery are via the inflow profile and the value of turbulence intensity. The 3-d model is sensitive to the cross sectional area of the domain. In this test the TI_{amb} value is small and

Not to be disclosed other than in line with the terms of the Technology Contract

causes a slower recovery in the models. However, the rate of recovery seen in the experiments is quicker than in other experiments where TI_{amb} is high. It should be emphasised that the error is of the order of 5-10%**.** In the case of these experiments there could be an important piece of physics missing such as rotor generated turbulence whereby the increase in turbulence due to the rotor is greater than TI_{amb}.

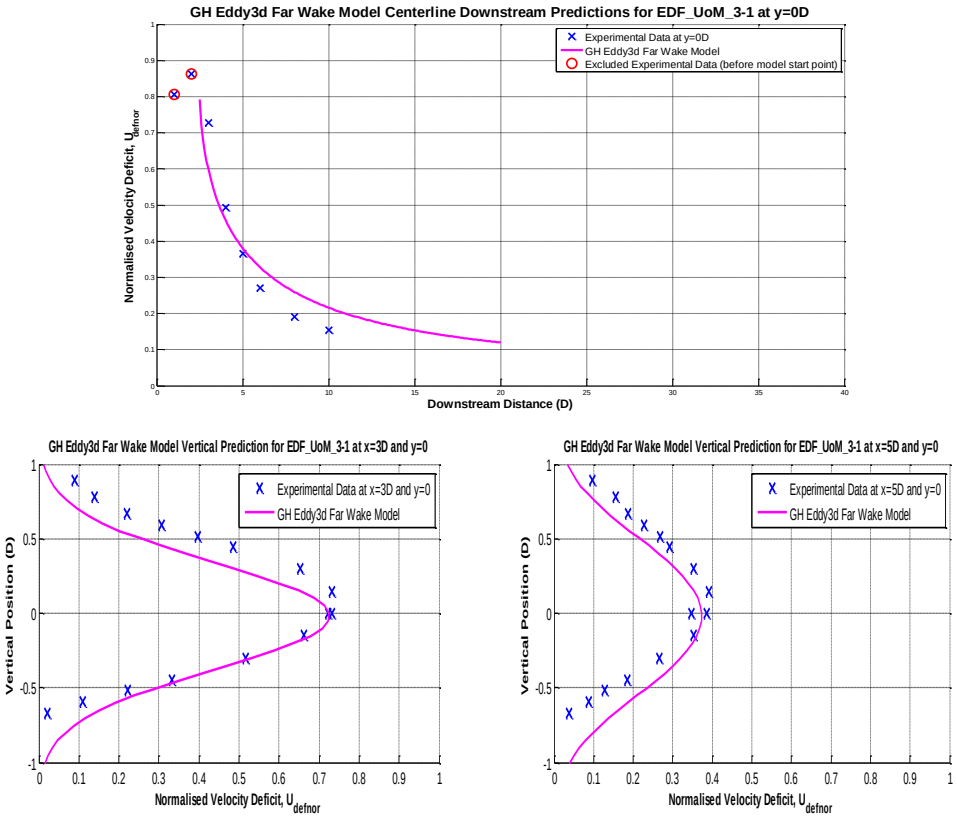

Figure 5-11: Centreline (top figure) and vertical (bottom figures) wake recovery profiles for the WG4 WP3 experiments of 1/70th scale rotor at inflow U0 = 0.55 m/s, TI_{amb} = 5 %.

A further comparison was made against the results provided by the wake mapping of the low-level rotor in figure 5-12. Here good agreement is found between the observations and the 2-d and 3-d model. In both sets of results, while the Gaussian approximation in the vertical appears to agree well with measurements, there appears to be a slight offset.

The results suggest that even for a low ambient turbulence intensity case, the flow recovers quickly. Given that other tests, which have been performed at greater TI values, show slower recoveries either the models should be parameterised to account for changes in vertical blockage, or there is a rotor generated turbulence intensity that will cause quicker regeneration of the fluid flow.

Not to be disclosed other than in line with the terms of the Technology Contract

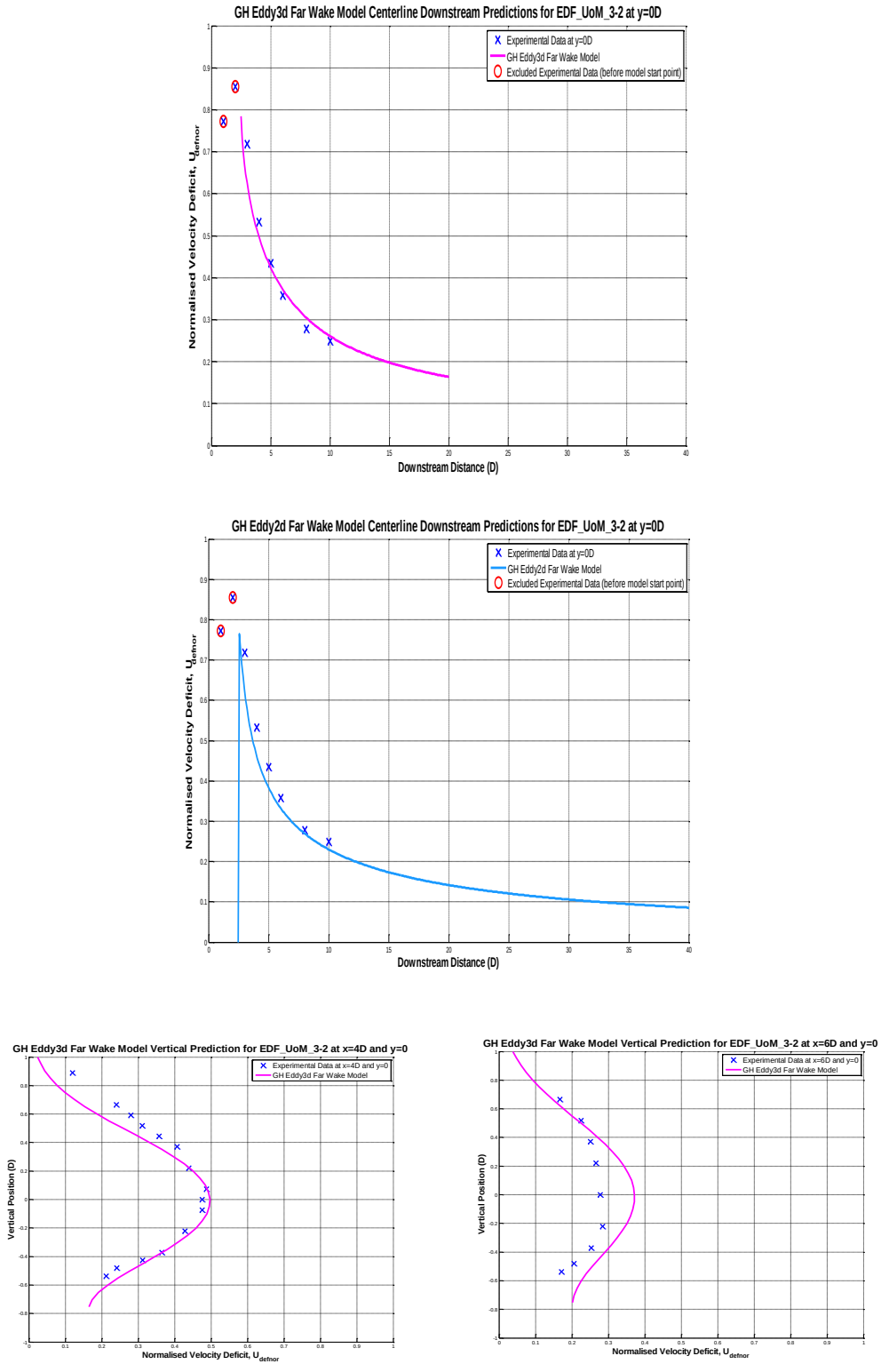

Figure 5-12: Centreline comparison with 3-d model (top), 2-d model (middle) and 3-d comparison with vertical profiles (bottom figures) for the WG4 WP3 experiments of 1/70th scale rotor at inflow U0 = 0.55 m/s, TI_{amb} = 8 %.

Not to be disclosed other than in line with the terms of the Technology Contract

5.6 Added turbulence intensity model

An increase in turbulence intensity is observed downstream of an operational tidal stream rotor. In order to predict the increase in these small scale turbulence structures a ratio of TI = u'/u_{wake} or, the ratio of turbulent velocity fluctuations to the flow velocity in the wake, was calculated from measured data. For the WG4 WP2 data we expect that the measurement error for the turbulence intensity is roughly ±2-5%. Figure 5-13 shows the centreline variation of the turbulence intensity for a variety of studies of different TI_{amb}.

In WG3 WP4 D5 the added turbulence intensity model is discussed whereby we define the added turbulence intensity TI_{added} and the ambient TI_{amb}. The added turbulence intensity is the increase due to the device above the ambient site conditions. Here we assume that the TI = $\sqrt{(TI_{amb}^2 + TI_{added}^2)}$ and so can be used to predict the increase in turbulence intensity given some background value and an empirically derived added value. The model is good at predicting the centreline increase in turbulence intensity, the outputs of which feed directly into the far wake models described herein.

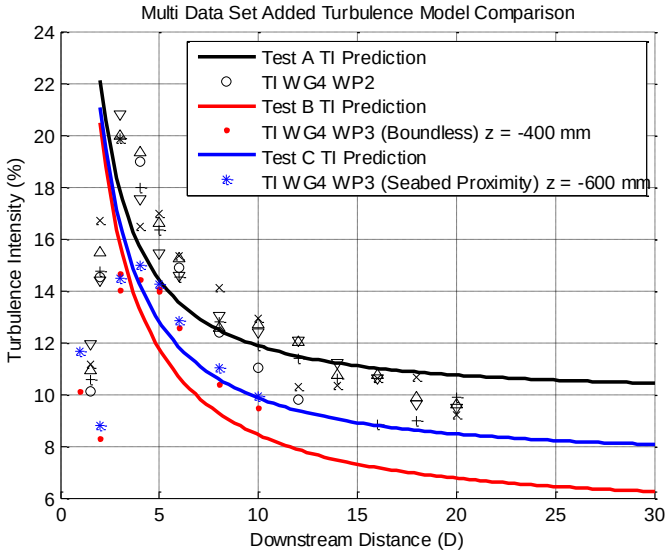

Figure 5-13: Comparison of added turbulence model and observations of turbulence intensity of the various experimental studies within PerAWaT.

5.7 Quantification of uncertainties

In the above study the models have been evaluated at the observed experimental value. The standard root mean square error method is used to judge how well the model prediction fits to the experimental data. This error gives an indication of the general degree of model closeness. A full spreadsheet showing the root-mean-square-error for each individual model comparison made in each test is attached in Appendix 1. The overall errors are then averaged to yield mean values. These values are listed in table 5-1.

From table 5-1 the accuracy with which all three models predict the test data is summarised. The 3-d model shows, on average, good results against all measurements with an average median root-mean-

Not to be disclosed other than in line with the terms of the Technology Contract

square-error of 3.8%. In addition, the average upper quartile of the root-mean-square-error of the 3-d far wake model is just 5.1%.

Table 5-1: Box and Whisker plots of the root mean square error between model and measured data for single row and multiple row tests: Centreline, lateral, and vertical profile comparisons were made. Shown are the minimum, maximum, median and quartile errors.

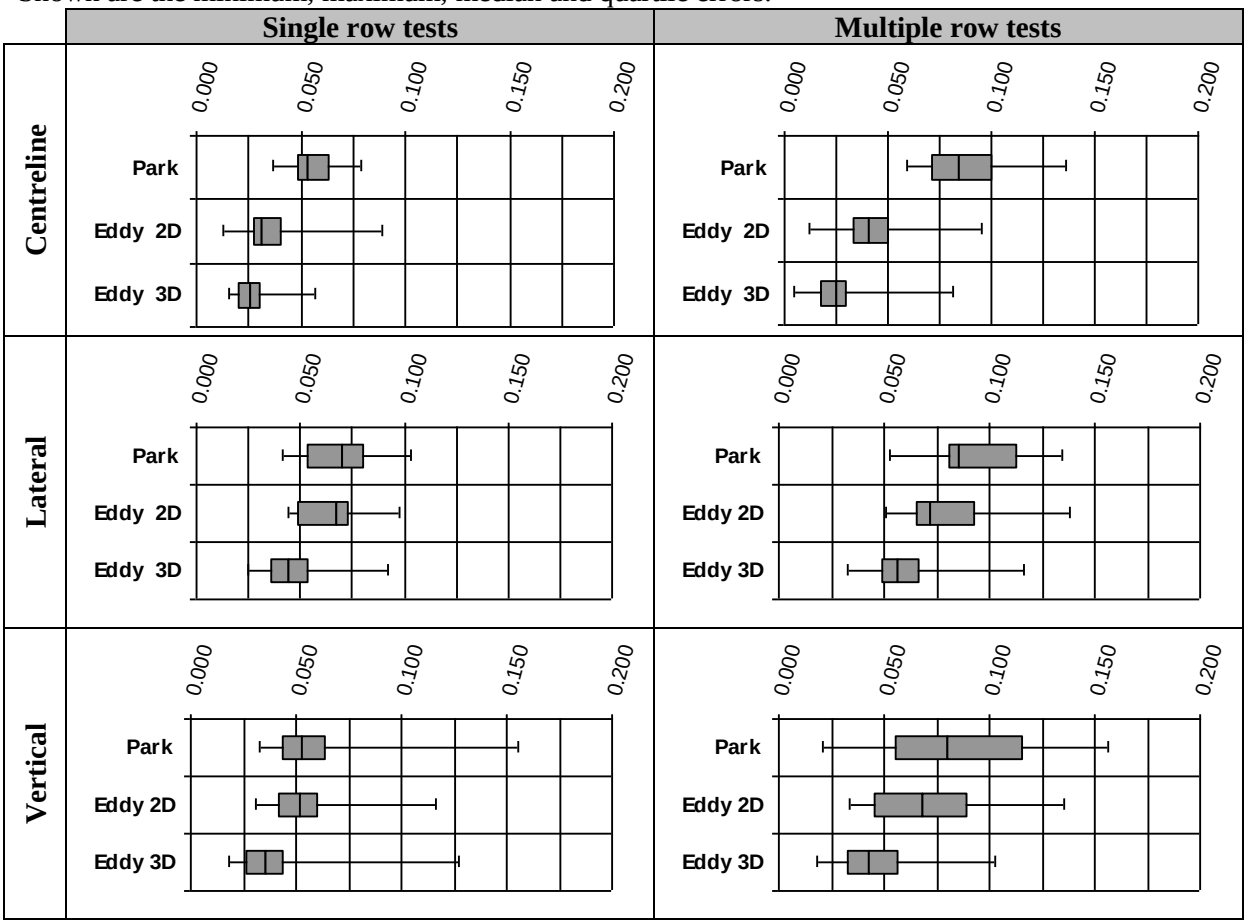

Table 5-1 clearly shows a drop-off between the accuracy of the 2-d and 3-d models. If the box and whisker plots are studied for the centreline root-mean-square-error for single row tests (the first row and first column in Table 5-1) it is observed that the median root mean square error (RMSE) for the 2-d and 3-d models is similar with values of 3.1% and 2.6% respectively. However, when a second or third row is introduced the centreline RMSE (see eq. 1-1) for the 2-d model rises to 4.1%. The 3-d model does not lose any prediction accuracy of the centreline velocity deficit with the introduction of multiple rows of turbines (2.6% estimated error for single row tests and 2.5% estimated error for multiple row tests).

Estimates of the error in comparison to the array scale experiments is shown to be low and gives an estimate of structural uncertainty of the model. However, this doesn't inform us of where the greatest sensitivities lie. For the interim, as simplistic models have been used it is easy to understand how model predictions change with model inputs. For instance, the effect of an increase in thrust coefficient is to increase the velocity deficit as more momentum is extracted from the flow. In addition the effect of an increase in turbulence intensity is to increase the rate of recovery of the wake deficit. It

Not to be disclosed other than in line with the terms of the Technology Contract

will be seen in section 6 that, as the models are simplistic, the sensitivities can be explored and this can help inform model uncertainty.

Just as in the near wake section, the measurement error for thrust coefficient and speed measurements was estimated to be 2-5%. To assess the impact of the measurement uncertainty upon the model outputs, two worst case scenarios were investigated (Ct + 5%, TI-5%) and (Ct-5%, TI+5%). This investigation represents the scenario where the initial deficit is large and turbulent mixing is low such that an over-prediction for the flow deficit will be obtained. The converse is when the initial deficit is low and the mixing is high, such that the resulting output should be an under-prediction for the velocity deficit.

Repeated readings of the wake of the $1/70^{th}$ single rotor were taken at multiple lateral and vertical traverses downstream. A comparison will be made at 8D downstream. The experimentally observed rotor averaged deficit at multiple points downstream is recorded in table 5-2. This value was derived by taking lateral (10 readings) and vertical (10 readings) measurements and so is derived from multiple readings according to eq. 5-1. Therefore it suffers from error propagation. In this case, we are calculating:

$$u_{rotor} = \Sigma_{i=1}^{N} u_{def}\, dS / A \quad [5\text{-}1]$$

where u_{rotor} is the rotor averaged flow speed, dS is the area segment of the rotor plane, A is the total swept area and u_{def} the velocity deficit along vertical and lateral traverses. The final estimate suffers from additive error progation, which for two uncorrelated/independent readings with associated errors da and db, can be calculated using $\sqrt{(da^2+db^2)}$. Here we shall assume that the measurement errors are in fact uncorrelated and each 2%. The uncertainty is combined to find that the total uncertainty of the observed deficit is approximately $\sqrt{(20(0.02)^2)} = 0.09$ or 9%.

From table 5-2 it is clear to see that the general trend of the data is followed well. However, while close to the rotor (x<8D) reasonable agreement is observed, it is clear that beyond that point, and after taking measurement error into account, the rotor averaged deficit is over-predicted by the models. However, it should be noted that the measurement error for each reading was conservative at 2% so the overall uncertainty attributable to the rotor averaged prediction may be greater.

Further trends can be observed whereby the difference between the upper bound and lower bound flow deficit for the far wake models decreases with increasing downstream distance. This is because, once the initial conditions are inputted into the model the effect of this input will diminish with increasing downstream distance as the equations transform the solution of the system spatially. In addition, the difference between the upper and lower bound predictions for the 3-d model is greater than the 2-d model such that one impact of increasing the model complexity is a greater increase in uncertainty of the final answer.

One of the largest errors when considering the results for $x \leq 8D$ and a 5% perturbation of the model inputs gives the 3d model at 8D whereby 0.2118/0.1681 gives a 25% error between model prediction and observed. When x > 8D then the results are not in as good agreement with observations and the outputs give a conservative estimate of the impact of the devices on the downstream flow speed. The preliminary studies in this section are extended in Section 6.

The rotor averaged deficit is a more rigorous test of rotor loading and therefore is the best metric to use as ultimately this value needs to be predicted in order to calculate the correct thrust C_t and power operating points C_p.

Not to be disclosed other than in line with the terms of the Technology Contract

Table 5-2: Table showing the rotor averaged deficit predictions made by the 2-d model and 3-d model when over and under-estimating the input parameters of thrust coefficient and turbulence intensity. The measured rotor averaged deficit is provided with uncertainty bounds.

Downstream distance	2-d under-prediction	2-d over-prediction	3-d under-prediction	3-d over-prediction	Rotor averaged deficit
4D	0.2866	0.3097	0.2924	0.3314	0.3300±0.03
6D	0.2193	0.2358	0.2294	0.2540	0.2193±0.02
8D	0.1821	0.1967	0.1850	0.2118	0.1681±0.02
10D	0.1587	0.1710	0.1611	0.1852	0.1411±0.01
12D	0.1410	0.1522	0.1448	0.1669	0.1146±0.01

5.8 Discussion of model validity, sensitivities and limitations

The Park, 2-d and 3-d models have been compared to data from multiple rotor experiments performed within the PerAWaT project. The start of the wake, s_0, was justified through comparison to the various data sets and the model was calibrated to the single-rotor tests performed in WG4 WP2.

The wake models have been shown to give good results when compared to scaled experiments with arrays of turbines. The Park model has given reasonable agreement while the 2-d models have been shown to give good predictions except for wake merging. For wake merging the 3-d model was shown to increase the model accuracy by incorporating the prediction of the multiple wake interaction within the core solver.

Different ambient turbulence intensities were investigated. For the WG4 WP3 investigations at different TI values it was seen that the rate of recovery could be dependent on geometry and rotor generated turbulence. For other investigations, in particular for the array scale experiments, when the turbulence intensity was increased on downstream rows, both the 2-d and 3-d model approximated the wake measurements well.

Here an overview of the assumptions is given and analysis of whether they produce reasonable results:

- Free-shear layer equations – Given that the models approximate the measurements well, this is the correct set of equations to solve for the problem at hand. In particular, assuming that the flow is predominantly in the axial direction, incompressible and the thin shear approximation gives good results.

- Unbounded – The boundary conditions applied to the 2-d and 3-d models have been found to be acceptable provided the flow is not laterally blocked. In this scenario the near wake profile and boundary conditions should be changed to account for this.

Not to be disclosed other than in line with the terms of the Technology Contract

- Eddy-viscosity model – In the 2-d model the rate of flow recovery has been well predicted, while the 3-d model appears to describe wake mixing and merging processes well, suggesting that the eddy-viscosity is a suitable closure model.

The current known limitations of the models are:

1. Further validation at different thrust coefficients and turbulence intensities is required. So far, high turbulence intensities are well modelled but low TI and low vertical blockage tests are not well predicted. This would be useful for the added turbulence model as well as the near wake model.

2. The model cannot emulate highly blocked channels. Investigation of inputting a modified near wake profile that better represents results in a very high recovery rate. Therefore, modelling high laterally blocked flows at present is not possible. This is not envisaged as an immediate problem as channels at real sites are typically wide enough such that lateral blockage is low.

3. Results from the wave current interactions in wave current interaction is not modelled. One solution could be to add a dependency on the model mixing parameters according to the wave number as deep water waves appear to result in faster wake recovery. This may merit further studying, however, waves only serve to increase recovery rate making the models conservative. The occurrence of deep water waves will be site dependent and the frequency at which these occur would typically be small.

4. The effects of large eddies on the wake recovery was not quantified. However, as discussed in section 5.1 and noted in (Ainslie, 1988) the wake models will over predict the wake deficit as the effect of large scale eddies will be to increase the rate of recovery. Comparison with field measurements from the ReDAPT project will allow us to quantify these effects.

5.9 Further work

The ReDAPT project will potentially provide data at different thrust coefficients which should allow further comparisons to aid model validation. Preliminary flow observations of the TGL device are given in figures 5-14 and 5-15. These are to be treated as preliminary results and should not be viewed as instructional. What can be seen is that there is roughly 50% wake deficit (although the operating point is not evaluated) and that this recovers rapidly to free-stream at around 7-8D downstream.

Figure 5-14 shows that the wake deficit in the vertical is well approximated by a Gaussian curve. As discussed, this data requires more thorough analysis as some of the measurements need to be referenced to other data sets. In addition, the ADCPs do not lie directly on the streamline of the wake.

However, what can be observed is that the centreline appears to follow a similar trend as seen in the experimental testing; the deficit recovery is quick and the shape of the near wake region is Gaussian in shape. In addition, these results now put the tidal industry in a similar position to the wind industry in terms of understanding the loadings, performance and wake effects of a device operating in real conditions.

One of the big unanswered questions of the PerAWaT project was whether the scaled testing would reflect the full scale device. We can clearly see that with data as shown in figure 5-14 and 5-15 these questions will be answered and that these answers will lend greater confidence to the models that have been developed through the PerAWaT project.

Not to be disclosed other than in line with the terms of the Technology Contract

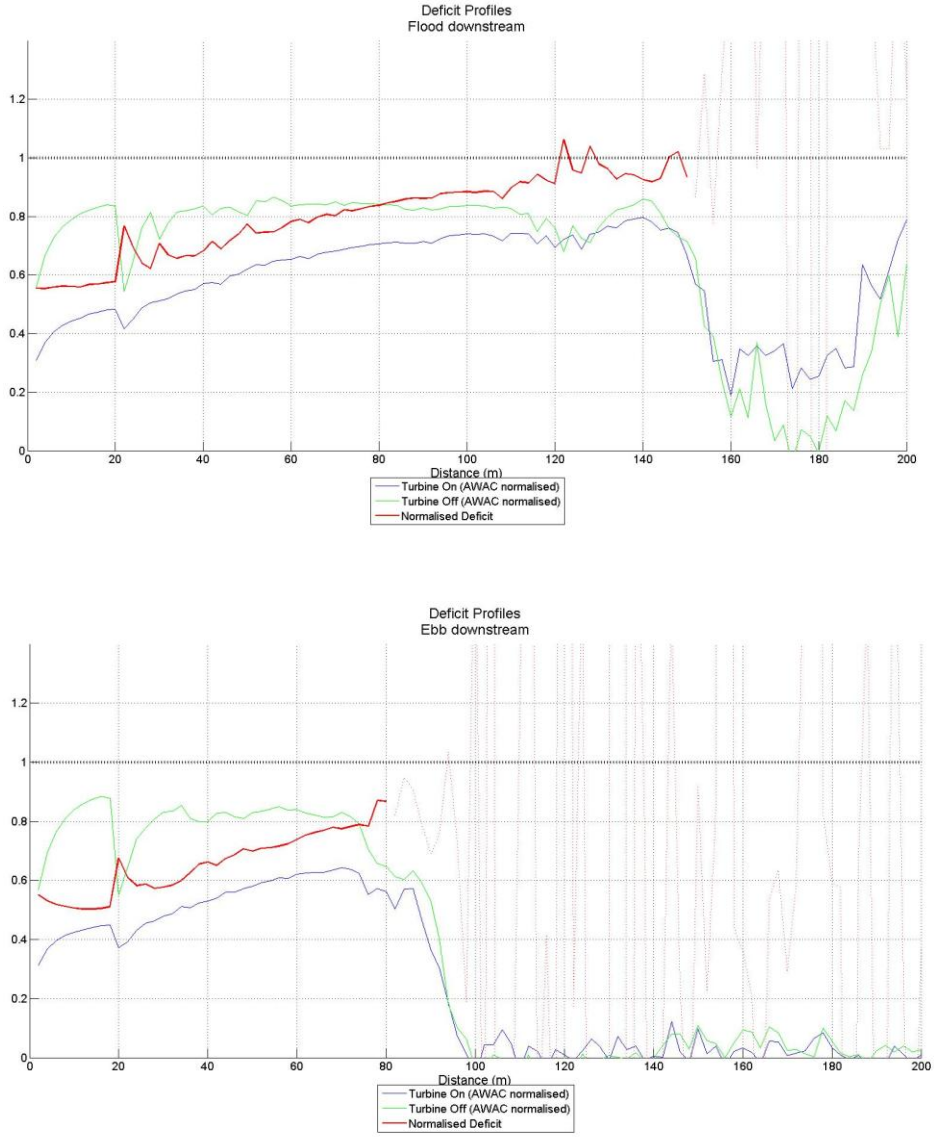

Figure 5-14: Centreline recovery for the flood tide (top) and ebb (bottom) of the TGL device. Measurements readdings taken by instrumentation on the TGL device are denoted green for fluid velocity when turbine is off, blue for when turbine is on and red gives flow deficit.

Not to be disclosed other than in line with the terms of the Technology Contract

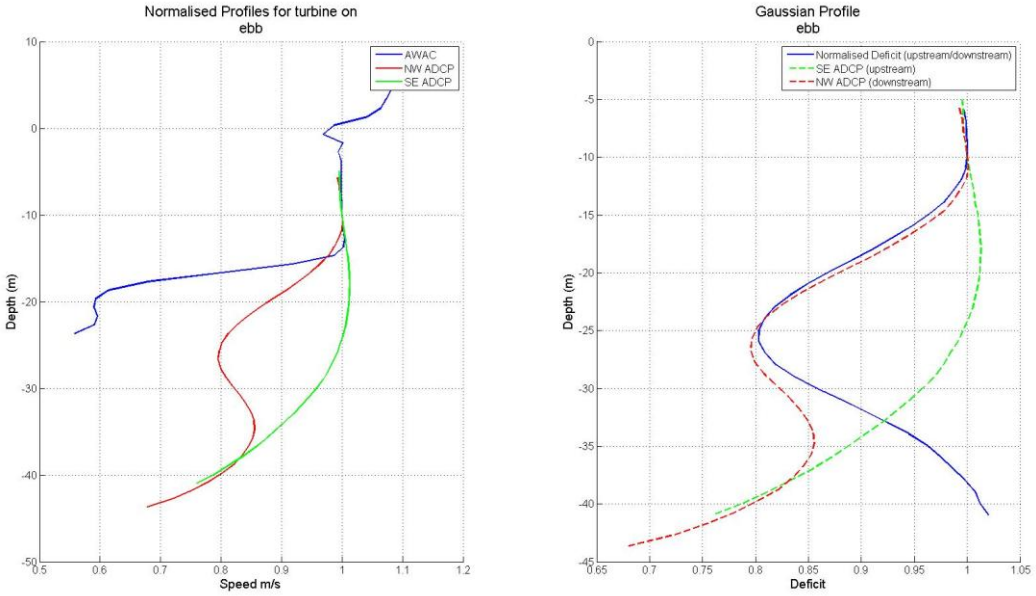

Figure 5-15: Vertical profiles taken at ADCP locations deployed downstream and upstream of the TGL rotor. Position of the devices is roughly 3D downstream of the devices. Right hand picture shows on/off profiles along with the normalised velocity when the device is operational.

Not to be disclosed other than in line with the terms of the Technology Contract

Not to be disclosed other than in line with the terms of the Technology Contract

6 ADEQUACY OF ARRAY SCALE MODEL

The numerical models that are combined within TidalFarmer are a simplification of the physical processes involved in tidal stream energy extraction. The approximations and assumptions made in the computer program make it possible to simulate a real world system at low computational cost. Whether the model is an accurate representation of the physical system requires careful assessment. The modelling framework must be examined to determine whether the models provide the practical insights that demonstrate that the current application is "fit for purpose".

The primary intention of TidalFarmer is to provide estimates of the long term energy yield of a Tidal project involving multiple devices (or 'Tidal Farm'). The modelling framework comprises a series of sub-models that are combined in order to arrive at an answer. Each of the sub-models makes assumptions concerning the environment and physics being modelled in order to arrive at an estimate. For instance, wake meandering, wave-current interactions, the drag generated by the tower and nacelle, may impact on the solution, yet at this stage have been neglected for simplicity. An order of magnitude assessment has been made to determine whether the model is missing important physics or if the focus should first be on reducing uncertainty in the model inputs.

This report presents a study using basic methods that allow us to assess the degree of uncertainty that it would be reasonable to attribute to the model outcomes. Given that TidalFarmer does not model every physical process, the following should be ascertained; first, whether the sub-models are sufficiently accurate to provide a reasonable assessment of the energy yield, second, quantify the uncertainties in the assessment, and third, to confirm that the uncertainties are not so large as to prevent an individual from achieving their objectives.

In the following sections, the system refers to the physical system (tidal flow, device operation, etc.) and related system properties (fluid velocity, thrust coefficient, etc.) that we wish to represent in the model or sub-model. The model refers to the assumptions and algorithms used to produce an estimate of a certain property of the system.

6.1 Methodology for assessing model uncertainty

TidalFarmer may be described as a simulation tool that takes inputs x and outputs an expected energy yield, $E = f(x)$. The function f, as described in Goldstein, *et al*, (2013) is a description of the way in which system properties determine system behaviour. In the complete model for a realistic site the inputs would be:

1. Bathymetry data.
2. Hydrodynamic model outputs.
3. Position and measured data provided by ADPs.
4. Flow speed bin specification.
5. The position of the devices, thrust and power curves as well as geometric information about the device such as hub height, rotor diameter.
6. Inputs to the wake modelling parameters as well as flow speed bin specification.

Not to be disclosed other than in line with the terms of the Technology Contract

In order to quantify the level of uncertainty of model outputs, a source of data, where the measurement uncertainty has been quantified is required. Our initial focus will be on tests A, B and C of the array scale experiments, (see Section 5, figure 5-4). This data set represents a steady state simulation of a rotor group, and the prediction for the inflow speed of downstream rotor groups by the model can be written as,

$u_{rotor} = f(C_t,\Lambda,u_h,\alpha,\nu)$

where we define the thrust coefficient C_t, turbulence intensity Λ, while α and u_h determine the power law fit and ν represents the wake mixing calibration constants.

The ability to predict the reduction in flow velocity using the wake models developed within TidalFarmer, and then comparison to measured data, is the primary focus of this study. The study itself will allow us to evaluate the model adequacy for predicting loadings on downstream rotors. Here a comparison is being made between the model and a scaled experiment and it is acknowledged that this may only partially represent reality. The scaled testing is reported in (Stallard *et al*, 2013) and will be informed through field measurements through other projects such as ReDAPT.

The simplest way to evaluate model adequacy is to make many model evaluations using a wide range of input parameters and analyse the impact of these on outputs. This a global method, known as a Monte-Carlo analysis, whereby a model is run repeatedly in order to gain an understanding of all the different possible outcomes. In ascertaining model adequacy the phrase model discrepancy is defined, which is the difference between the model properties and system properties.

Following Goldstein, *et al* (2012), the approach adopted is Bayesian such that we make a judgement on the potential uncertainty surrounding each input and then use this to assess the level of uncertainty in the model outputs. By relating our best current judgements to model inputs in a probabilistic form, all uncertainties can be drawn together into a common framework such that a probabilistic assessment can be produced. This assessment then represents the best current judgement of the expert in a form that is appropriate for use in subsequent decision analysis, such as independent energy yield calculations for example.

6.2 Sources of model uncertainty

The sources of uncertainty that are important for the study of model adequacy will be i) input of forcing function uncertainty, where it is unclear as to the appropriate value of the inputs at which to evaluate the model ii) functional uncertainty, the process whereby the system properties are transformed by the model into outputs, iii) general aspect, when we train the model against a certain data set and intend to use it in another application. TidalFarmer will be viewed as acceptable if model discrepancy is small. These are two basic sources of model discrepancy.

Internal discrepancies

The first is referred to as internal model discrepancy that can be quantified as part of the model output itself. A further sub-division of internal model discrepancy is defined.

The first type is due to a lack of precise knowledge of the input and model parameters. We judge that the model parameters are inappropriate to be specified as inputs as the model requires pre-calibration.

Not to be disclosed other than in line with the terms of the Technology Contract

A second aspect of internal model discrepancy lies in how the solution techniques, employed to arrive at a solution, transform the model inputs and the impact this has on the outputs of the model. This is sometime referred to as structural uncertainty. For example, when calculating the solution of the far wake the model inputs are used as both initial conditions and model parameters, and then a system of parabolic partial differential equations is solved using a Crank-Nicholson finite difference technique. At each time step a degree of error is introduced, however, with respect to mesh resolution the truncation error is known to be $O(dx^2)$. This allows the cumulative error to be understood.

An illustration is provided, through figure 6-1, showing how input and structural uncertainty can impact on the final result leading to discrepancy between the model outputs and system properties. Input uncertainty for the flow and the near wake profiles are represented by the red and green curves. Changes in the input from their 'real' value causes errors to propagate through the model. For the flow profile, this will be directly due to model inputs, however for the near wake model it is dependent on both thrust coefficient and turbulence intensity (see Section 3). Both the thrust coefficient and turbulence intensity are dependent on accurately resolving the upstream wake effects such as the increase in turbulence intensity and the decrease in flow speed. In order to calculate the wake affects, the far wake model is used to transform the near wake prediction into a deficit at all points downstream. The final profile, which is then compared to measured data, is a combination of the flow profile, the near wake and then finally the far wake model. In figure 6-1, this final profile is represented by purple lines, and represents the discrepancy between system and model properties arising from input and structural uncertainty.

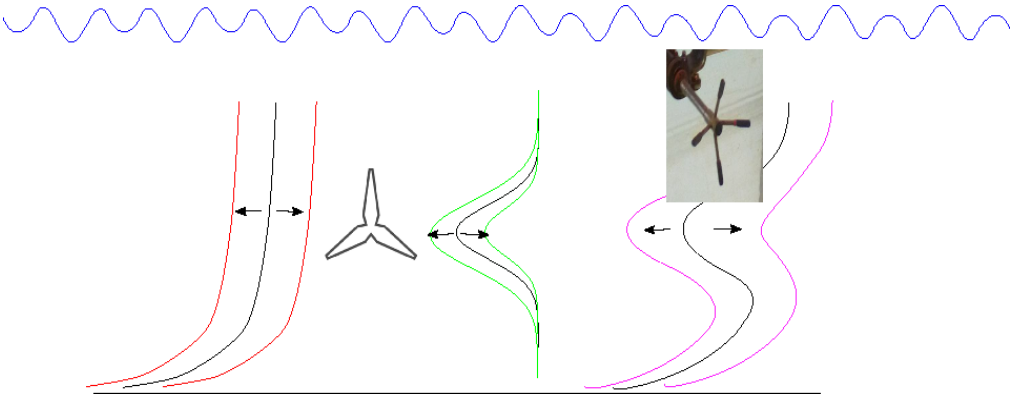

Figure 6-1: Depiction of the combined effects of internal model discrepancy on final velocity profile. Red curves represent input uncertainties for the flow profile, the green curve represent model uncertainties of the near wake. Purple curves show the combined model discrepancy between a measured inflow profile and model prediction.

To understand internal model discrepancies, thought experiments of model behaviour can be performed, whereby we consider how inputs are transformed by the equations into an output. If we want an order of magnitude assessment of the internal model discrepancy then a simplistic model can be used to provide us with valuable insight into changes in the model behaviour in response to different values of various input parameters. For example, we can use the simple fact that the wake recovery scales with the reciprocal of the downstream distance and then use this first order assessment of the wake deficit to scale the free-stream velocity u_0, resulting in a value for the downstream flow speed u using the following equation,

$u = u_0 (1- k C_t /(x - x\_0)^n)$ for $x > x_0$

Not to be disclosed other than in line with the terms of the Technology Contract

here we define x_0 to represent a calibration constant, n is a value the type of wake flow, such as a plane or axisymmetric wake (Pope, 2000), and k is some dissipation parameter that can be used to fit to measured data. The leading order terms in the velocity deficit are the flow speed u_0 and then the thrust coefficient C_t. While this is a gross over-simplification of the actual model, we have represented the flow profile, the near wake and far wake model in this one-line equation. We can see that the flow speed will be corrected by the downstream distance, turbulence dissipation parameter and the thrust coefficient. The impact of the thrust coefficient diminishes with downstream distance as this is an initial condition and as the flow recovers the dependence on the input becomes negligible because $1/(x - x\_0)^n \rightarrow 0$ as $x \rightarrow \infty$. However, the dependence on the flow speed velocity will always remain. A number of conclusions can be drawn; first, the flow speed inputs will have a strong impact on the model discrepancy and second, ii) the importance of the thrust coefficient decreases with increasing downstream distance.

External discrepancies

The second aspect of model discrepancy arises from external features that we cannot quantify by directly evaluating the model. This may for instance be represented by physical processes that we acknowledge are not explicitly modelled in TidalFarmer - for instance, large scale turbulence, the effect of global blockage on the performance of the array etc. Provided that appropriate model inputs are used to evaluate the system, the sum of the measurement error, internal and external discrepancies would equal the total error. Assuming that the measurement error and internal model discrepancies are quantified, any further lack of fit will be a guide to external model uncertainty.

6.3 Model discrepancy

Our uncertainty specification is formulated as

$$\varepsilon = y - f(x^*)$$

where ε is the model discrepancy, y is the 'true' value of the unobserved system output and f the present value of the system when forced by the appropriate representation of the actual system properties x*. An approximate 'true' value for y can be observed through scaled testing. As discussed above the model outputs will be compared to the measured rotor-averaged flow speeds from scaled testing and so,

$$u_{rotor} = y - e$$

where u_{rotor} is the measurement of y and e is the associated measurement error. In line with our discussion, the overall model discrepancy is decomposed into a sum of the internal model discrepancy ε_I and the external discrepancy ε_E

$$\varepsilon = \varepsilon_I + \varepsilon_E.$$

The internal discrepancy accounts for the uncertainty in predicting the input parameters as well as errors relating to how inputs and parameters are transformed by the model. The external discrepancy represents all other discrepancy, except measurement error e, such that

$$u_{rotor} = f(x^*) + \varepsilon_I + \varepsilon_E + e.$$

Not to be disclosed other than in line with the terms of the Technology Contract

We regard the discrepancy and error terms, ε_I, ε_E and e to be uncorrelated random quantities each with expectation zero and respective variance σ_I^2, σ_E^2 and σ_e^2 respectively. The implausibility I(x) of a model input x is defined to be

$$I(x) = \max |u_{rotor} - f(x)|/\sigma \quad [6\text{-}1]$$

where

$$\sigma^2 = \mathrm{Var}[u_{rotor} - f(x^*)] = \sigma_I^2 + \sigma_E^2 + \sigma_e^2 \quad [6\text{-}2]$$

This definition of I(x) is most stringent, demanding that none of the observed model outputs fails the criterion set out in eq. 6-1. Previously (section 6.2) uncertainty and model discrepancy were discussed. The implausibility statistic is a combination of both these quantities that helps assess whether the model is adequate, by simultaneously analysing the accuracy and dispersion of model outputs. If the model is accurate then the numerator $u_{rotor} - f(x^*)$ should be small, likewise if the model predicts wildly different results for different input values then the dispersion or denominator σ, will be large. This dispersion is related to the uncertainty, because the information that is required is a degree of certainty that, if a tidal farm were to constructed, then the upper and lower bounds on energy yield take a certain range.

In order to understand what value of I(x) should be assigned as a tolerance to define implausibility, we specify the probability of a `failure' as

$$p = P[I > m \mid x = x^*] = 1 - (2\Phi(m) - 1)^N \quad [6\text{-}3]$$

where Φ is the cumulative distribution function of the standard normal distribution and N is the number of model outputs that are compared to observations. Hence, m is chosen so that the probability p in eq. 6-3 is small. Inverting the relationship we find that

$$\Phi(m) = \tfrac{1}{2}\,(1 + (1-p)^{1/N}).$$

When $N \geq 3$, and $p \sim 0.01$ then $m = 3.0$. Thus an input is implausible if $I > 3$. Indeed, we are only interested in the case where we input values to the models that accurately represent system properties. If all the inputs to the model are found to be implausible, when applying the Monte-Carlo analysis, then the message is that there is something missing in the physics of the model. This is because the model has transformed system properties to an output value that is not correct. Otherwise, if all inputs are observed to be plausible then this suggests that greater effort should be made in quantifying the uncertainty in measurements of the relevant input parameters.

6.4 Assessment of model adequacy

In this section, the different tests that will be analysed are discussed in order to assess model performance. The model is compared to a variety of experimental tests (test A, test B and test C) as discussed in Section 5 (figure 5-4) that assess the functionality of the model including the ability to model staggered rows and the impact of closely spaced devices in the longitudinal direction. Experimental measurements will be used as inputs to the model and compared to the model outputs. This tests whether the system can transform system properties into a result that is close to the experimental observations.

Not to be disclosed other than in line with the terms of the Technology Contract

Second, for each of the experiments, the model is evaluated repeatedly while varying the input parameters using a Monte-Carlo technique such that the input space is fully explored. The outputs are compared to the experimental measurements in order to assess the internal model discrepancy. A best current judgement is made in how much to perturb the input variables by, in order to account for epistemic uncertainty and measurement error. If parameters are badly predicted, then the errors will aggregate potentially increasing the error in the output. In this case, the measurement error for thrust coefficient was observed to be ±5 % while for flow speed and turbulence intensity it is ±2-5%. This dictates that we should associate a higher uncertainty to inputs when evaluating the model. Once the simulations have been undertaken, the discrepancy between the model outputs and experimental outputs is evaluated and an implausibility test is then specified to determine model adequacy.

6.4.1 Observational uncertainty

To quantify the uncertainty of the measurement error, an understanding of the errors in the flow velocity readings and the thrust coefficient is required. A type A standard uncertainty for measurement error is typically obtained by calculating the sample standard deviation (JCGM, 2008). In this way, if the experiment is repeated, then future sample means should lie within one standard deviation of the observed mean. For time series data, where the mean of the readings is the measurement required, the analysis described above is not applicable. As reported in WG4 WP2 D4, the 60s sample mean converged to within ±2% of the 90s sample mean. In addition, it was found that the thrust measurements also varied by around ±5% of the 90s sample. If the 90s sample is assumed to be the population mean, then to have converged within ±2% for repeated measurement campaigns shows evidence of repeatability and that future measurements may be observed to lie within this interval. Therefore, without performing further analysis it is assumed that ±2% represents our standard uncertainty for flow speed measurements.

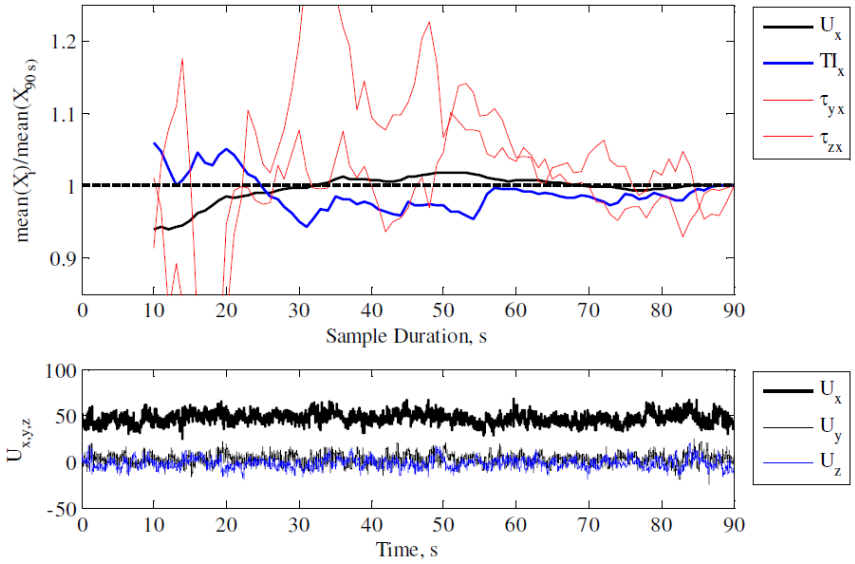

Figure 6-2: Convergence of mean values (of Ux, TIx and Lateral and vertical Reynolds stresses) with sample duration for a continuous 90 s sample at 200 Hz.

To calculate the rotor averaged flow velocity, a weighted average was used such that flow speeds along vertical and lateral traverses were multiplied by the corresponding area segment using eq. 5-1. The uncertainty attributed to this measurement is the root mean square of the uncertainty of each

Not to be disclosed other than in line with the terms of the Technology Contract

measurement made to predict the velocity deficit. Therefore, in the case where 20 bins are used, and assuming that each flow measurement has an uncertainty of 2%, then if lateral and vertical measurements are used the uncertainty is approximately 9% (see Section 5-7). In regions where only lateral traverses were used the error is around 6%. These estimates give an under-estimate, as in some cases a 5% measurement uncertainty was attributed to flow speed observations.

6.4.2 Investigative case

In the following study the model is evaluated using inputs that best describe the system, for each of the experimental tests. This allows us to examine the discrepancy between the models, assuming no uncertainty in the measurement data and no model discrepancy. The placement of the devices and inflow is provided by the experiments discussed in Section 5 and presented in figure 5-4. The model takes the experimental inputs of the calibrated power law profile, operating thrust and turbulence intensity, and then, using the wake models, will output a prediction of the inflow to the last row of turbines for each test case.

The inputs that best describe the experimental test were observed (from experimental measurements) to be a thrust coefficient of 0.88 for both the first and second row of devices, the turbulence intensity for the first row were observed to be 10%. For subsequent rows this increased due to added turbulence for the upstream rows. This only affects the results of the test C where u_{rotor} is calculated for the final row. In this case the second row turbulence intensity inputs over the rotor plane were informed from experimental observations and set to be symmetric across the rotors Y= -2.25, -0.75, 0.75, 2.25 and took values 17, 24, 24, 17 % respectively. The shaping parameter used for the power law profile (defined in equation 4-1) was N = 1/10.6 and the maximum flow speed was set to $u_h = 0.5067$.

The results of these studies are presented in table 6-1, where the predicted rotor averaged velocity has been calculated using both the 2-d and 3-d wake models (see Section 5). The results have been compared to the laterally averaged flow speeds observed in the experiments, calculated in eq. 5-1 and denoted Ux(Yav). The observations of laterally and vertically averaged inflow in test A, for the rotors Y = -1.5D, 0.0D and 1.5D were found to be 0.3797, 0.3767 and 0.3838 m/s respectively. It is clear that for the aligned case there is very good agreement across both models and between the different methods of deriving the rotor inflow speed from measurements, where possible. The one result of note is at Y=-2.25D where the experimental reading shows some asymmetry in comparison to the models and the reading at y = 2.25D. Given the symmetry in the experiments it is expected that these values should also be similar, yet it disagrees by roughly 5%.

Although in other experiments, only the lateral traverse can be used to predict the deficit, as no vertical measurements were made in the relevant positions; it appears from test A that the two approaches yield similar answers.

Not to be disclosed other than in line with the terms of the Technology Contract

Table 6-1: Tabulation of model outputs using 2-d and 3-d wake models and observations for the three separate experiments. Dark blue represents the inflow to second row of the aligned test (test A), pink is the inflow speed to the second row of the staggered case (test B) and purple is the inflow to the last/third row of the large staggered formation (test C). All units are m/s.

Downstream of:	***1 row of 3turbines/devices***			*2 rows 3 then 4 devices at 4D*		
Rotor positions	*At 8D*			*At 4D: row 3 inflow*		
Y	*2-d*	*3-d*	*Ux(Yav)*	*2-d*	*3-d*	*Ux(Yav)*
-3.0D				*0.4200*	*0.4180*	*0.4278*
-2.25D	*0.4301*	*0.4258*	*0.4063*			
-1.5D	*0.3827*	*0.3873*	*0.3762*	*0.3091*	*0.3263*	*0.3015*
-0.75D	*0.4007*	*0.3836*	*0.3729*			
0	*0.3827*	*0.3810*	*0.3689*	*0.3098*	*0.3258*	*0.3126*
+0.75D	*0.4006*	*0.3838*	*0.3729*			
+1.5D	*0.3827*	*0.3873*	*0.3820*	*0.3092*	*0.3258*	*0.3078*
+2.25D	*0.43042*	*0.4298*	*0.4205*			
+3.0D				*0.4206*	*0.4184*	*0.4287*

6.4.3 Small aligned array – test A

Here a Monte-Carlo type study is undertaken to quantify the overall contribution of the internal discrepancy σ_I to the total model discrepancy. This will be achieved by perturbing different features of the model and focusing on how they perturb the output deficit on downstream rows. In this study, both the measurement error σ_e and the external model discrepancy σ_E are set to zero. If implausible inputs are observed, then using the most implausible, an estimate for both the measurement error and external discrepancy for which the input would then be plausible is made. This is achieved by rearranging eqs. 6-1 and 6-2 such that

$$\sigma_E^2 + \sigma_e^2 = (\max |u_{rotor} - f(x)|)/ I(x)^2 - \sigma_I^2 \quad [6\text{-}4]$$

To illustrate the approach adopted; the thrust coefficient, turbulence intensity, power law, and speed adjustment are individually perturbed. The case where all parameters are perturbed together is also considered.

Not to be disclosed other than in line with the terms of the Technology Contract

An example is provided by investigating changes in $C_{t,}$ by replacing the thrust coefficient variable with η C_t. Here the random variable η is drawn from a normal distribution such that E[η] = 1 and SD[η] = p, that corresponds to a small percentage in change of the input value. Thus, we will obtain inputs for the thrust coefficient of the form E[η C_t] = C_t and SD[η C_t] = pC_t. In this and all other Monte-Carlo simulations p = 0.1. This perturbation accounts for both input uncertainty (based on measurement error) and structural uncertainty whereby errors propagate resulting in incorrect input values for downstream rows. None of the perturbed inputs are believed to be implausible (i.e. no negative turbulence intensities have been inputted into the simulation)

Figure 6-3 shows the results of n_{sims} = 500 simulations and the variation in model outputs (prediction of rotor averaged flow speed) due to perturbing the input for the thrust coefficient. In this scenario the thrust coefficient was perturbed by p = 0.1, such that 70% of the time the input value lies within a tength of its original value. From inspection of table 6-1 typical values of u_{rotor} for this experiment are approximately 0.37-0.38 m/s. The results therefore show a bias to over predict the flow speeds.

From visual inspection the model outputs vary between 0.37-0.40 m/s. Therefore, the final distribution has a standard deviation of 0.0114 m/s. Normalised to obtain a percentage of the rotor averaged in flow speed gives a 0.0114/0.37 ~ 3-4 % standard deviation of the flow speed. Therefore, from a perturbation of 10% of the input thrust coefficient the resulting distribution of model outputs has a standard deviation of 3-4% of the value of u_{rotor}. To investigate the form of the outputted distribution a histogram of the flow speeds has been plotted in figure 6-2 which follows the shape of the normal distribution.

Further information from the simulations can be obtained by calculating the normalised error of the model predictions, or $1 - f(x)/u_{rotor}$ and plotting this value against the inputted value. This analysis is presented in figure 6-2 where each of the input parameters, in turn, has been perturbed by 10%. So, for instance in the thrust coefficient sub plot, only thrust coefficient has been perturbed, while all other inputs were held constant to the same values defined in section 6.4.2.

Not to be disclosed other than in line with the terms of the Technology Contract

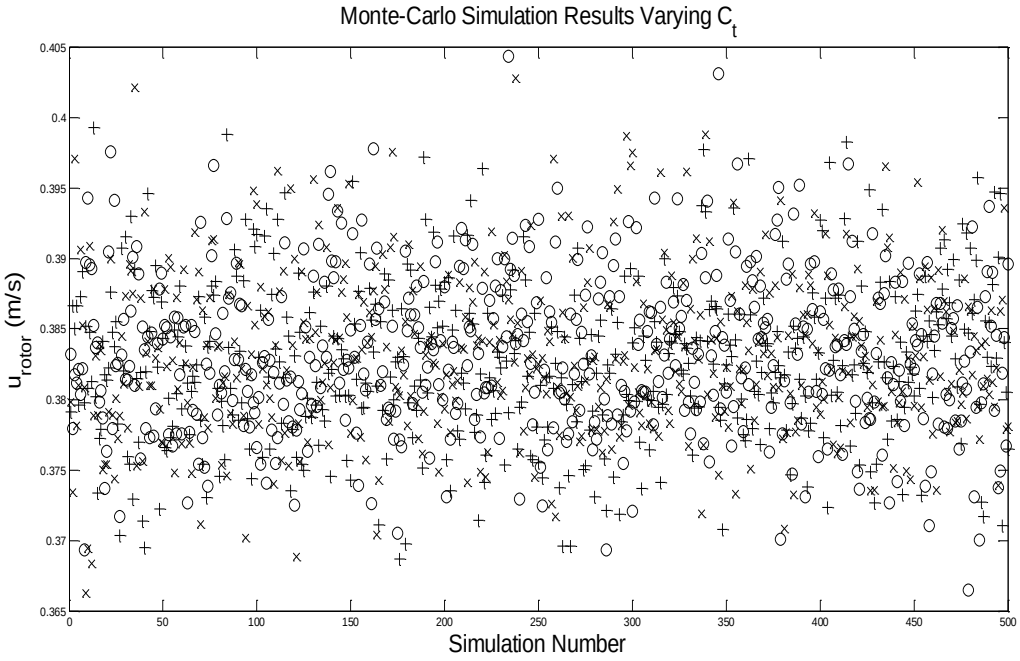

Figure 6-2: Monte-Carlo simulation predictions for u_{rotor} when thrust coefficient input is randomly perturbed. The randomness of the model input is reflected in the outputs.

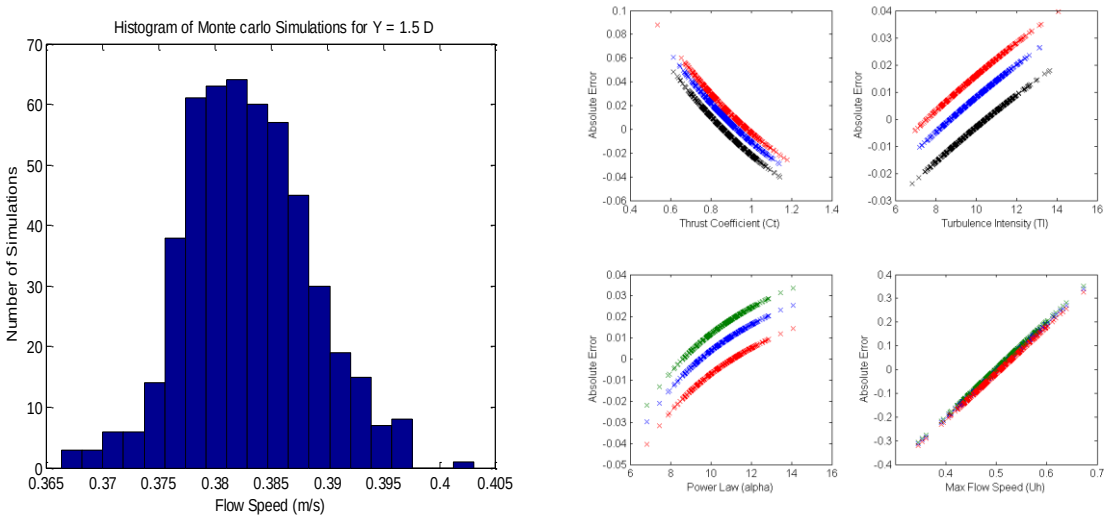

Figure 6-2: Histogram of u_{rotor} predictions from Monte-Carlo simulations shows a normal distribution (figure on left) and absolute error of model outputs against input value (figure on right).

The results are in line with intuition. As the value of thrust coefficient C_t is increased, the velocity deficit grows and this means the model begins to under-predict the experimentally observed value. Likewise for investigation into the turbulence intensity TI parameter it is observed that an increase leads to an over-prediciton of the flow speeds. From variation in the power law shape profile $N = 1/\alpha$ the relationship is not linear and reflects the non-uniform shape of the flow profile. It is noted that, the input value for both thrust coefficient and turbulence intensity are varied for each rotor separately. In

Not to be disclosed other than in line with the terms of the Technology Contract

the case of the velocity profile, only one input parameter is being varied. The differences between the u_{rotor} predictions is due to asymmetries in the experimental data and the symmetry in the model outputs. The final input parameter that was perturbed was u_h. For a perturbation of p = 0.1, the variation in the absolute error is much greater for this parameter than for all the other model inputs.

A second more detailed study was undertaken. The results of n_{sims} = 3000 simulations, for each of the inputs parameters discussed above, for both the 2-d and 3-d model are presented in table 6-2. The model outputs for the rotor average speed were compared to the vertically and laterally averaged measurements of the inflow to the rotor. This gave an estimate for the internal discrepancy which is presented in table 6-2. We can see that the greatest sensitivities lie with the parameter u_h, whereby the variation is approximately 10% of the flow speed at the downstream rotors. In addition, the thrust coefficient is also a sensitive parameter such that a 2% variation is found. For the other parameters we find that the turbulence intensity and power law shaping parameter produce a 0.8 % variation in the final output.

Table 6-2: Tabulation of model outputs using 2-d and 3-d wake models and observations for test A. Results for the internal discrepancy, for each rotor, proportion of implausible inputs and the required variance in external discrepancy and measurement error for all simulated inputs to be plausible.

	Internal discrepancy, $\sigma_I = \sqrt{Var[f(x) - u_{rotor}]}$ (m/s)			Proportion of implausible inputs	(m/s)
2-d model	Y = -D/2	Y = 0	Y = D/2	P(I(x)>m|x=x*)	Max($\sigma_E + \sigma_e$)
C_t	0.005682	0.005670	0.005699	0.018667	0.009136
Λ	0.002363	0.002414	0.002323	0.118667	0.003718
α	0.002886	0.002886	0.002886	0.060000	0.003632
u_h	0.038081	0.038081	0.038081	0.003222	0.031275
All	0.038081	0.038704	0.038505	0.003889	0.032600
3-d model					
C_t	0.009591	0.009616	0.009515	0.006222	0.010128
Λ	0.002769	0.002269	0.002744	0.177222	0.003887
α	0.002725	0.002682	0.002725	0.168556	0.004100
u_h	0.038282	0.037659	0.038282	0.002222	0.034225
All	0.039282	0.038998	0.039694	0.001889	0.040209

The 3-d model shows similar results although with a higher sensitivity to the thrust coefficient. In addition, model implausibility has not necessarily improved with the level of modelling.

Not to be disclosed other than in line with the terms of the Technology Contract

For this test, the measurement uncertainty is 9% (Section 6.4.1), thus it is expected that future observations of the flow speed would lie within the range 0.3767±0.033 m/s. In addition, if an estimate of $\max(\sigma_E + \sigma_e) > 0.03$ then the model discrepancy is greater than observational error and therefore the external discrepancy must be non-zero.

If implausibility of inputs is tested then it is found that the parameters with the least sensitivity are also the most implausible inputs. However, upon examination of the external discrepancy and measurement error via eq. 6-4, it is then seen that these inputs are in fact plausible to within measurement error. For instance, in the case of turbulence intensity in the 3-d model we see that 17.7 % of the runs result in implausible inputs. However, by calculating the combined external discrepancy and measurement error according to eq. 6-4, an estimate is found for $\max(\sigma_E + \sigma_e) = 0.003887$ m/s. This is around 1% of the rotor averaged velocity predicted from the experimental data and within the potential 9% (or 0.03 m/s) experimental uncertainty.

Results from simulations where all model parameters are randomly drawn from normal distributions, result in the occurrence of a small number of implausible inputs. These are again within experimental uncertainty except in the 3-d model case, where there must be an implausible input that can only be explained by a loss of physical modelling. In most cases, it can be seen that the internal discrepancy, when varying all parameters, is comparable to the internal discrepancy when varying just u_h.

Following on from the discussion given in section 6.3, the order of the model error was found to scale like $\sim k\, u\_0\, C_t/(x\text{-}x\_0)^n$. Therefore, if the model parameters are perturbed, u_0 by a random variable η and C_t by another random variable ζ both with expectation 1 and variances of p and q respectively then we observe that the variance of the internal model discrepancy will behave as follows

$$\sigma_I^2 = p^2 - (k\, pq/(x\text{-}x\_0)^n)^2.$$

This then means that the magnitude of the internal discrepancy is primarily dictated by the flow speed and that the wake modelling is a secondary effect. If p, q = 0.1 then it is found that $\sigma_I^2 \sim 0.10$ dependent on the downstream position. This prediction holds well in the aligned case as it predicts the centreline velocity well.

In staggered or off-centre layouts the wake width and wake merging algorithms would then bring a level of model uncertainty that is not easy to quantify using analytical expressions as there are many variables. This is because the velocity deficit between two centrelines is dependent on both the wake width, the distance from the centrelines and the wake merging algorithm plus upstream affects. This does not account for the sensitivity to minor parameters such as the turbulence intensity and the flow profile shape parameters.

In the 3-d model, where an attempt to resolve the wake mixing by solving for the entire flow field implies that the velocity deficit between two centrelines is then a function of the domain geometry, model parameters, the flow gradients across the shear layer and the magnitude of the deficit. This cannot be readily expressed using a simple analytical formula. To quantify all these effects in one study is best approached using a Monte-Carlo type method as implemented above.

6.4.4 Small staggered array – test B

A Monte-Carlo analysis will be used to examine the wake merging functionality of the TidalFarmer models. The input parameters were again drawn randomly from a normal distribution with expectation 1 and standard deviation p = 0.1. For this series of experiments the measurement for the rotor averaged

Not to be disclosed other than in line with the terms of the Technology Contract

flow speeds were found to be roughly 0.3729±0.02 m/s (see table 6-1) for the central rotors (Y = -0.75D, 0.75D) and 0.4205±0.03 m/s for the outboard rotors (Y= -2.25D, 2.25D).

From table 6-3 calculation results for the 2-d model show that the thrust coefficient, turbulence intensity and the power law shape profile parameters were almost all observed to be implausible inputs. The maximum combination of measurement error and external discrepancy however was found to be within measurement error, which in this test was 6% (0.02-0.03 m/s). A familiar pattern is also observed with respect to the sensitivity of input parameters with the flow speed and thrust coefficient being the most important input parameters. It is particularly worthy to note that an insensitivity to the thrust coefficient means that accounting for blockage may not be as important as previously thought.

Table 6-3: Tabulation of model outputs using 2-d and 3-d wake models and observations for test B. Results for the internal discrepancy, for each rotor, proportion of implausible inputs and the required variance in external discrepancy and measurement error for all simulated inputs to be plausible. All units are m/s.

	Internal discrepancy, $\sigma_I = \sqrt{Var[f(x) - u_{rotor}]}$ (m/s)				Proportion of implausible inputs	(m/s)
2-d	Y = -2.25D	Y = -0.75D	Y = 0.75D	Y = 2.25D	$P(I(x)>m\|x=x^*)/n_{sims}$	$Max(\sigma_E + \sigma_e)$
C_t	0.003969	0.004189	0.004235	0.003883	0.832417	0.013822
Λ	0.000573	0.000915	0.000915	0.000563	1.000000	0.010332
α	0.002860	0.002664	0.002664	0.002863	0.921250	0.011172
u_h	0.043499	0.040522	0.04052	0.043534	0.007000	0.053011
All	0.043499	0.040860	0.040823	0.043726	0.007833	0.053119
3-d						
C_t	0.006490	0.008099	0.008250	0.005981	0.159583	0.011499
Λ	0.000964	0.001229	0.001292	0.000774	1.000000	0.007492
α	0.002848	0.002566	0.002567	0.002874	0.826000	0.008486
u_h	0.043802	0.039463	0.039475	0.044207	0.004917	0.035001
All	0.044270	0.040248	0.040108	0.044419	0.004333	0.039967

The 3-d model in this test shows an improvement over the 2-d model. While the turbulence intensity and the flow profile shape parameters are predominantly implausible inputs (to within measurement error it is found that they are plausible) the thrust coefficient inputs are now primarily plausible. This perhaps reflects that the model is better at resolving the wake between rotor centrelines.

Not to be disclosed other than in line with the terms of the Technology Contract

It is observed, from table 6-3, that the thrust coefficient does not have as large a variation in these tests as before. Again this relationship is linked to the interaction between the two models, where the magnitude of the inflow centreline deficit is fed into the far wake model and then recovers the flow to free-stream. Thus, given the staggered formation, where the centreline deficit is not as important as wake mixing, less response to the value of this parameter is found and the relationship is mirrored by the results.

When perturbing all the parameters, or varying the flow speeds for both the 2-d and 3-d models we observe the occurrence of a small number of implausible parameters. The external discrepancy is not zero in these cases and is approximately twice the magnitude of the measurement error. This however, can be explained by the observed flow speed at Y= -2.25D, that was shown to be asymmetric, in table 6-1, for test B, leading to a small number of non-zero external discrepancies.

6.4.5 Large staggered array – test C

The large staggered formation allows a reasonable stress test of the model. Whereas in the previous tests the rows were 8D apart, here they are only 4D, which means that the flow will essentially be in full recovery when a further row is initialised. In addition, the sensitivity to thrust coefficient may be expected to increase as the wake model will not have had sufficient time to `wash out' the initial condition.

From table 6-1, the measurement error in this set of experiments for the rotor averaged flow speeds was found to be roughly 0.30±0.02 m/s (see table 6-1) for the central rotors (Y = -1.5D, 0.0D, 1.5D) and 0.42±0.03 m/s for the outboard rotors (Y= -3.0D, 3.0D).

Concerning the 2-d model, it is observed from the results shown in table 6-4, the impact of the sensitivity to thrust coefficient is seen to be larger than in the small arrays. Again the turbulence intensity and power law shape parameters do not show as much sensitivity. A further interesting observation that is that the outermost devices show the least sensitivity to inputs of thrust and turbulence intensity, presumably as they are in the wake flow of only the second row of devices and are not as sensitive to the initial conditions of the system inputs.

The 3-d model shows a greater sensitivity to the thrust coefficient than the 2-d model. There is also a higher proportion of implausible inputs for the 3-d model. In fact, it is observed that the external discrepancy plus measurement error calculated from results using the 3-d model is generally greater than for the 2-d model and this has been observed for all the different tests. However, this discrepancy is usually within experimental uncertainty. We also see a similar trend concerning the position of the rotors. For instance, the outer rotors are shown to be less dependent on input parameters then central rotors as they are impacted by the downstream effects of two rows of rotors.

This last case highlights an interesting point that as wake effects become more significant the sensitivity to the input parameters grows. Therefore, while in the immediate future the most important aspect to focus on appears be flow speed, when calculating losses there will be further work required in order to understand the wake impacts of larger farms as this becomes increasingly dependent on other wake modelling parameters.

As a final note, as in test B, it is seen that there exist implausible inputs whose combined external discrepancy and measurement error are of the same magnitude or greater than the experimental uncertainty. For instance, when we perturb the flow speed for the 2-d model we observe that 0.34% of the inputs are implausible and that the largest discrepancy is 0.030264 m/s. Through the presentation of the data we have lost information concerning which observation and model output were compared

Not to be disclosed other than in line with the terms of the Technology Contract

to arrive at this answer. While it is not clear what exactly has caused the implausible input we can argue that these are observed for such a low number of cases and that it is within twice the measurement uncertainty. Only further investigations will reveal whether this is a modelling error or otherwise. However, it is clear that there is large sensitivity to flow speed and so if this input is incorrect by a large amount the final result will also be incorrect.

Table 6-4: Tabulation of model outputs using 2-d and 3-d wake models and observations for test B. Results for the internal discrepancy, for each rotor, proportion of implausible inputs and the required variance in external discrepancy and measurement error for all simulated inputs to be plausible.

	Internal discrepancy, $\sigma_I=\sqrt{Var[f(x) - u_{rotor}]}$ (m/s)					Proportion of implausible inputs	(m/s)
2-d	Y = -3.0D	Y = -1.5D	Y = 0.0D	Y = 2.25D	Y = 2.25D	$P(I(x)>m\|x=x^*)/n_{sims}$	$Max(\sigma_E + \sigma_e)$
C_t	0.005405	0.006458	0.006227	0.006432	0.005305	0.034067	0.009051
Λ	0.000706	0.002288	0.002289	0.002319	0.000688	0.532867	0.004346
α	0.002831	0.002083	0.002088	0.002084	0.002835	0.330600	0.006410
u_h	0.042896	0.031564	0.031635	0.031579	0.042950	0.003400	0.030264
All	0.043252	0.032380	0.032342	0.032420	0.043389	0.002933	0.029860
3-d							
C_t	0.007767	0.010143	0.009651	0.009948	0.007740	0.106733	0.017729
Λ	0.000695	0.002590	0.002348	0.002582	0.000698	0.998200	0.010548
α	0.002815	0.002197	0.002194	0.002197	0.002817	0.893067	0.009687
u_h	0.042051	0.032823	0.032780	0.032774	0.042088	0.006200	0.031628
All	0.042577	0.034292	0.034055	0.034360	0.042843	0.006267	0.034344

6.5 Conclusions

While a simplified model of the dependencies in fluid flow reduction of the centreline helped quantify the internal model discrepancy, it is difficult to understand the impact on the wake merging between the centreline velocity deficits as these are dependent on many parameters. Therefore, the approach that has been adopted is to test model sensitivity to the various input parameters by repeatedly evaluating the model by using a space filling algorithm of the model inputs and then test against experimental evidence. Here we have made an order of magnitude assessment of the overall model

Not to be disclosed other than in line with the terms of the Technology Contract

adequacy accounting for measurement error and internal discrepancy in the way inputs are transformed into outputs by the system and then external discrepancy whereby we acknowledge limitations in the physics.

The models that have been developed and combined to produce the TidalFarmer methodology are relatively simplistic in comparison to state of the art CFD software programs and allow us to understand the process of energy extraction and the simple relationships between the physical parameters being modelled. This has allowed us to perform a detailed analysis of the models making many evaluations at a wide range of values and then quantify the model discrepancy, both through examination of the model outputs but also comparison against a range of experiments that test the physics of energy extraction.

A general trend has been observed whereby the external discrepancy plus measurement error is greater for the 3-d model than the 2-d model. This should perhaps serve as a lesson that, by increasing the complexity of a model, it does not necessarily decrease the uncertainty around the outputs. In fact, in the case of the 3-d model, an erroneous input will propagate through the mesh and so will have a greater global impact. In comparison, the 2-d model is a much simpler description of the problem and the uncertainty attributable to model outputs is less.

Furthermore, the parameters that are the most sensitive are the flow speed and thrust coefficient. The turbulence intensity and power law shaping parameters tend to have less influence on the final result. In conclusion, the model has been found to be adequate and that implausible inputs can be explained via a lack of inclusion of the measurement error in the calculation, an asymmetry in experimental output or a genuine sensitivity to an input value. The perturbation of the flow speed is roughly in line with the internal model discrepancy while the thrust coefficient was also found to be a reasonably sensitive parameter.

The model was tested against flow speed measurement taken of scaled rotors operating in an idealised channel geometry in steady conditions. While these have been argued to be representative of full scale, the next goal should be to assess model adequacy against field measurements of operational devices or arrays in order to check that the model is still adequate. However, the experiments have been analysed and it is thought that they are representative of the full-scale conditions such that they test the model in idealised conditions to the best of their ability.

Assessment of the model adequacy leads us to conclude that the model is fit for purpose and that efforts would be better spent on quantifying the uncertainty around particular model inputs. Above all, flow speed sensitivity was found to be the single largest contributor to model uncertainty. Therefore, projects where measurements of real tidal sites, such as the on-going studies within the ReDAPT project, are important. This is particularly noteworthy given the literature on the current limitations in the understanding of the resource (Kutney, *et al*, 2013).

For initial demonstration projects, field measurements will be of the utmost importance and quantifying the uncertainty in these measurements will then feed directly into the TidalFarmer tool. This is of direct implications for numerical modelling of the flow around islands as while depth-averaged flow speed is important, the vertical flow profile shape is not as important for energy yield. Therefore, whether external model outputs are sufficient to make a reliable prediction can be inferred from the study undertaken here. In the future however, larger arrays will mean that the modelling will require further assessment as the sensitivity to other inputs grows with array size and so, further research will be required into wake losses.

Not to be disclosed other than in line with the terms of the Technology Contract

Not to be disclosed other than in line with the terms of the Technology Contract

7 REFERENCES

Anderson J.D (1995) *Fundamentals of Aerodynamics*. McGraw-Hill Fourth Edition.

Ainslie, J.F. *Calculating the flowfield in the wake of wind turbines*, Journal of Wind Engineering and Industrial Aerodynamics, 27, 213-224, 1988.

Arango, H.G., and Shchepetkin, A.F. (2012) Regional Ocean Modelling System (ROMS). URL https://www.myroms.org/wiki/index.php/ocean.in.

Blom, P. and Booij, R. Turbulent free-surface flow over sills. Journal of Hydraulic Research, 33, 663–682, 1995.

Bahaj A. S., Myers L.E., Thomson, M.D. and Jorge N. *Characterising the wake of horizontal axis marine current turbines* Proceedings of the 7th European wake and Tidal energy conference, Portugal 2007.

Bai, L., Spence, R. R. G., Dudziak, G., *Investigation of the influence of array arrangement and spacing on tidal energy converter (TEC) performance using a 3-dimensional CFD model*. Proceedings of the 8th European wave and tidal energy conference, Uppsala, Sweden, 2009.

Blom, P. (1993). *Turbulent Free-Surface Flow Over a Sill*. Ph.D. thesis, Technical University of Delft, Delft, Netherlands.

Bravo, H. R., and Zheng, Y. H. (2000) *Turbulent flow over step with rounded edges experimental and numerical study*. Journal of Hydraulic Engineering, 83-85.

Burton, N., Jenkins, N., Sharpe, D., and Bossanyi, E. (2011) *Wind Energy Handbook*, 2nd edition, John Wiley & Sons.

Buvat, C., Peyrard, C., Menon, J.-M., and Fil, C. (2010a) *Construction of the scale model of a horizontal-axis turbine device and installation of the experimental test platform WG4 WP1 D2*. EDF ETI marine programme project.

Buvat, C. (2010b) *Calibration of tests without turbine WG4 WP1 D3*. EDF ETI marine programme project.

Buvat, C. (2012) *Performance of tank tests with physical scale model of horizontal-axis turbine device installed. Analysis of results WG4 WP1 D4*, ETI Marine programme project.

Chanson, H. (2004) *The hydraulics of open channel flow: An introduction.* Elsevier Butterworth-Heinemann.

Duckworth, A., and Barthelmie, R. J. (2008) *Investigation and validation of wind turbine wake models*. Wind engineering, 32, 5, 459-475.

Not to be disclosed other than in line with the terms of the Technology Contract

Durski, S.M., Glenn, S.M., and Haidvogel D. B. (2004) *Vertical mixing schemes in the coastal ocean: Comparison of the leve l 2.5 Mellor-Yamada scheme with an enhanced version of the K profile parameterization.* Journal of Geophysical Research, 109.

Dyer, K. R. and Soulsby, R. L. (1988). *Sand transport on the continental shelf.* Annual Review of Fluid Mechanics, 20, 295–324.

Garrett, C. And Cummins, P. (2005) *The power potential of tidal currents in channels.* Proceedings of the Royal Society, 461, 2563-2572.

Giles, J., Myers, L., Bahaj, A., O'Nians, J., Shelmerdine, B. (2011) *Foundation-based flow acceleration structures for marine current energy converters, IET renewable power generation*, 5, 4, 287-298.

Gretton, G. I. (2011) *Development of a computational fluid dynamics model for an open-centre tidal current turbine WG3 WP5 D2*, ETI Marine programme project.

Gunn, K., and Stock-Williams, C. (2012) *Falls of Warness 3D Model Validation Report*, ETI ReDAPT project.

Gunn, K., and Stock-Williams, C. (2013) *On validating of numerical hydrodynamic models of complex tidal flow*, Proceedings of the 10th European Wave and Tidal Energy Conference, 2013, Aalborg, Denmark.

Hogan, R. 2006 *How to combine errors* [online article] url: http://www.met.rdg.ac.uk/~swrhgnrj/combining_errors.pdf

Jackson, P. S. and Hunt, J. C. R. *Turbulent wind flow over a low hill*. Quarterly Journal of the Royal Meteorological Society, 101, 929–955, (1975).

JCGM, *Evaluation of measurement data - Guide to the expression of uncertainty in the measurement*, JCGM Std.100:2008, 2008.

Kutney, T., Karsten, R., and Polagye, B. *Priorities for Reducing Tidal Energy Resource Uncertainty*, Proceedings of the 10th European Wave and Tidal Energy Conference, 2013, Aalborg, Denmark.

MacKay, D. (2008) *Sustainable Energy: Without the Hot Air*, www.withouthotair.com, UIT.

Martin, V., Pham, C. T., and Saviot, S. (2012) *Tidal basin modelling: The Alderney Race, the Pentland Firth and the Paimpol-Bréhat sites modelled in Telemac software*, ETI Marine programme project.

McNaughton, J., Rolfo, S., Apsley, D., Afgan, I., Stansby, P., and Stallard, T. *CFD Prediction of Turbulent Flow on a Laboratory Scale Tidal Stream Turbine using RANS modelling* 1st Asian Wave and Tidal Conference Series 2012

McIntosh, S. C., Fleming C. F., and Willden, R. H. J. (2011) Performance and wake structure of a model horizontal axis axial flow turbine. ETI Marine programme project.

Not to be disclosed other than in line with the terms of the Technology Contract

Myers, L., Bahaj, A. S., Rawlinson-Smith, R. S., Thomson, M. (2008) *The effect of boundary proximity upon the wake structure of horizontal axis marine current turbines*. In Proceedings of the 27th International Conference on Offshore Mechanics and Arctic Engineering, Estoril, Portugal.

Olczak, A., Stallard, T., and Stansby, P. *The influence of waves on Tidal Stream Turbine Wake Recovery*, Proceedings of the 10th European Wave and Tidal Energy Conference, 2013, Aalborg, Denmark.

Paterson, A. R. (1983) *A first course in fluid dynamics*. Cambridge University press.

Pope, S. B. (2010) *Turbulent flows.* Cambridge University press.

Salmon, R. (1998) *Lectures on Geophysical Fluid Dynamics*. Oxford University Press.

Schlichting, H., Gersten, K,. (2000) *Boundary layer theory*, Springer-Verlag Berlin.

Song, Y., and Haidvogel, D. (1994) *A semi-implicit ocean circulation model using a generalized topography-following coordinate system*. Journal of Computational Physics, 115, 228-244.

Stallard, T. (2012) *Design and specification of ducted disc experiments WG4 WP3 D1,* ETI Marine programme project.

Stallard, T., Collings, R., Feng, T., and Whelan, J. I., *Interactions between Tidal Turbine wakes: Experimental study of a group of 3 bladed rotors*, Proceedings of the 9th European Wave and Tidal Energy Conference, 2011, Southampton, UK

Stock-Williams, C., Parkinson, S. G. and Gunn, K. *An investigation of Uncertainty in Yield Prediction for Tidal Current Farms*, Proceedings of the 10th European Wave and Tidal Energy Conference, 2013, Aalborg, Denmark.

Telemac modelling system 2013 [online] http://www.opentelemac.org/

Tennekes, H., and Lumley, J. L. (1972) *A first course in turbulence*, MIT Press.

Thomson, M.D., and McCowen, D. (2010a) *GH Blockage modelling report WG3 WP4 D1,* GL Garrad Hassan. ETI Marine programme project.

Thomson, M.D., Gill, L., and Collings, R. (2010b) *Near wake modelling report WG3 WP4 D2*, GL Garrad Hassan. ETI Marine programme project.

Thomson, M.D., Whelan, J.I. (2010c) *Device scale modelling report WG3 WP4 D3*, GL Garrad Hassan. ETI Marine programme project.

Thomson, M.D., Collings. R., and Stallard, T. (2011a) *Array scale experimental test report WG4 WP2 D5*, GL Garrad Hassan. ETI Marine programme project.

Thomson, M. D. And Gill, L. (2011b) *Rationalised flow field modelling report WG3 WP4 D4*, GL Garrad Hassan. ETI Marine programme project.

Not to be disclosed other than in line with the terms of the Technology Contract

Thomson, M.D., Gill, L., and Collings, R. (2011c) *Far wake modelling report WG3 WP4 D5*, GL Garrad Hassan. ETI Marine programme project.

Trefethen, L. N. (2000). *Spectral Methods in Matlab*. Society for Industrial Mathematics.

Vermeer, L. J., Sorenson, J. N., Crespo, A. (2003) *Wind turbine wake aerodynamics*. Progress in Aerospace Sciences, 39, 467-510, 2003.

Weideman, J. A. C. and Reddy, S. C. (2000). *A MATLAB differentiation matrix suite*. ACM transactions on mathematical software, **26**, 465–519.

Whelan, J. I., Graham, J. M. R., and Piero, J. (2009) *A free-surface blockage correction for itdal turbines in an array*. Journal of Fluid Mechanics. 624, 281-291.

Whelan, J. I., and Stallard, T. *Arguments for modifying the geometry of a scale model rotor*, Proceedings of the 10th European Wave and Tidal Energy Conference, 2011, Southampton, UK.

Wickham, A., and Way, S. P. (2012) *Construction, calibration, testing and reporting of coastal basin scale experiments*. GL Garrad Hassan. ETI Marine programme project.

Wood, R. M. and Harris, R. G. (1920), *Some notes on the theory of an airscrew working in a wind channel*, Reports & Memoranda No. 662, Aeronautical Research Committee.

Ni, Z. H. and , Song Z. Y. and Zhang, X. J. and Wu, L. C. and Yi, J. *A Modification to vertical Distribution of Tidal Flow Reynolds Stress in Shallow Sea*, Chinese Ocean Engineering, 26, 431-442, 2012.

Not to be disclosed other than in line with the terms of the Technology Contract